October 2011

The Beacon Locator Project: A Passive Direction Finding System for Locating Pulsed Emitter Signals

Christopher Benjamin Massa
Worcester Polytechnic Institute

Erik Chapman Silva
Worcester Polytechnic Institute

Samantha O'Connor Kuhlwein
Worcester Polytechnic Institute

The Beacon Locator Project

A Passive Direction Finding System for Locating Pulsed Emitter Signals

A Major Qualifying Project
submitted to the faculty of
Worcester Polytechnic Institute
in partial fulfillment of the requirements for the
Degree of Bachelor of Science

Submitted by:

Erik Silva
Samantha O'Connor
Christopher Massa

Submitted to:

Project Advisors:
Professor Edward Clancy
Professor Germano Iannacchione

Project Supervisors:
Scott Bailie, MIT Lincoln Laboratory
Lisa Basile, MIT Lincoln Laboratory
Christopher Strus, MIT Lincoln Laboratory

October 13, 2011

This work is sponsored by the Department of the Air Force under Air Force Contract #FA8721-05-C-0002. Opinions, interpretations, conclusions, and recommendations are those of the author and not necessarily endorsed by the United States Government.

Abstract

RF emitters can be tracked through their electromagnetic energy transmissions by passive direction finding systems. These systems have many applications, including aircraft tracking, radio navigation and emergency aid. Our sponsor, MIT Lincoln Laboratory, has an interest in using direction finding systems to locate friendly and hostile emitters via airborne test platforms. In order to analyze potential designs, we simulated three direction finding methods, time difference of arrival (TDOA), phase difference, and amplitude comparison, in MATLAB and compared the accuracy of their direction calculations. TDOA had the greatest error, as high as 70°. Phase difference produced the smallest error, less than 0.01°, but resulted in multiple ambiguous solutions. Amplitude comparison had a moderate error, less than 2°, but did not result in ambiguous solutions. For this reason, the amplitude comparison method was implemented in an FPGA based development module as a proof of concept. This design was able to meet most of the performance requirements set forth for the system by MIT Lincoln Laboratory. However, the design could be improved in the future by integrating it with a phase difference system and using the amplitude comparison design to eliminate ambiguities in the phase difference results.

Acknowledgements

The authors would like to thank the following people for their guidance and assistance through our work on this project:

- Our WPI advisors: Professor Ted Clancy and Professor Germano Iannacchione
- Our Lincoln Laboratory staff: Chris Strus, Scott Bailie, and Lisa Basile
- Emily Anesta and Seth Hunter for organizing the WPI MQP projects at Lincoln Laboratory
- The members of Group 108 at MIT Lincoln Laboratory for their role in helping our group in various ways throughout the course of this project

Statement of Authorship

The contributions of the authors Christopher Massa, Erik Silva, and Samantha O'Connor are as follows:

Christopher designed and implemented the radar signal emulator used to simulate a receiver front-end during the summer at Lincoln Laboratory. For this project, he coded and implemented our algorithm design in hardware using VHDL. Chris verified that the implemented system had the capability of meeting all project specifications, and evaluated ADC performance through hardware testing to determine the resolution of the prototype system. He performed the hardware tests for system functionality and headed the discussion on hardware results and analysis in our paper. He also conducted background research on the time difference of arrival (TDOA) direction finding method, authored the section on TDOA direction finding in our paper, and wrote the TDOA position location algorithm in MATLAB.

Erik led the investigation of the ability for our hardware to meet project specifications through analysis in MATLAB. He modeled the ability for our hardware to achieve direction finding within ±2.5° of accuracy for input signals covering 40 dB of dynamic range, and examined ways to improve our design to fully meet the system requirements. Additionally, he conducted research on the phase comparison direction finding method, authored the background section on phase comparison in our paper, and wrote the phase comparison direction finding algorithm in MATLAB. Erik also created the capability for signal detection within our MATLAB simulations, as well as designed the Hilbert filter used to generate in-phase and quadrature signal components in the phase and amplitude comparison methods.

Sam conducted preliminary background research on available methods of direction finding, and the various wave characteristics used to achieve angle of arrival calculations. She also spearheaded research on the amplitude comparison direction finding method, authored the background section on amplitude comparison in our paper, and developed the algorithm in MATLAB. Sam executed the testing and analysis of all three simulated direction finding methods in MATLAB. She identified sources of error within each algorithm, analyzed the impact of these error factors, and hypothesized modifications to each system to improve accuracy. Her analyses of sources of error included, but were not limited to, the symmetry of system geometries, timing errors due to closely spaced receivers, the impact of noise on intermediate frequency signals, and the resolution of the lookup table used for amplitude comparison angle determination. Additionally, she performed the cross correlation analysis to verify correct time delay calculations within the TDOA algorithm, accounting for the impacts of microwave frequency and interpolation factor in her analysis.

This project has been completed in partial fulfillment of the requirements for the degrees of Bachelor of Science in the fields of both Physics and Electrical and Computer Engineering.

Executive Summary

Any system that uses an RF emitter, such as radar or a cell phone, operates by generating electromagnetic energy and transmitting that energy into the surrounding environment. These electromagnetic waves can be observed by a passive receiver in the field of view of the emitter to determine the direction from the receiver to the emitter. These direction finding systems have many applications, including aircraft tracking, radio navigation and emergency aid. Our sponsor, MIT Lincoln Laboratory, is interested in developing a direction finding system to passively locate friendly and hostile emitter signals from an airborne platform. Passive direction finding systems can provide important situational awareness without emitting RF energy. Rather than transmit signals themselves, the passive systems operate by tracking signals transmitted from other sources.

MIT Lincoln Laboratory has taken initiative to research and develop such direction finding systems. They have conducted an earlier project to analyze the relative advantages and disadvantages of several methods of direction finding. Resulting from this project was a set of suggestions for selecting a method to implement. Lincoln Laboratory wished to continue the work of this project by utilizing these suggestions to begin prototype development work. In particular, they wished to model several direction finding methods in simulation to predict their feasibility and performance in practical systems, as well as to prototype a direction finding hardware device implementing one of the simulated methods. Accordingly, the goals of our project were to:

- Design MATLAB simulations for three different methods of computing angle of arrival to investigate feasibility of various systems.
- Design and prototype a signal processor for an airborne direction finding system capable of determining the angle of arrival of a pulsed emitter signal to within ±2.5° of accuracy over 40dB dynamic range.

The methods investigated through simulation were time difference of arrival (TDOA), phase difference, and amplitude difference. The simulations compared each method over a range of input signal characteristics and system geometries. Each simulation was designed to imitate the respective algorithm's functionality in hardware as closely as possible by adhering to system geometry limitations for implementation on an airborne platform, as well as limitations induced by our development board. The signals used to drive our simulations were restricted to an intermediate frequency of 20 MHz, assuming that the radio frequency signal detected at the antennas was successfully down converted in a radar system's front end. The sampling rate was set to 250 MHz, as determined by the 14-bits of resolution for the A/Ds in our system with 10 effective bits. Additionally, since our direction finding system is only concerned with resolving azimuth angles of arrival, we are restricting our simulations to perform direction finding with one degree of freedom over a 90° azimuth extent.

Our procedure for analysis of the three direction finding systems in simulation followed a four-step process: creating a uniform test environment, designing systems for each of the three direction finding methods, gathering information about the accuracy of the resolved angles of arrival from each system in the test environment, and comparing the results of these simulations between each method.

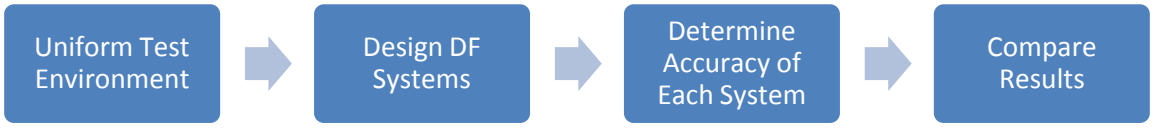

Figure 1. Four-step procedure for designing each of the three direction finding systems for simulation.

To create the uniform test environment, our group utilized MATLAB to simulate a pulsed radar beacon at a known location in space. This signal exhibited the same wave characteristics (amplitude, frequency, pulse width, etc.) in the simulation of all three methods, and would be detected by each of the three systems at the same true angle of arrival and from the same true distance away from the system's receiver array. Our group designed systems for each of the direction finding methods. Each of the methods required a unique receiver array, shown in Figure 2 below, which was dependent on the angle of arrival algorithm of the systems. The TDOA method used four omnidirectional receivers spaced in a diamond formation to imitate the placement of these receivers on the nose, tail, and wings of an aircraft. The phase comparison method used a receiver geometry of two omnidirectional antennas spaced 10cm apart from each other. The amplitude comparison method used two directional horn antennas located next to each other but offset by 90° such that their beam patterns intersect at the 3dB point. The antennas shown in the figure below for amplitude comparison are triangular to differentiate from the omnidirectional antennas used for phase comparison and TDOA direction finding. Our group developed algorithms for determining the angle of arrival using each of the three methods and ran each simulation in the test environment to collect data on the accuracy of the resolved signals from each system. The results were compared to determine which method would be most appropriate for our project.

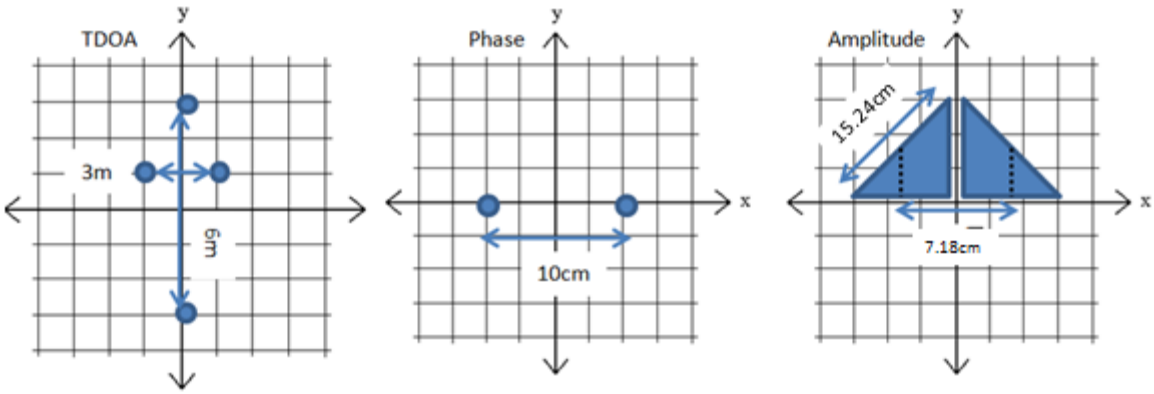

Figure 2. Antenna geometries for each of the three direction finding systems.

Analysis of the results of our simulations allowed our group to make several determinations about the accuracy of each direction finding method and its respective appropriateness for use in our project. The TDOA algorithm relies on the intersection of hyperboloids at specific points in space to determine the source location of a detected signal. While adhering to the specification of implementation on an airborne platform, the TDOA method was only able to resolve 22% of angle calculations across the full azimuth extent within the required ±2.5° of accuracy, and was unable to resolve angles close to the boresight of the system due to a fault in the algorithm for small antenna geometries and insufficient sampling rate (Figure 3). Due to these inaccuracies, our group determined that the TDOA algorithm was not the best method to implement for our prototype.

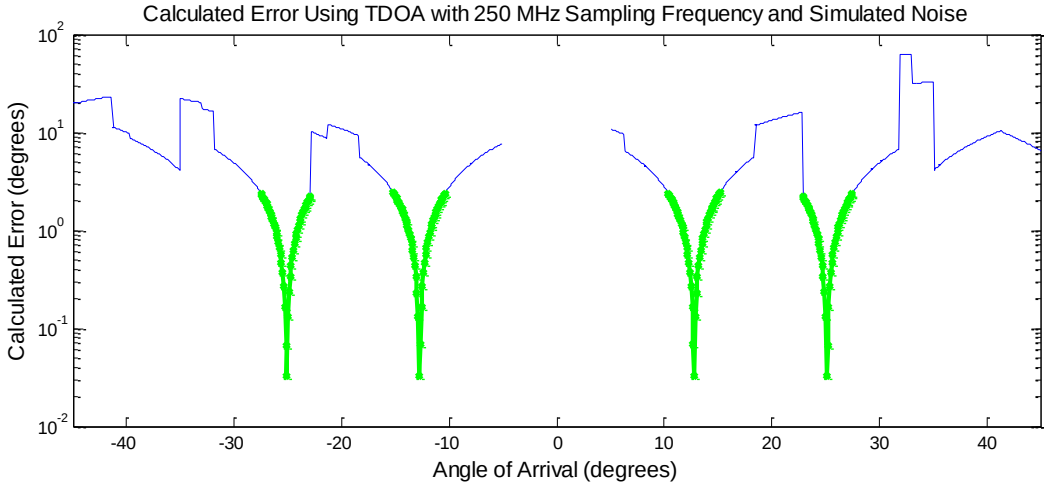

Figure 3. Error in angle calculations from the TDOA method over the full azimuth extent. Calculations shown with green dots meet the requirement of ±2.5° accuracy.

The phase comparison method was able to resolve an angle of arrival with the highest degree of accuracy out of the three simulated systems by comparing the incident phase of a signal detected at two omnidirectional signals. However, since the phase comparison method cannot differentiate between signals that are 360° out of phase, the simulation with antennas separated by 10cm yielded 2 or 3 possible angles of arrival for signals detected over ±45° (Figure 4). While one of the calculated angles of arrival was resolved with an accuracy of within one-thousandth of a degree of the simulated angle, the other calculated angle(s) of arrival were typically off by 10s of degrees. Our group determined that while adhering to our design, the phase comparison method, on its own, would not be appropriate for use in our project due to this ambiguity of angle calculation.

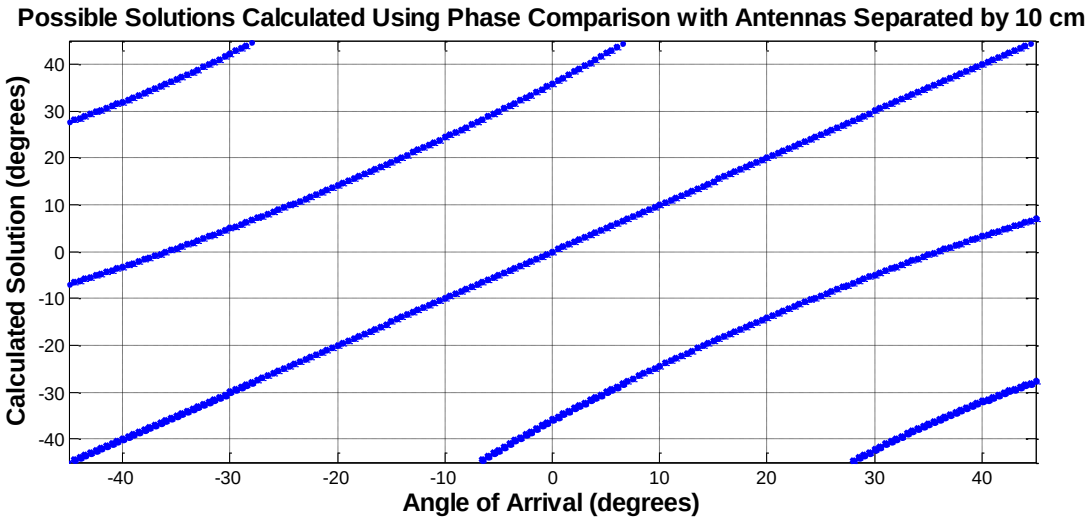

Figure 4. Possible angles of arrival calculated using the phase comparison method for direction finding with antennas separated by 10cm.

The amplitude comparison method resolved angles of arrival to within 2° of the simulated angle using a lookup table with 1.8° resolution (Figure 5). This algorithm compares the voltages induced at two offset directional antennas with a known gain pattern, computes a ratio of voltage magnitudes from the two antennas, and uses a lookup table of ratio values to determine an angle of arrival. Since this antenna geometry was appropriate for an airborne platform and the accuracy of the system met the specifications of our sponsors, our group determined that the amplitude comparison method would be the most appropriate for our project.

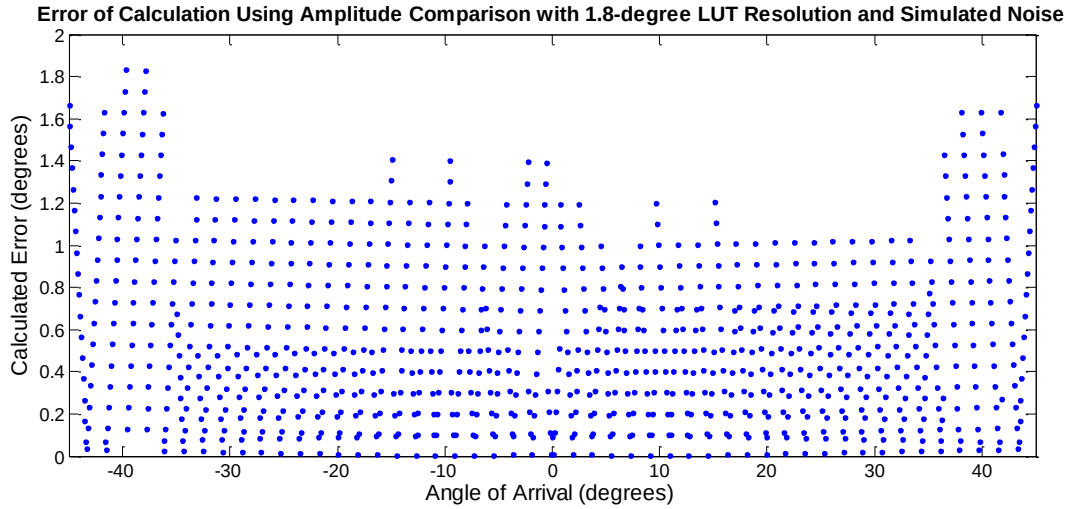

Figure 5. Error of angle calculations from the amplitude comparison method over the full azimuth extent. All angles can be determined with the use of a lookup table of 25 values to within the required degrees of accuracy.

The final component of our project was the design and development of a signal processing hardware device capable of performing direction finding on intermediate frequency

signals and that met all criteria specified by our sponsors. Following from our simulation results, we designed hardware components to implement the amplitude comparison direction finding algorithm. Our hardware design was realized in VHDL and tested using a commercial off-the-shelf development board with a Xilinx Virtex 5 FPGA core. Two ADCs were included with this board which we utilized for the acquisition of intermediate frequency signals. These ADCs were clocked at 250 MHz, which covered our specification of 100 MHz of input bandwidth, and provided an effective 10 bits of resolution when accounting for noise. Our system was able to receive two intermediate frequency input signals, determine an angle of arrival, and transfer the result across the LAN through an Ethernet connection to a separate graphical software display.

We tested our system in a lab with intermediate frequency input signals covering the 90° azimuth extent of the system in order to measure its accuracy. The results of our testing are given below in Table 1. For most input angles, the hardware device was able to meet the ±2.5° accuracy specification. However, larger errors occurred at the extremes of the field of view (near ±45°), and system output for a beacon signal with a 44.6° angle of arrival was not within accuracy specifications. We investigated the cause of these inaccuracies and determined that they can be mitigated with additional hardware components. As such, we believe that our design will be able to achieve performance near our accuracy specifications once these components are integrated with our design.

Input Angle	Calculated Angle	Error
-44.6	-42.5	2.2
-40.5	-40.8	-0.4
-30.4	-31.0	-0.7
-20.3	-22.1	-1.8
-10.2	-10.2	-0.1
0.1	0.1	0.0
10.2	10.3	0.1
20.3	20.3	0.0
30.4	30.8	0.5
40.5	39.1	-1.4
44.6	40.7	-3.9
All values in degrees.		

Table 1. Average calculated angles of arrival from the direction finding hardware and the errors from the true value.

Recommendations

After our group identified the limitations and restrictions of each of the direction finding methods in simulation, we explored various ways to increase the accuracy of each of the systems. By slightly modifying some of the specifications for our project, each of the direction finding systems could be improved to resolve angles with greater accuracy.

The TDOA method is usually implemented with receivers separated over a significantly larger area than is possible on an airborne platform. However, to accurately represent this algorithm in terms of our project specifications, our simulation employed a receiver geometry that imitated possible distances between receivers on an aircraft. Our design also used a sampling frequency of 250 MHz as characterized by our ADCs. With improved technology, the use of ADCs with a higher sampling frequency would greatly improve the accuracy of our TDOA system design while maintaining the current receiver geometry for airborne implementation. In addition, larger and more complex TDOA systems have been designed to overcome inherent problems with TDOA position location, which could be an avenue for further research.

The phase comparison method produced 2 or 3 possible angle of arrival calculations when the antennas were separated by 10cm. Reducing the size of the antennas to a point where they could be separated by just 3cm (one wavelength) would result in a single calculation for the angle of arrival with less than 1° of error and no ambiguities. However, it is impractical to consider such small separation between antennas as this would induce timing errors as a result of very small differences in incident phases for signals detected at the two antennas. Instead, the phase comparison method could be combined with addition direction finding techniques to reduce the extent of azimuth range and eliminate ambiguities in angle calculations. For example, if an additional direction finding method were first used to locate the angle of arrival of a signal to within a few degrees, the phase comparison could then calculate the angle of arrival within that reduced range with a high level of accuracy.

The amplitude comparison method, as calculated for our project, had the greatest degrees of error for wide angles of arrival (approaching ±45° from the central median of the antenna array), but was able to calculate angles of arrival over the full azimuth extent to within the required degrees of accuracy. Increasing the size of the lookup table resulted in even more accurate calculations for angle of arrival over the full extent.

For the direction finding hardware device, there are several avenues of further work which could improve its performance. First, additional hardware would be able to mitigate the issues with system accuracy. Once these issues are mitigated, our hardware should be able to achieve performance close to its desired accuracy specifications. Second, the functionality of the device could be extended to account for pulsed waveforms and multiple emitters. Currently, our system is only able to determine angles of arrival for a single, continuous wave beacon emitter. However, practical applications would likely involve multiple pulsed-wave emitters, which should be taken into account. We had initially intended to develop this functionality, but we were unable to complete it due to time constraints. The addition of such improvements and functionality extensions would allow our system to be accurate and robust for use in practical applications on an airborne platform.

Table of Contents

1. Introduction

Any system that uses an RF emitter operates by generating electromagnetic energy and transmitting that energy into the surrounding environment. These electromagnetic waves can be observed by a passive receiver in the field of view of the emitter to determine the direction from the receiver to the emitter. These direction finding systems can be used to track many different types of systems for various applications, ranging from avoiding aircraft collisions to aiding emergency rescue missions. One area of interest is in developing direction finding systems that are able to passively locate emitter signals, such as radar beacons, from an airborne platform.

While the information collected by radar systems is highly beneficial to operators, the signals transmitted by the system can be used by hostile targets to obtain information about the aircraft. Passive direction finding systems reverse this situation by not emitting radar signals and instead tracking the signals emitted by hostile targets. Additionally, it is useful to know the location of other radio frequency beacons in the environment, for purposes ranging from tracking hostile radar systems to radio navigation. These benefits will serve to improve situational awareness as part of the goals of our sponsors at MIT Lincoln Laboratory to reduce vehicle vulnerability and increase survivability of aircraft in the United States Air Force.

Due to the high importance of increased situational awareness for military aircrafts, there is an ever increasing demand for more sophisticated direction finding systems. As such, numerous attempts have been made in recent years to combine existing technologies and create more accurate direction finding systems. In fact, Lipsky makes the observation that "in no other field perhaps have there been as many false starts, aborted designs, and abandoned systems [Lipsky, 2004]." Experimentation with hybrid systems utilizing a combination of existing direction finding techniques has shown significantly greater accuracy than earlier systems were capable of achieving. Several devices have been created that measure different properties of detected signals to determine the bearing of the signal's transmitter. For example, numerous devices have been created that use measurements of both a signal's amplitude and its incident phase to calculate the angle of arrival [Carr and Marvin, 1989; Carter et al., 1997]. These devices usually compare a signal's amplitude as detected at two receivers that are differentially oriented and either collocated or separated by a known distance in space to determine the location of an emitter to within a few degrees. Then, a phase analysis is used to increase the accuracy of the target's location. Other devices have been developed that utilize information about the time a signal arrives at two separated receivers, along with the incident phase [Lioio et al., 1998]. Even more designs have been created using other combinations of wave characteristics, vector sensors, and various antenna types. The variety in direction finding system designs allows for the creation of highly specified systems that can utilize various methods to calculate a signal's angle of arrival depending on unique specifications for a wide range of projects.

Our sponsors, MIT Lincoln Laboratory, wished to design and develop such a device for their own needs. Currently, direction finding systems are not readily available in packages viable for the airborne platforms our sponsors work with. Though our sponsors had acquired background knowledge on available direction finding methods, they did not yet have a device capable of performing any of these methods. An earlier project they conducted involved an analysis of available direction finding methods to ascertain their complexity and accuracy. Resulting from this project was a set of suggestions for selecting a method to utilize for development. However, before our project began, our sponsors had not yet begun development work.

This project continued our sponsors' previous research and utilized it to develop functional direction finding systems for MIT Lincoln Laboratory. Our group researched several of the direction finding methods covered by the previous project in order to determine their functionality, advantages/disadvantages, and required calculations. Using these data, we simulated each method within computer software to better analyze their implementation complexity and output accuracy. Further, we selected the direction finding method we felt was most appropriate for a prototype direction finding system, and we designed and implemented a hardware system to perform the method. The results of our work were a set of virtual testing environments, a prototype hardware device to perform the core functionality of a direction finding system, and a set of data consisting of accuracy and error information obtained from simulations as well as laboratory hardware testing. These results form a base on which future projects could expand towards the goal of a practical direction finding system usable on an airborne platform.

2. Background

2.1 Project Motivation and Specifications

The motivation behind this project involved aiding the Tactical Defense Systems group at Lincoln Laboratory in their goal of improving airborne situational awareness of the United States Air Force (USAF) aircraft. Our goal was to develop a passive direction finding (DF) system to determine the angle of arrival of a pulsed radar beacon signal, modeled as a pulsed sinusoid, coming from an emitter that could be located on the ground or on another aircraft. Passive direction finding allows our system to detect both cooperative and non-cooperative targets without providing a beacon of our own location in the form of emitted radar signals.

The project entailed the creation of a prototype DF system according to a set of specifications from our sponsor. The system must utilize one of three possible direction finding methods, time difference of arrival (TDOA), phase comparison, or amplitude comparison, to determine the angle of arrival of a pulsed radar signal with one degree of freedom. The angle of arrival should be calculated to within ±2.5° accuracy over 40dB of dynamic range. Also, the system must be able to identify up to three simultaneous emitters, and include a real-time display that indicates each individual emitter and corresponding angle of arrival in an intuitive way so that it can be interpreted by the operator of an aircraft. Since the desired platform for our prototype is airborne, the size and weight are physically limited to fit within the constraints of a USAF aircraft.

The scope of our project is limited to processing intermediate frequency (IF) signals over a 100 MHz bandwidth, instead of an entire DF system, which could operate over several gigahertz. This narrow scope is a result of the fact that it is impractical to master and prototype an entire functional DF system during the nine week time constraint of this project. The prototype system developed by our group instead used input signals generated by a hardware signal emulator, which will be described in greater detail later in this chapter.

While the given specifications are desirable of a functioning system, they may not be achievable with the provided hardware, or within the time constraints of our project. Accordingly, the successful completion of this project will be defined as building a direction finding system that is able to locate a single beacon adhering as closely as possible to the given specifications. If a specification cannot be met, we will describe why it is beyond the capabilities of our project, and provide a simulation of a functioning system that meets the specifications.

2.2 Emitter Signals

Before discussing the techniques used to locate the angle of arrival of an emitter signal, it is necessary to provide some basic background on the nature of radar signals and systems, as

radar shares many characteristics with more general systems that could be integrated with our design. Radar systems operate by feeding high frequency electrical signals, specifically radio frequency (RF) signals in the range of several MHz to 10's of GHz, to transmitter antennas that then emit the energy as electromagnetic waves. After objects in the path of the beam distort and reflect these waves, a portion of the transmitted energy can be detected and converted back to electrical signals at receiver antennas. Radar processing circuitry analyzes these return signals to determine characteristics of the surrounding environment, which could include information about the location, direction, or speed of objects in the path of the beam. Since we are designing a passive system, our project will deal with the second half of this system, where the signal is received and processed.

Before our project can process pulsed emitter signals, they must first be detected and pre-processed by a receiver frontend. The following sections will provide a brief overview of a receiver system that could be integrated with our project. First, the signals that would be detected at a receiver will be described, along with the parameters that are used to characterize them. Second, basic antenna behavior and the antenna geometry that will be used for this project will be introduced and explained. Third, the analog circuitry necessary to manipulate received signals for digital system processing is presented. Fourth, the in-phase and quadrature signal components are described, as well as the signal processing calculations that utilize these components.

2.2.1 Pulsed Radar Signal Characteristics

The most common type of radar signal is a series of sinusoidal waveform pulses that are repeated in time, frequently referred to as a pulse train. This is the type of signal that our system is designed to process and an example of such a waveform is shown below in Figure 6.

There are many parameters that are used to describe the behavior of a radar signal. The most important of these parameters are described here, as well as being labeled in Figure 6. The time of arrival (TOA) describes when a pulse starts in time. Some radar systems use differences in time of arrival for the same signal at multiple locations to determine the direction of origin of a signal. The pulse amplitude (PA) describes the strength of a signal in terms of the power associated with the waveform. Pulse amplitude is affected by several factors, including the input signal strength and the angle at which the signal reaches the antenna, and, like TOA, is used in some radar systems to calculate the angle of arrival of a signal. The carrier frequency (RF) is the frequency at which each pulse oscillates. This characteristic is modulated in time for many radar systems; however, our project will only deal with fixed carrier frequency signals. A common use of the carrier frequency is to differentiate between multiple signals in an environment. If two signals with different carrier frequencies are detected by a receiver, they can be separated and individually processed by applying the proper filter to the input signal. Another method by which receivers can differentiate multiple signals is through the pulse repetition interval, which describes the length of time between the start of each pulse. Though

signals with the same carrier frequency cannot be separated through linear filtering, it is still possible to differentiate between the signals if they are transmitting at different points in time. The pulse width defines the length of time that each pulse is transmitted. Since increasing the duration of a signal increases the amount of energy contained in that signal, pulse width is part of what determines the amount of energy associated with a signal. This relationship, combined with the fact that radar receivers are limited by the strength of signals they can detect, mean that pulse width is a large component of what determines the maximum range at which a signal can be detected.

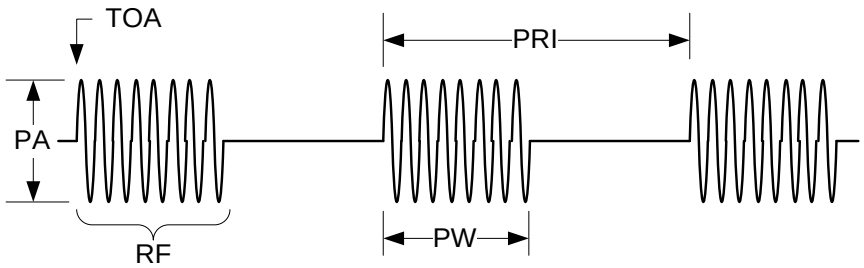

Figure 6. Example pulsed radar signal and the parameters that are used to characterize the waveform [From Scott Bailie, 2011]

2.2.2 Receiver Front-End Geometry

Before a received signal pulse can be processed by the frontend hardware or digital circuitry, it must first be detected by the receiver antenna. There are many different types of antennas in use today for various purposes ranging from radar to television broadcasting. The shape and size of the antennas determine their behavior and include omnidirectional antennas that emit and receive energy equally in all directions along a horizontal plane, as well as directional antennas that are able to transmit and receive signals more strongly in one direction than others.

Due to the need for accurate angular measurements and desire to aim all available power at a single point in space, most radar systems use highly directive antennas. These directional antennas have an angle of greatest gain, known as the boresight axis, where they are most effective at transmitting and receiving energy. The boresight is often located along the axis of symmetry of the antenna. As shown in Figure 7 below, the amplification of received signals is highest near the boresight axis and rapidly drops off as the input signal moves farther towards the edges of the beam. Note that this pattern only shows the horizontal plane of the antenna. Realistic antennas vary gain in two dimensions; however, since our project is only concerned with azimuth angle of arrival, our design will use a symmetric one-dimensional gain model.

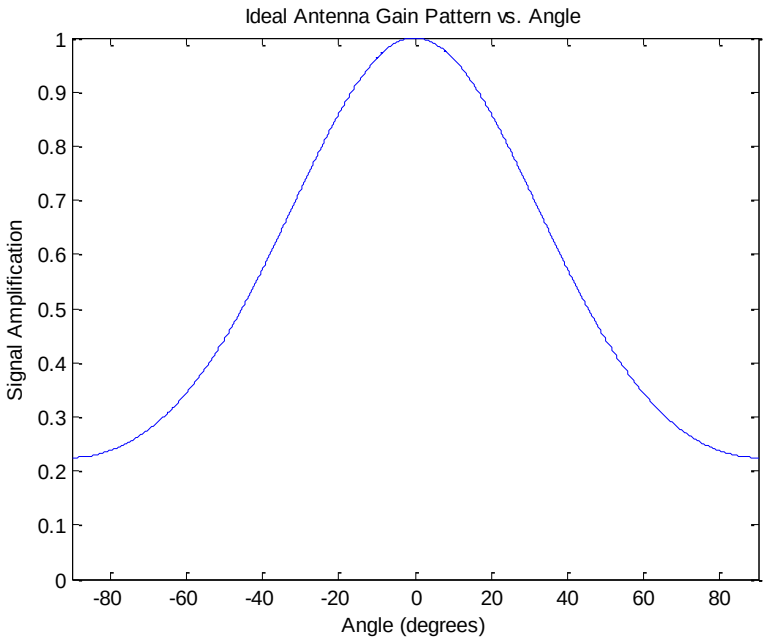

Figure 7. Ideal gain pattern for a directional antenna with respect to signal angle of arrival

It is important to note that input signal power is not solely dependent on the angle of arrival of the signal. The distance over which the signal travels is also important. A simplified form of the radar range equation treats transmitter power as being evenly distributed over the surface of a sphere:

$$Power\ Density = \frac{P_t}{4\pi R^2}$$

Equation 1

Since the energy will be distributed across a larger area the farther one is from a source, the lower power will be received and the harder the signal will be to detect. This equation is a simplified version, however, and more complex equations exist to describe the power density for directional antennas. [Skolnik, 2001]

2.2.3 Receiver Frontend Circuitry

Due to limited analog to digital converter speeds, before a digital receiver can process the information contained in an RF signal, the signal must first be down converted to baseband frequency. Several architectures exist for performing this conversion, but one of the most common is the super-heterodyne architecture, which mixes the RF signal down to an Intermediate Frequency (IF) before mixing it a second time to baseband. The additional stage increases the amount of analog hardware associated with the system, but significantly increases the sensitivity and selectivity of the receiver [Bowick et al, 2008].

Like most receivers, super-heterodyne systems start with an RF filter that attenuates frequencies outside the desired RF band, occasionally adding multiple RF filters to switch between frequency channels. The signal is then sent to a Low Noise Amplifier (LNA) that increases the signal strength to reduce the effect of noise contributions at later stages in the channel. Because of its impact on noise figure, the effectiveness of this stage is a primary factor in determining the selectivity and sensitivity of a receiver. In order to down convert the signal to IF, it is mixed with the output of a Local Oscillator (LO) offset from the signal frequency by a fixed amount. Further filtering and amplification is performed to improve the signal quality and the signal is then sent to further stages for conversion to baseband. [Bowick et al, 2008]

The receiver for our project will be different from a standard super-heterodyne receiver in that it will not use the conversion stage from IF to baseband and will instead sample the IF signal directly. The system is able to use IF because the ADC's sampling rate of 250MHz is fast enough to cover the target IF band of 12.5-112.5MHz. There are several reasons why using IF is advantageous for our project. Primarily, in order for a system to convert a signal from IF to baseband frequency, it must know which frequency band it is monitoring to select the proper frequency for down conversion. Our system is instead searching over a range of frequencies for any strong signal, so in order to use the baseband signal, it would need to constantly adjust the LO to monitor a different frequency. In addition, using IF rather than baseband frequency will reduce the amount of hardware that needs to be implemented in the receiver frontend, reducing the cost of the system and allowing us to focus our time on implementing the signal processing algorithms.

2.2.4 In-Phase and Quadrature Signal Analysis

There are many ways to view and analyze detected radar signals, and one of the most useful methods for doing so are through the in-phase and quadrature components of the signal. The in-phase and quadrature components, or I and Q, of a signal represent the real and imaginary portions of that signal, respectively, as seen in Figure 8 below. Various digital and analog methods are used to obtain these signals, ranging from Hilbert filters, which are filters designed to introduce 90° phase shifts across all frequencies while ideally not affecting signal amplitude, to mixing signals in hardware with sine and cosine functions of the same frequency. The choice of method will depend on the system being utilized, however each technique will produce the same output of two signals with the same frequency and amplitude, but 90° out of phase from each other.

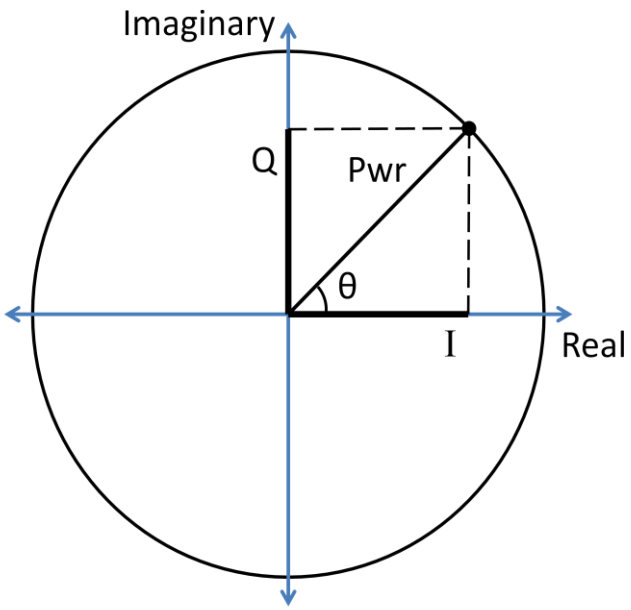

Figure 8. Graphical representation of the in-phase and quadrature components of a signal as well as useful signal characteristics that can be calculated using those values.

The primary benefit of using the in-phase and quadrature components of a signal comes from the simplification of calculations associated with treating real signals as complex entities. Since I and Q represent the real and imaginary components of input signals, certain mathematical properties can be leveraged to instantaneously calculate many signal characteristics. For example, without I and Q, a signal must be monitored over several periods, squared, and averaged in order to calculate the power of a signal. However, by using the Pythagorean Theorem to measure the magnitude of the complex signal, the amplitude can be calculated from a single sample. Alternatively, using the inverse tangent function with I and Q enables one to measure the instantaneous phase of a signal, which can be very useful in calculations of frequency or phase difference. The graphical representation of both of these calculations can be seen above on the unit circle in Figure 8.

2.3 Direction Finding

While there are various applications for radar systems, such as obtaining information about weather patterns or landscape images, the type of radar involved in this project involves obtaining directional information about a target. The various characteristics of radar signals can be used to determine the angle of arrival at a receiver. Direction finding refers to this ability to determine the direction from which a signal is emanating, and can be resolved with one or two degrees of freedom covering azimuth and/or elevation depending on the complexity of the system. While direction finding has several applications, including radio navigation and emergency aid, it is a valuable capability for airborne platforms involved in air

defense. Active direction finding techniques rely on the use of directional antennas, which are more sensitive to signals arriving from certain directions than from others. Because of this variation in sensitivity, different types of directional antennas have different gain patterns. Legacy systems were able to accomplish direction finding by pointing a directional antenna in the direction at which the incoming signal is received the strongest. However, to achieve a greater degree of accuracy, more sophisticated procedures are required.

2.3.1 Passive Direction Finding

Passive direction finding allows a system to locate a transmitted signal without producing a signal of its own. This ability is advantageous for aircrafts to search for non-cooperative emitters without inadvertently providing information about their own bearings [Skolnik, 2001].

This type of direction finding requires an array of directional antennas to intercept a signal and draw information about its angle of arrival based on a comparison of data from each antenna. Several methods of passive direction finding exist which perform this comparison using different sets of signal characteristics. Many of these methods involve antenna arrays that are relatively inexpensive and small enough to be mounted in an aircraft. The three methods that were considered for our project were time difference of arrival (TDOA), phase comparison, and amplitude comparison. [Lipsky, 2004]

2.3.2 Time Difference of Arrival Direction Finding

Time difference of arrival (TDOA) direction finding utilizes small differences in the travel times of a signal to a set of receivers in order to determine the location of the signal source. The basis of this method is that if a signal produced at a certain location arrives at two or more receivers separated in space, variations in distance will result in different signal travel times to each receiver. Therefore, each receiver would encounter the signal at a different point in time. The resulting differences in arrival time could then be used to calculate the location in space of the signal source.

2.3.2.1 TDOA System Geometry

The configuration of a TDOA direction finding system can be visualized as a set of points in space: one source point and multiple receiver points (see Figure 9). Each receiver point is an unknown distance from the source. The travel time of a signal originating from this source point would vary between receivers due to any differences in these distances. If each receiver records the time at which they encounter the signal, a set of time of arrival differences, or TDOAs, may be calculated. The differences in distance can then be determined directly from these TDOAs.

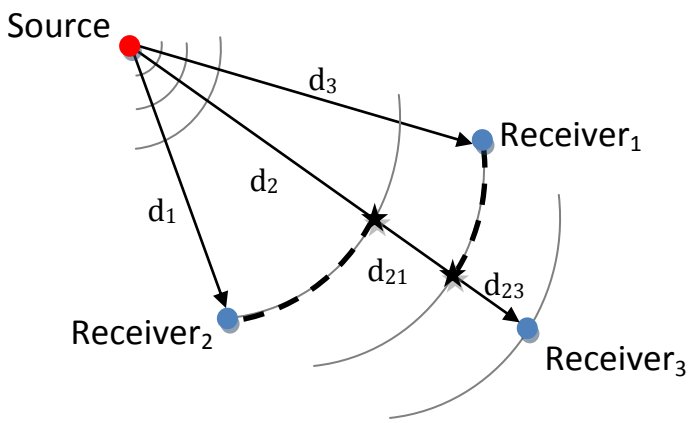

Figure 9. Geometry of a TDOA direction finding system consisting of a single source and three receivers at separate distances away. Differences in distance result in differences in arrival time.

2.3.2.2 Calculation of Source Position

An exact location of the signal source can be derived from equations for the differences in receiver distance. For each difference between two receivers, there exists a set of points in space at which the signal source could possibly be located. Combining the results of multiple receivers can reduce these sets of locations to a single point. The result of the derivation is then a set of equations for the location of this point in space. Bucher and Misra [2002] have completed a full derivation of the coordinate equations for a signal source location; some of these equations have been adapted here to help illustrate the mathematical basis of TDOA direction finding.

The calculation of signal source location is based primarily on formulas for distance. Consider a TDOA system consisting of an unknown source location (x, y, z) and a set of N receivers at known locations (x_i, y_i, z_i), where i denotes a single receiver. The distance from the source to a receiver can then be calculated using the distance formula:

$$d_i = \sqrt{(x_i - x)^2 + (y_i - y)^2 + (z_i - z)^2}$$

Equation 2

An additional formula can be used to calculate this distance based on the travel time of the signal in question. This formula calculates the distance traveled by a moving object as its speed multiplied by the total travel time. Given that electromagnetic signals travel at a known speed, the speed of light (c), the distance traveled by the signal in question to a receiver i can be calculated from the following equation:

$$\mathrm{d_i} = \mathrm{c} * \mathrm{t_i}$$

Equation 3

where t_i is the travel time of the signal to the receiver. As the source location and the travel times for the signal are unknown, these distances cannot be calculated directly from these equations. However, a system of equations for multiple receivers can be used to pinpoint the source.

Using the TDOAs between receivers with a system of distance equations allows for the calculation of possible signal source positions. Consider two receivers i and j and their distances calculated from travel time: $d_i = c * t_i$ and $d_j = c * t_j$. Subtracting the latter from the former results in the equation:

$$\mathrm{d_{ij}} = \mathrm{c} * (\mathrm{t_i} - \mathrm{t_j})$$

Equation 4

where d_{ij} denotes $d_i - d_j$. Note that $t_i - t_j$ is the TDOA between receivers i and j. As such, it is possible to calculate a value for the difference in distances from a signal source between two receivers. Applying this knowledge with Eq. (4) results in the equation:

$$d_{ij} = \sqrt{(x_i - x)^2 + (y_i - y)^2 + (z_i - z)^2} - \sqrt{(x_j - x)^2 + (y_j - y)^2 + (z_j - z)^2}$$

Equation 5

which, when rearranged, becomes the following:

$$\sqrt{(x_i - x)^2 + (y_i - y)^2 + (z_i - z)^2} = (d_{ij}^2 + x_i^2 - x_j^2 + y_i^2 - y_j^2 + z_i^2 - z_j^2 + 2x_{ji}x + 2y_{ji}y + 2z_{ji}z)/2d_{ij}$$

Equation 6

where x_{ji} denotes $x_j - x_i$, y_{ji} denotes $y_j - y_i$, and z_{ji} denotes $z_j - z_i$. This equation, when squared, becomes the equation for a hyperboloid [Bucher and Misra, 2002]. As the unknown x, y, and z values in this equation define the location of the signal source, it follows that each point on this hyperboloid is a valid possibility for the source location. The results from this equation are therefore ambiguous; however, with upwards of two receivers and their resulting TDOAs, more hyperboloids may be calculated which can reduce the number of possible source location points (see Figure 10).

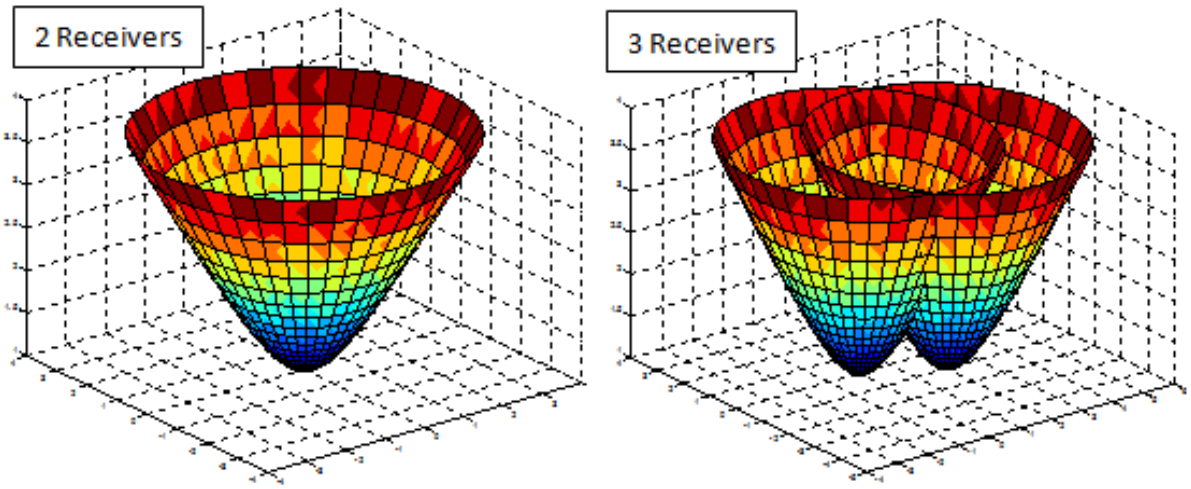

Figure 10. Hyperboloids of possible source locations. Each hyperboloid is calculated from a TDOA between two receivers. Two hyperboloids reduce the possible locations to the intersecting curve. Three or more further reduces the possible locations to a single point.

The intersections of several hyperboloids may be used to reduce the number of possible source locations. As each hyperboloid must contain the actual point in space of the signal origin, the point at which a set of hyperboloids intersect must be this origin. With a third receiver, a second TDOA may be calculated and used to form a second hyperboloid. The intersection of the two hyperboloids found thus far will be a curve on a 2D plane. The set of possible source locations is therefore reduced to the points located on this curve. Utilizing the intersection of a third hyperboloid with the curve would reduce the possible locations to a single point. Theoretically, a third hyperboloid could be calculated with three receivers as there would be three distinct receiver pairs. Unfortunately, due to the square root terms, the system of equations for three receivers does not reduce to a simple, satisfactory solution [Bucher and Misra, 2002]. Instead, four or more receivers can be used to simplify the equations. By using a system with four receivers, the equations can be reduced down to the coordinates of the source location.

2.3.2.3 Advantages and Disadvantages of TDOA Direction Finding

Several advantages are inherent with this particular direction finding method. The most pronounced advantage is the ability to pinpoint an exact emitter location in space rather than determining only a direction. The results of this method therefore provide information outside of the capabilities of other methods. In addition, a full TDOA direction finding system (with four or more receivers) can easily cover 180° with no ambiguities, whereas other methods have more limited fields of view or have inherent difficulties with resolving ambiguities. By simply adding a fifth receiver, this field of view may be expanded to a full 360°. [Bucher and Misra,

2002] Other systems may require many more components to achieve a full viewing angle. These features make TDOA direction finding very appealing for various applications.

However, in the context of this particular project, there are some serious drawbacks to using this method. First, for a field of view limited to azimuth only, this system will require more components than other available methods. Position locating in 2D space using TDOA requires three receivers in order to locate a point [Thai et al., 2008]. Typically, a TDOA direction finding system would require fewer antennas than other systems would. However, if a direction finding system is needed only for azimuth in a narrow field of view, then the TDOA system will actually require more components than other systems.

Second, calculating TDOAs on received electromagnetic signals within the space limitations of an aircraft will produce sub-optimal results. Typically, systems which perform position locating using the TDOA method utilize receiver bases which are more than kilometers apart. However, our system would have to be limited to the space provided by an aircraft, which would be on the order of only a few meters. Note that for such a separation of receivers, the maximum possible TDOA between them for an electromagnetic signal would be only a few nanoseconds. Unfortunately, most modern high-speed ADCs have sampling periods also on the order of nanoseconds, which would induce large errors in the calculated TDOAs.

Finally, the algorithms required for TDOA direction finding are far more complex than those of other direction finding methods. These algorithms require a great number of time-consuming calculations on large sets of stored samples, all of which must occur in real-time. The development and optimization of a system consisting of these algorithms would therefore require far more development time than other available methods, which posed a serious issue given the limited time frame of the project. In addition, given various receiver and source locations, realistic noise levels, and practical system sampling rates, the simple four-receiver algorithm described here may not converge on a single point. More advanced systems have been developed to mitigate some of the inherent practical issues with TDOA direction finding, but attempting to develop such a system would compound the issue of long development time. With all of these disadvantages considered, it appears that TDOA direction finding should not be the immediate focus of this project.

2.3.3 Phase Difference Direction Finding

Whereas TDOA systems use differences in travel time to locate signals, phase difference DF systems calculate direction based on differences in phase between signals received at multiple locations. When the same signal is received at two separate receivers, but travels slightly farther to reach one receiver than the other, the extra distance can be detected as a phase shift in the signal. By analyzing the phase difference, distance between the antennas, and wavelength of the RF signal, one can calculate the angle of arrival (AOA) of the signal and locate the transmitter.

2.3.3.1 Phase Comparison System Geometry

Phase difference DF arrays require at least two antennas to provide a direction, however more are frequently included to resolve ambiguities associated with the calculations that the system performs. As many as five antennas can be spaced linearly apart at fixed distances based upon the target frequency band in order to construct an unambiguous system. These antenna arrays operate as several two-antenna systems in parallel and combine the information after processing. The calculations for such a configuration are therefore similar to more basic systems. As phase difference DF systems generally monitor a 90° target quadrant, four systems would be combined to produce a full 360° field of view. [Lipsky, 2004]

2.3.3.2 Calculation of Angle of Arrival

The first step of phase comparison calculations is that the system will use the in-phase and quadrature components of the signal at each receiver to measure the phase at each receiver. It then calculates the difference in phase between the receivers, which will be used in later calculations.

Once the system measures the phase difference between the two receivers, the AOA can be calculated with some assumptions and simple trigonometry, as seen in Figure 11 below. When the average distance between the transmitter and the receivers (R) is much greater than the distance between the receivers (d), the direct paths from the transmitter to the receivers (r1 and r2) are approximately parallel. This relationship is a safe assumption for most radar applications and allows us to treat angle α as the AOA.

A point P is then selected along line r1 such that the distance from the transmitter to Rx2 is equal to the distance from the transmitter to P. Since these two distances are the same, the phase of the transmitted signal will be identical at points P and Rx2. Therefore, any differences in phase detected at the receivers can be used to calculate the distance between P and Rx1 according to the equation:

$$|\overline{P\ Rx1}| = \left(\frac{\Delta\theta}{2\pi} + K\right) * \lambda$$

Equation 7

where Δθ is the phase difference in radians between the two receivers, K is any integer value, and λ is the wavelength of the RF signal. Equation 7 derives from the fact that signals cover one wavelength of distance for every 360° of change in phase angle. Additionally, since r1 and r2 are effectively parallel, the points at P, Rx1, and Rx2 will form a right triangle with the distance between the receivers as the hypotenuse, as indicated in Figure 11 below. This orientation means the definition of the cosine function in a right triangle can be used, namely $cosine(angle) = \frac{length\ of\ adjacent\ side}{length\ of\ hypotenuse}$, to calculate the angle of arrival. Using Equation 7 as the length of the adjacent side and the distance between the receivers as the hypotenuse produces the equation:

$$\cos(\alpha) = \left(\frac{\Delta\theta}{2\pi} + K\right) * \lambda * \frac{1}{d}$$

Equation 8

where α is the angle of arrival and d is the distance between receiving antennas. [Broadbent, 2010; Lipsky, 2004]

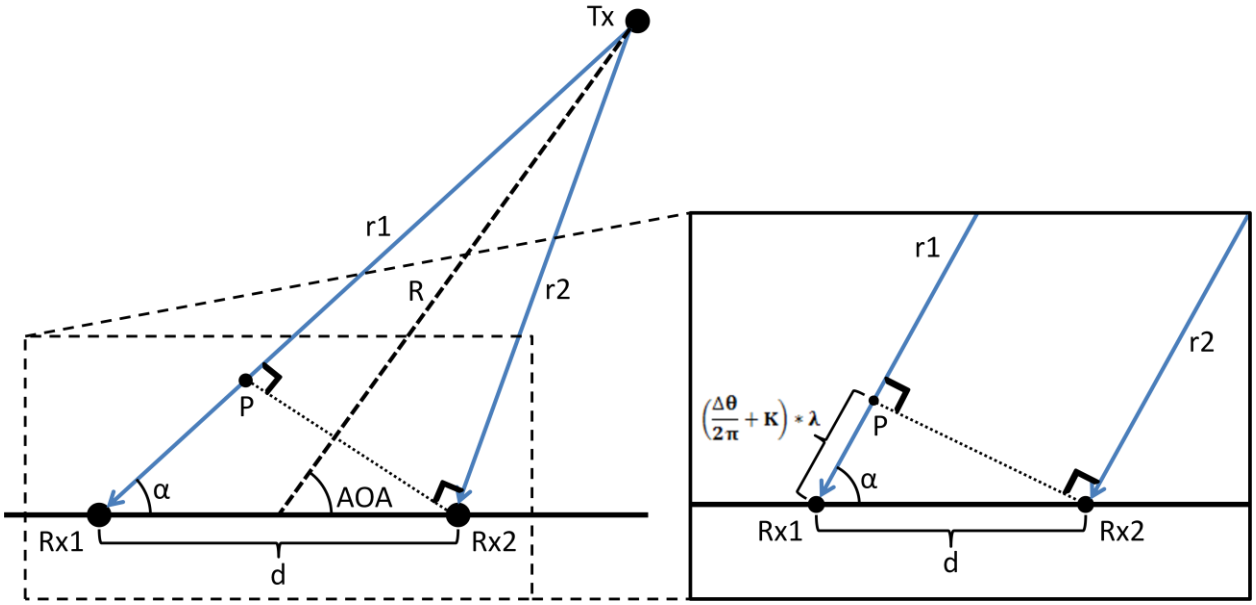

Figure 11. Geometric relationship of phase angle and angle of arrival within a phase interferometry direction finding system [Adapted from Broadbent, 2010]

Not all of the variables in Equation 8 can be measured directly from the input signals. In order to calculate Δθ instantaneously, a Hilbert filter can be used to generate the in-phase and quadrature components of each received signal. From those components, we can then calculate the instantaneous phase of each signal and the phase difference between the two signals. The wavelength of the RF signal can be measured indirectly due to the fact that $\lambda = \left(\frac{c}{f}\right)$, where c is the speed of light and f is the radio frequency of the signal. By measuring the phase change over a known number of clock ticks and converting that value to a phase change per unit time, the IF of the signal can be calculated. Then, as long as the mixing frequency used to down convert the RF signal is known, we can calculate the original frequency and wavelength of the RF signal.

2.3.3.3 Advantages and Disadvantages of Phase Comparison Direction Finding

Utilizing phase difference for direction finding can produce highly accurate results. Due to the high frequency of RF signals, a small change in distance results in a large change in phase. For example, a signal with an RF frequency of 10GHz would have a wavelength of 3cm, which would mean a change in distance of merely 0.5cm would result in a 60° change in phase. With

this fact and Equation 8, it is possible to design DF systems with less than 1 degree of error in angle of arrival calculations. Indeed, this high precision is one of the primary strengths of phase difference DF systems. [Lioio et al, 1996]

Despite the high accuracy of phase interferometry systems, however, the periodic nature of the signals that makes these systems possible also introduces an ambiguity when calculating AOA. Systems measuring the phase difference between two signals cannot resolve phase shifts greater than 360°. Therefore, if receiver antennas are spaced more than one wavelength apart for a given frequency, there may be multiple solutions to Equation 8 when locating signals on that frequency. This ambiguity is often resolved by combining phased interferometry with other DF methods such as TDOA or by constructing an array of antennas to detect the phase at additional locations for comparison. [Lioio et al, 1996; Lipsky, 2004]

An additional challenge that phase difference DF systems share with TDOA systems is the need for highly accurate synchronization between channels. The phase of a signal is directly related to time, which means that any difference in delay between the receiver channels would affect the accuracy of the system. The techniques for avoiding this problem include using the same local oscillator for each down converter and the same clock to trigger both ADCs. [Broadbent, 2010]

2.3.4 Differential Amplification Direction Finding

In addition to the phase and time difference methods of direction finding, some systems take advantage of differences in signal amplitude to locate RF beacons. These systems are usually smaller, less expensive, and simpler both to understand and implement than the previously mentioned techniques of direction finding. For these reasons, amplitude comparison has been chosen as the predominant method for implementation for this project.

2.3.4.1 Amplitude Comparison System Geometry

The amplitude comparison method uses two offset directional antennas to determine the angle of arrival of an incoming signal. Figure 12 shows a two antenna system that can be used for amplitude comparison direction finding, where d is the distance between the boresights of the two antennas, and θ indicates the angular displacement of the boresight of each antenna from a central median. While this figure shows two antennas that are separated by a non-negligible distance, some amplitude comparison systems can use collocated antennas with boresights that are angled away from each other. Specifically, our project involves a pair of directional horn antennas located adjacent to each other with a known overlapping antenna beam pattern as shown in Figure 13. A signal will induce a different voltage amplitude at the output of each antenna depending on the angle at which the signal intersects each of the radiation beams.

For the purposes of this project, our group is only concerned with using amplitude comparison to determine the azimuth angle of arrival of a beacon signal with one degree of

freedom. As such, our descriptions of the angle of arrival method of direction finding will predominantly focus on antenna arrays for azimuth direction finding. To apply the amplitude comparison method over more than one degree of freedom, additional antennas can be added to the array to expand the dimensions of beam pattern overlap to additional degrees of freedom. In fact, for any known antenna pattern and system geometry, the amplitude comparison method can be used to determine the induced voltages at each antenna to compute the angle of arrival of a signal. [Mahafza, 1998]

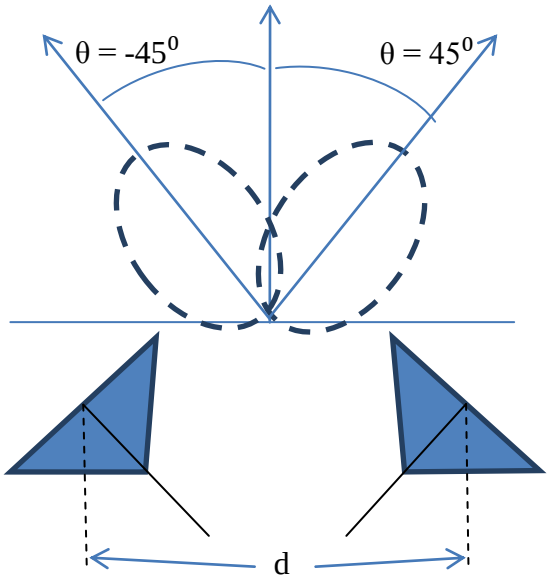

Figure 12. Two-antenna system for amplitude comparison direction finding. The antennas are separated by a distance, d, and offset from a central median by 45-degrees in opposite directions. This offset causes their boresights, and accordingly, the peak of their gain patterns, to be located 90-degrees apart. The gain patterns intersect at the 3dB point.

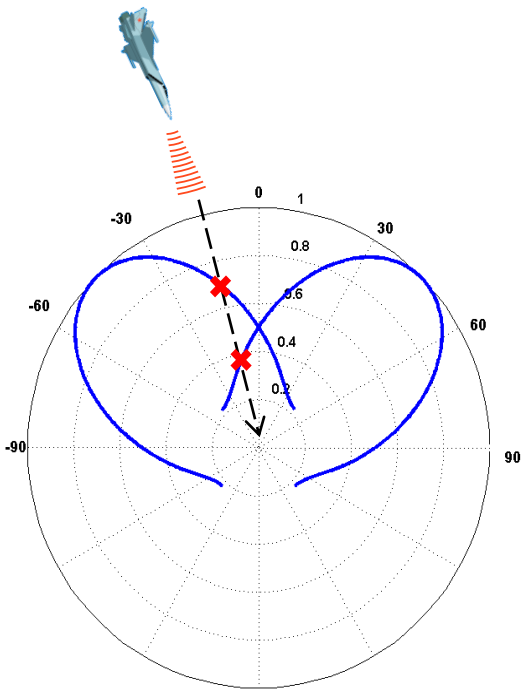

Figure 13. Antenna pattern of horn antennas showing intersection of incoming signal at different gain levels for each antenna.

The antenna pattern in Figure 13 shows two antennas offset ±45° from a central median. Due to this offset, the signal will induce different voltages that vary according to the angle of arrival of the signal at each individual antenna. The different voltage levels are determined by the point of intersection of the incoming signal by the antenna patterns, which are marked by red x's in Figure 13. A signal that originates closer to the boresight of one antenna will induce a larger voltage in that antenna than would be induced in the antenna angled away from the source. This voltage difference occurs as a result of the directionality of the antennas which provide the highest gain at an angle perpendicular to the face of the antenna. Offsetting the antennas guarantees that for every angle of arrival within our ±45° range, the ratio of received voltages can be calculated to yield a unique angle of arrival. [Skolnik, 2001]

2.3.4.2 Calculation of Angle of Arrival

To determine the angle of arrival, the magnitude of the incoming signals must be compared with angular information from a known antenna pattern. When a signal is received at the antenna, it is sent through an analog to digital converter (ADC). By converting the signal to digital, each antenna will register a different binary representation of the signal's voltage magnitude at the point when it is intercepted at the receiver, which can be used for digital processing and calculations. This magnitude varies according to the antenna gain pattern, and is determined by the signal's angle of arrival.

In order to accurately compare the instantaneous amplitudes measured at each antenna using only real components, the signals must arrive at the antennas in-phase with each other. Incoming waves induce a voltage at the receiving antenna, and this voltage is dependent upon the phase at interception. Taking instantaneous amplitude measurements at different phases could result in comparing a peak amplitude reading at the first receiver and a nodal reading at the second receiver, which would lead to inaccurate calculations for angle of arrival. The two antennas involved in this project are set apart at a non-negligible distance, which implies that there will be a phase difference between the received signals at the two antennas. Therefore, we still need a method of accurately comparing signal strength at the two receivers that can be used regardless of this phase ambiguity.

Since the instantaneous signals from the antennas will be out of phase, our amplitude comparison combines both in-phase and quadrature signals to calculate signal power. The in-phase and quadrature components of a signal are obtained using a Hilbert filter programmed in hardware, which makes it possible for our design with two ADC's to obtain a set of in-phase and quadrature components to represent signals from each of the two antennas. The original signal and its quadrature phase component for any given amplitude are used to calculate the instantaneous power of that signal using Equation 9, below, shows the calculation of the power levels, A and B, of the signals detected at the two antennas. In these equations, the in-phase and quadrature signal magnitudes are represented by a_I, b_I and a_Q, b_Q respectively.

$$A = \sqrt{a_I^2 + a_Q^2}\ ,\ B = \sqrt{b_I^2 + b_Q^2}$$

Equation 9

The process of taking the square root of the sum of the squared initial and quadrature shifted signals at a single antenna results in the power received at that antenna. Performing the calculation twice, for both A and B, results in power levels at each of the two antennas. The ratio ($\frac{A}{B}$) of these power levels is then used to determine the angle of arrival through the use of a look-up table. The LUT can be constructed from the known antenna pattern, with a specific angle associated with the corresponding ratio of antenna gain. This ratio can be compared with the calculated power ratio between the two antennas to determine the angle of arrival of the received signal. [Skolnik, 2001]

However, with our antenna configuration of two ideal directional antennas offset by 90°, this process of using the ratio calculation to determine angle of arrival is limited to calculations within the ±45° azimuth extent. Beyond this limit, since the beam pattern of the directional antennas used in this project are symmetric, angles that intersect the radiation beam at plus or minus any given angular displacement from the boresight axis will induce the same voltage at the antenna. For example, since the boresight of one antennas points to -45°, signals that intersect this antenna's radiation beam at -50° and -40° will induce the same

voltage at that antenna. Therefore, to eliminate this ambiguity, this antenna geometry will only be used to resolve angles of arrival within the ±45° azimuth extent.

2.3.4.3 Advantages and Disadvantages of Amplitude Comparison Direction Finding

There are several advantages to using amplitude comparison to determine direction of arrival. Beyond the fact that amplitude comparison DF utilizes relatively straight-forward equations for calculating angles, two aspects that make this method most appealing are its low cost and relatively small size. A system comprised of a minimum of four antenna receiver systems, known as a four-quadrant amplitude comparison DF system (Figure 14), can achieve 360° azimuth extent. With an array of four antenna receiver systems, any incoming signal over 360° is guaranteed to cross through two of the four main radiation beams, providing enough information to compare received signal amplitudes and calculate the angle of arrival. Though real antennas have more than just a main beam, the gain levels of the secondary beams are low enough to not interfere with signal detection in the main beam. While this method is accurate enough to meet most of our project specifications, additional antennas could be added to the system to improve accuracy and sensitivity. For our purposes, an amplitude comparison antenna-receiver system is small enough to operate on an airborne platform. Since amplitude comparison only requires the use of two receivers to cover 90° azimuth extent, implementation of this method would also be less expensive than other options, such as TDOA analysis, which require additional components. [Mahafza, 1998]

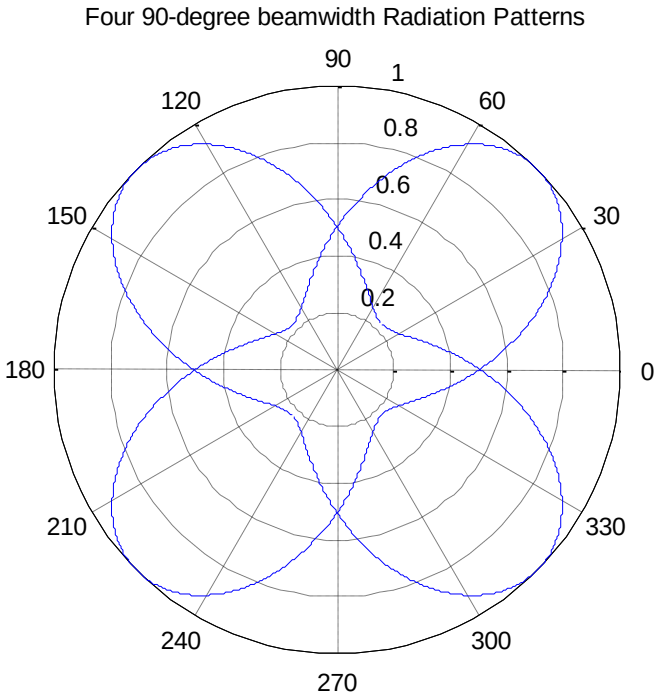

Figure 14. Four main beam antenna radiation patterns, with 90-degree offset between antennas, can achieve 360-degree azimuth extent.

A significant drawback of amplitude comparison DF systems is the high degree of error for calculations at large angles of arrival. For this project, our group will be using the properties of directional horn antennas for all calculations. This specific model of antenna has a gain pattern that indicates low voltage changes along the outer limits of our specified angular range, which could limit the accuracy of measurements at these points depending on the resolution of the A/D in our hardware.

These limitations can be seen in Figure 15, which shows the power ratio between the two antennas in our system over the specified ±45° extent. Toward the center of the graph, which represents a signal emanating from a point equidistant between the two antennas, there is a relatively steep variation in power ratio. This steep incline indicates that small deviations in angle will produce large variations in power, reducing the resolution required to accurately measure the angle of arrival. However toward the outer portions of the graph, as it approaches ±45°, the slope levels out to show very little variation in power ratio for small angle ranges. For this reason, at angles approaching ±45°, there will be very little change in power ratio for a large range of angles, thus decreasing the accuracy of our calculations.

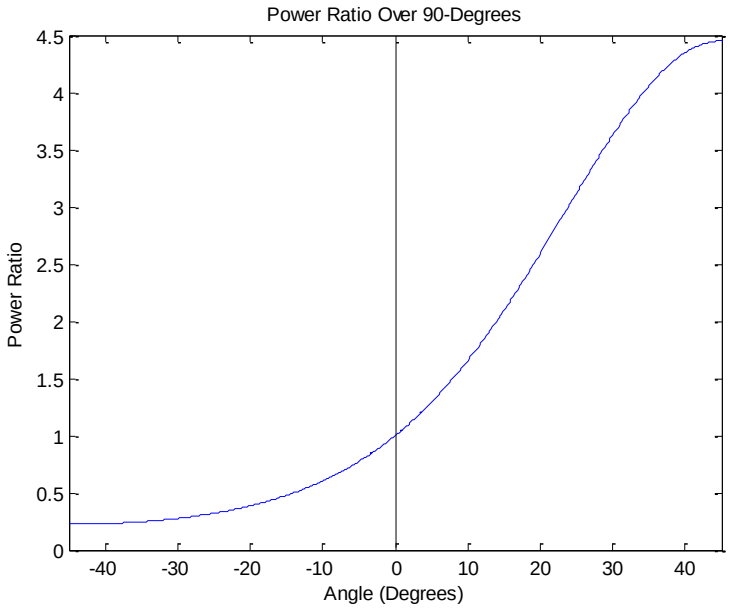

Figure 15. Ratio of power levels used to determine the angle of arrival in the amplitude comparison method over 90-degree azimuth extent.

2.4 Real-time Signal Processing

In order to implement a direction finding algorithm, digital signal processing must be done to extract and manipulate the necessary information from an input signal. Such information could be amplitude, time-of-arrival, or phase, and each may be extracted with a variety of signal processing techniques. Additional processing will also be needed to identify different time coincident signals at the input and to track those signals for more accurate

results. Finally, the direction finding algorithm must also be implemented, taking into account the signal information and analyzing it to produce an angle of arrival.

Several hardware platforms are available for performing the digital signal processing required to implement a direction finding method. These platforms include such devices as central processing units (CPUs), digital signal processors (DSPs), graphical processing units (GPUs), and field-programmable gate arrays (FPGAs). Each of these devices ranges in its specialization, and each has its own merits given a certain application. These four devices were analyzed and compared in order to select a single platform for project development.

2.4.1 Central Processing Unit (CPU)

A CPU is a general-purpose processing element used in a wide variety of applications. It has been designed to perform basic data manipulation functions, such as simple arithmetic and data loading and storing. Such simple functions are intended to be used as building blocks for more complex operations. To perform these functions, it reads in a program of binary instructions built from an instruction set pertaining to the abilities of the device. [Hennessy et al., 2007] The building-block functions of the device combined with the ability to be configured with a customizable program allow the CPU to be utilized for nearly any algorithm. The features which make this device attractive are its general-purpose nature and the ease with which a program design may be edited. However, as the CPU is not inherently tuned to any specific algorithm, it performs much slower than any other similarly-priced option. CPUs do exist which contain features that allow for high-performance digital signal processing, but these are often more expensive and consume more power than other available options. [Eyre and Bier, 2000] In addition, though such high-speed CPUs would excel at sequential calculations, their parallel calculation performance would be limited.

2.4.2 Digital Signal Processor (DSP)

Similar to CPUs, but much more specialized for digital signal processing, are the DSPs. These devices are microprocessors containing architecture specifically designed for implementing digital signal processing tools, such as finite-impulse response (FIR) filters and the Fast Fourier Transform (FFT). DSPs are controlled in a similar fashion to CPUs in that they both read in binary programs built around a device-specific instruction set. As such, DSPs combine the relative simplicity of programming a general purpose CPU with the hardware support for high speed mathematical operations. The advantages of such a specialized processor include better performance and lower processing latency, the latter especially important in real-time applications. Unfortunately, this specialization often also requires becoming familiar with a specific chip as the features and specifications vary from processor to processor. In addition, the specialized architecture and irregular instruction sets of DSPs necessitate program optimization in assembly code to achieve efficient execution. These issues require that

additional time be spent at low-level programming and component analysis rather than algorithm development. [Lipták, 2006; Eyre and Bier, 2000]

2.4.3 Graphics Processing Unit (GPU)

Though GPUs are developed primarily for graphics processing, their programmability and stream processing capabilities allow them to be effective for digital signal processing applications. GPUs contain circuit architecture designed to pipeline streams of data and apply parallelized operations on large amounts of data at once. To account for advancements in technology and graphical effects, GPUs also contain programmable processors for manipulation of data in the pipeline. It is therefore possible to implement a customized digital signal processing algorithm by importing signal data into the device and programming it to perform digital signal processing techniques. With proper optimization, a GPU could outperform a CPU substantially for identical operations on large data sets. However, as GPUs are very specialized devices and are not primarily built for digital signal processing applications, much work and familiarity with the device architecture would be necessary for implementing and optimizing the digital signal processing for the direction finding algorithm. [Radhakrishnan, 2007]

2.4.4 Field-programmable Gate Array (FPGA)

An FPGA is an integrated circuit designed to be reconfigured by the end user. It consists of many independently configurable logic blocks which can be set up to perform different functions. By configuring and connecting these logic blocks in various patterns, different hardware designs may be realized within the FPGA. Old designs may be erased and replaced with new designs at any point, making the FPGA a reconfigurable device for implementing hardware systems. [Kuon et al., 2008] Hardware description languages (HDLs) allow engineers to design and edit these designs in an intuitive, simple-to-understand environment. These languages are text-based expressions for specifying how a hardware system is connected and operates. Existing tools make it possible to realize very complex digital designs, locate logical errors, and test for proper functionality. Once the system is fully described, a simulator can be used to execute the code, or an FPGA configuration can be synthesized and implemented. The generic nature of the device and the ease with which a design may be modified in an HDL allow the device to be fully configurable and reusable.

Several advantages and disadvantages are inherent with using an FPGA for system development. One major disadvantage is the development time required. In general, FPGAs require additional development time and programming efforts over other available platforms. This additional work may be attributed to the fact that in the case of an FPGA, physical hardware components must be designed, whereas other platforms require only that an algorithm is translated into their native machine language. However, the result of designing with an FPGA is a hardware solution that is tuned to the specific algorithms required for a given

task. In real-time digital signal processing applications, it is very desirable to have such an algorithm-specific device as it provides the least amount of processing latency possible. In addition, many different components and systems may be synthesized together on an FPGA and function in parallel. FPGAs therefore allow the greatest degree of parallel processing out of all the devices we have considered. Finally, hardware designs developed in an HDL allow for more flexibility when integrating with other designs. The text-based nature of the designs allows for simpler modification if the device must be adapted for a new application. In addition, these designs typically utilize only a portion of the FPGA resources. As such, multiple HDL designs may be adapted to interact and synthesized on the same FPGA, allowing for system integration in a manner that may often be more straightforward than when utilizing other hardware.

3. Specification Analysis

In order to accurately model the hardware systems through MATLAB simulations, it was necessary to first test the capabilities of the ADC compared to the listed values on data sheets. These tests enabled us to build better simulations for comparing different types of direction finding systems. Additionally, the measured hardware specifications were used to analyze the plausibility of meeting the provided design requirements and provide alternate solutions to meet those requirements in the event that the current hardware was insufficient. This section describes the tests for the effective number of bits of the ADC and the analysis of the relationship between accuracy in angle of arrival calculations and dynamic range.

3.1 ADC Resolution Analysis

The Innovative Integration X5-400M module used for this project, shown below in Figure 16, contains 2 Texas Instruments ADS5474 14-bit ADCs for data acquisition; however, not all of these bits can reliably be used due to noise constraints. A certain amount of noise is introduced through the ADC, which causes lower bits to toggle randomly at the output. This noise causes all ADCs to have an effective number of bits (ENOB) less than the actual number of bits. Texas Instruments specifies 11.2 effective bits for the ADS5474; however, the receiver front end and circuit board parasitics also degrade the ENOB, so the X5-400M data sheet specifies 10.4 effective bits.

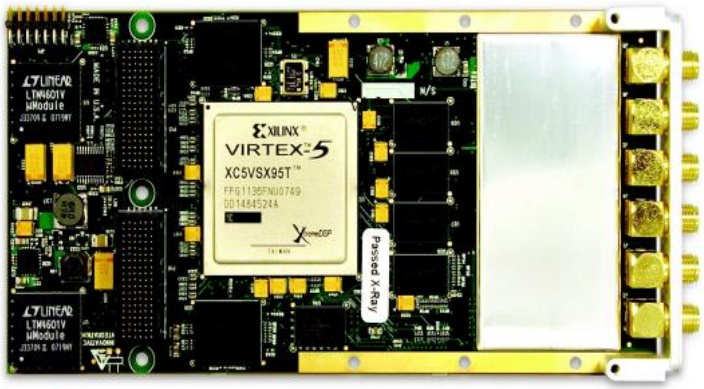

Figure 16. The Innovative Integration X5-400M module used as the hardware platform in this project. [Innovative Integration, 2007]

To measure the total ENOB for the ADC as implemented on the X5-400M, we connected a 50Ω terminator to the inputs of the ADCs and collected noise data for each ADC. Under ideal conditions, the ADC should produce a constant value of 0 since there would be no induced voltage. However, due to the noise at the input and noise inherent to the ADC electronics, there exists a random variation in the signal. Subtracting the minimum from the maximum recorded value produced the range of uncertainty in the output as a result of noise, and taking the base-2 log of that value gave us the number of uncertain bits. These bits were subtracted from the actual number of bits at the ADC to determine the ENOB.

To measure the ADC noise, we recorded 5 MB of samples from each of the two 50Ω-terminated ADCs, corresponding to about 10ms of recording time. We calculated the average of the recorded values for each ADC in order to determine any DC components present. We then subtracted these DC components from each sampled value in order to produce an offset adjusted waveform for the random noise voltages. We found the minimum offset adjusted value to be -10 for both ADCs and the maximum to be 9 for ADC0 and 10 for ADC1. The total noise extent was therefore 19 counts for ADC0 and 20 counts for ADC1. We then calculated the effective number of bits using the following equation:

$$ENOB = A/D\ Resolution - \log_2(Noise\ Counts)$$

Equation 10

Using Equation 10 and the A/D resolution of 14 bits, we calculated an effective 9.75 bits of usable resolution for ADC0 and 9.68 bits for ADC1, which initially appeared to indicate much worse resolution than the 10.4 bits specified in the X5-400M datasheet. However, as the datasheet does not specify the method used to calculate ENOB, these values may not be directly comparable. We investigated the noise further by producing histograms for the two noise waveforms, calculating a percentage of occurrence for each recorded noise value (see Figure 17). We then used the data from the histograms to calculate the percentage of time that the ADCs exhibited a number of effective bits. Our calculations indicated 11 effective bits for 96.64% of the time for ADC0 and 95.84% of the time for ADC1. In addition, both ADCs were found to exhibit 10 effective bits for 99.99% of the time. In order to minimize the impact of noise on the system, calculations in our ensuing simulations involving ENOB used a value of 10 effective bits. It should also be noted that with post-sampling processing, such as signal averaging, the ENOB could potentially be improved beyond our measured values, but our calculations do not take averaging into account.

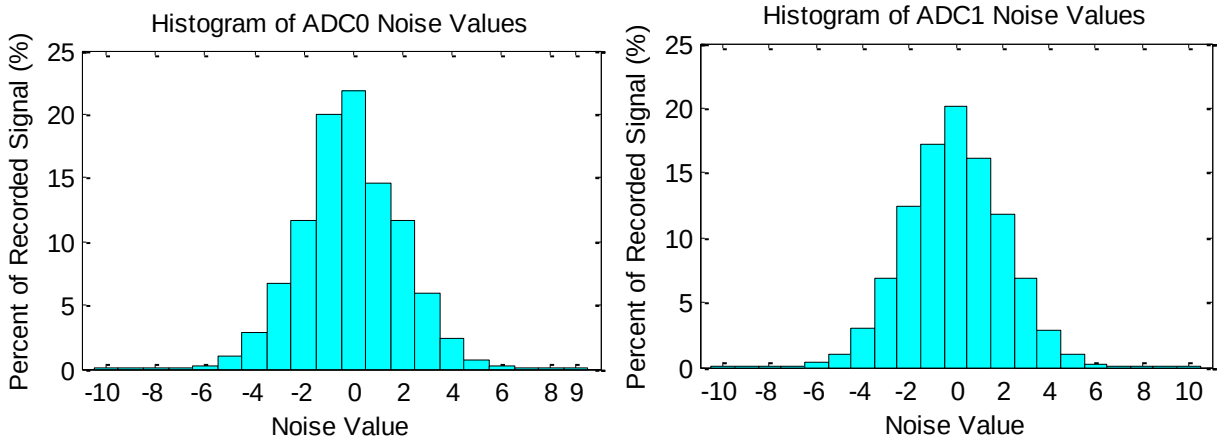

Figure 17. Histograms of recorded noise values from the two development board ADCs. In the recorded noise, over 95% of the noise values are between -4 and 4, and roughly 99% of values are between -8 and 8.

3.2 Dynamic Range Analysis

After having calculated the effective number of bits of the ADC, we were able to examine one set of requirements provided by our sponsors at MIT Lincoln Laboratory. These requirements included the restriction that the device must accurately calculate the angle of arrival to within ±2.5° for input signals covering 40 dB of dynamic range. This analysis assumes that the amplitude comparison method of direction finding is being used as this is the method we selected for our hardware implementation.

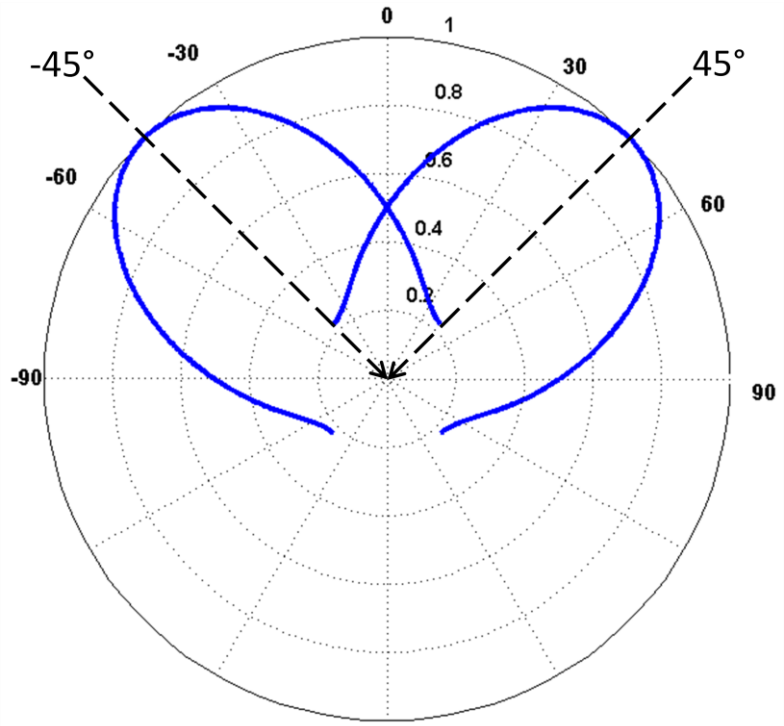

Figure 18. The normalized gain patterns of two 90° beamwidth antennas are shown in the azimuth plane. The boresights are angled 90° apart to match the field of view of the system.

The first step for analyzing the dynamic range of the system is to model the gain patterns of the antennas being used. As has been stated previously, different types of antennas produce different gain patterns and variations in the design between antennas of the same type will also affect the pattern. The MATLAB script 'pattern.m' constructs ideal gain patterns for horn antennas of specified dimensions and was used in this analysis to produce patterns for antennas with 90° and 60° beamwidths. A visual representation of two 90° beamwidth antennas as they would be implemented in the direction finding system is shown above in Figure 18. The boresights of the antennas are angled 90° apart from each other in order to match the field of view of the system. It is important to understand the relationship between these gain patterns in order to understand where the system will have the most trouble accurately resolving an angle of arrival. Figure 19 shows the difference in gain, referred to as ΔG in this section, between the two configured antennas in Figure 18 over the 90° field of view

of the system. Additionally, two 10° changes in angle of arrival, between -5° and +5° and between +35° and +45°, are marked on the figure along with their corresponding changes in ΔG. Notice how the -5° to +5° change in angle of arrival induces a much larger 2.24 dB change in ΔG than the 0.41 dB change induced by the shift from +35° to +45°. This difference is because the slope of ΔG decreases at the edges of the system field of view, meaning that for any given change in angle of arrival, it will induce a much smaller change in ΔG at the edges of the field of view than it would closer to the boresight of the system. This effect, combined with the fact that it is more difficult to accurately resolve the angle of arrival of weak input signals, means that the reference angles for estimating worst-case dynamic range are ±45°.

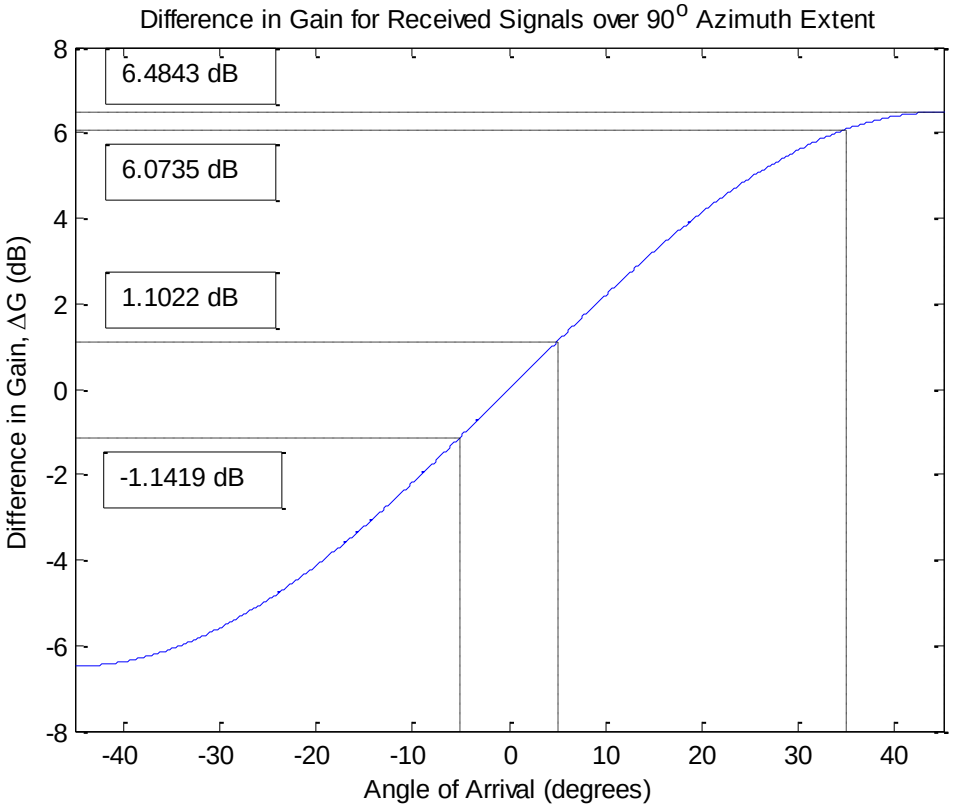

Figure 19. The difference in gain between the two antennas in Figure 18 (the gain of the right-facing antenna minus the gain of the left-facing antenna) for angles of arrival over the full ±45° azimuth extent. The change in the difference in gain between -5° and +5° is 2.24 dB and the change between +35° and +45° is 0.41 dB.

In order to estimate the expected worst-case dynamic range of the system for a given accuracy of angle of arrival, we must first understand the relationship between input signal strength and angle calculation. In the analog receiver front-end of the direction finding system, each signal power corresponds to a particular voltage measured at the ADCs. However, since the ADCs are constrained to a particular number of effective bits, there is a limit to the accuracy of the voltages that can be represented in the digital subsystem. This limit corresponds to the

voltage level of the least significant bit (LSB) and is equal to the voltage range of the ADC divided by 2 to the power of the effective number of bits. Any changes in signal voltage that are less than the LSB voltage will not be detected by the direction finding system. By calculating the change in voltage vs. input signal power for a given change in ΔG and comparing the result to the LSB voltage, we can determine the minimum signal strength at which the change in ΔG will be detected. This process is depicted graphically in Figure 20 below for a 0.104dB change in ΔG, which shows the intersection of the red and blue lines at the minimum detectable input signal power. Using Figure 19 and the maximum input signal power of +10dBm, we can then convert the change in ΔG to a change in angle of arrival and convert the minimum detectable signal strength to a dynamic range.

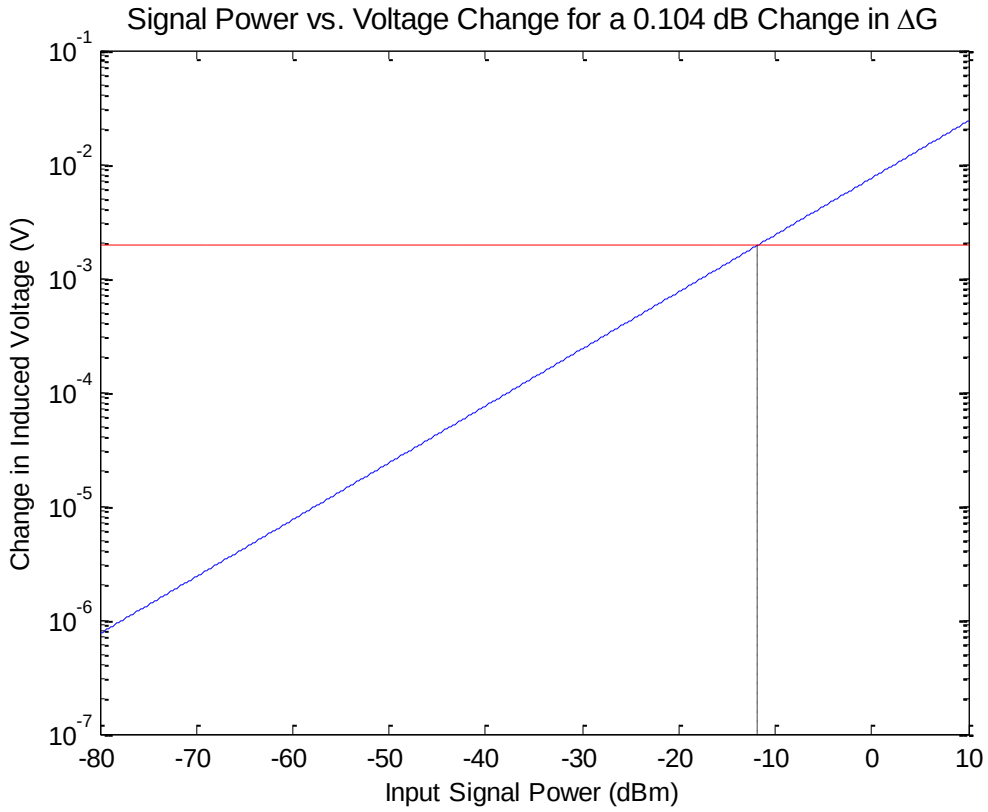

Figure 20. Graphical representation of the change in voltage induced by a 0.104 dB change in the gain difference (ΔG) between antennas over a range of input signal powers, shown in blue. The voltage for the LSB of the ADCs is shown in red.

This method provides us with the dynamic range at one reference angle of arrival for one level of angular accuracy. However, the steps can be repeated in MATLAB with various input values to plot how the dynamic range of the system changes with respect to different reference angles of arrival or desired accuracies. Changing the desired accuracy, while keeping a constant angle of arrival, demonstrates the relationship between accuracy and signal strength

for a given system. Alternatively, changing the angle of arrival while keeping accuracy constant shows which angles of arrival will meet the specifications for the system.

3.2.1 Results

The dynamic range for an amplitude comparison based direction finding system is primarily dependent on the accuracy that the designer wishes to achieve and the angle of arrival used as a reference in the calculations. The graphs in Figures 21 – 26 model the relationship between these parameters for three direction finding systems with different fields of view and effective numbers of ADC bits

Figures 21, 23, and 25 display the range of input signal strengths that can be detected with a given accuracy under worst-case conditions. Any signal that falls within the shaded upper right portion of the graph can be detected with the accuracy indicated along the x-axis. As a point of reference, 2.5° of accuracy at -30dBm is marked with a red circle to indicate the specifications of ±2.5° of accuracy over 40dB of dynamic range. If this point is within the shaded portion of the graph, then the system meets the given specifications under worst-case conditions. All calculations assume that there is no use of signal averaging or other techniques to improve the dynamic range after sampling.

Figures 22, 24, and 26 display the expected dynamic range over the system's field of view while maintaining a constant accuracy of ±2.5°. A line at 40 dB dynamic range is included to show the angles of arrival at which the system will meet the given specifications. Angles where the blue simulation line is above the red limit line meet the specifications of ±2.5° of accuracy over 40dB of dynamic range. For all other angles, the accuracy of the angle of arrival calculation cannot be guaranteed.

The plots in Figures 21 and 22 show the relationships between angle of arrival, target accuracy and dynamic range for a system with a 90° field of view and 10 effective bits. This setup is our current hardware configuration using the given specifications and hardware capabilities. As shown in Figure 21, at +45° and -45° in this system, maintaining an accuracy of ±2.5° will result in a minimum detectable input power of -11.86dBm and a dynamic range of 21.86dB, which is well below the given specifications of 40 dB. However, the dynamic range varies greatly with angle of arrival, and the system meets the specifications for angles between +25° and -25°, as can be seen in Figure 22.

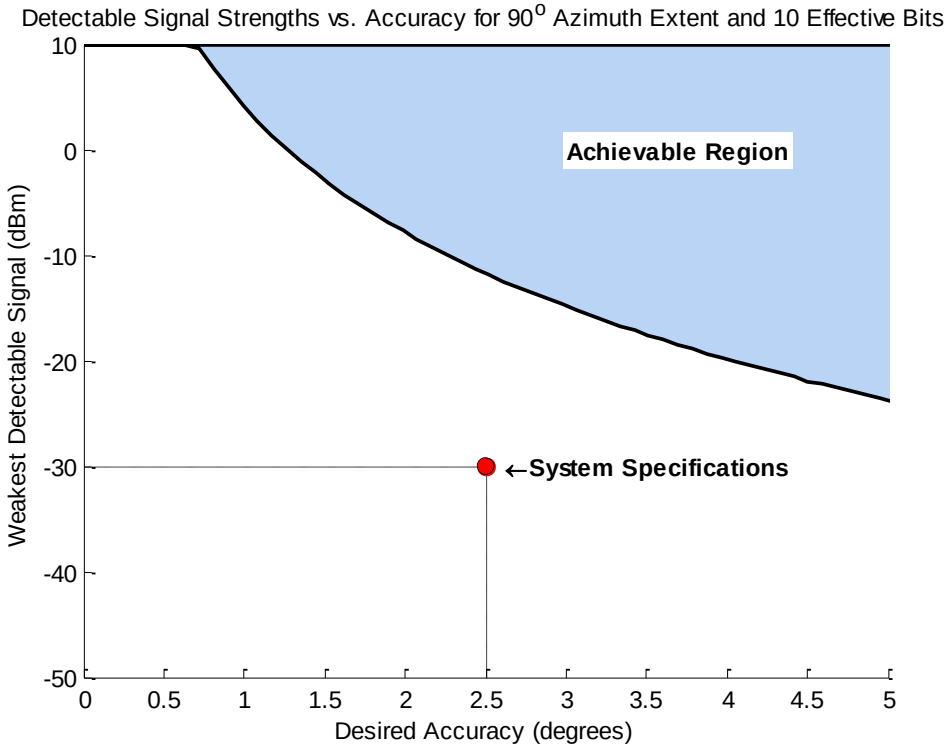

Figure 21. Solid line shows weakest detectable signal with a given accuracy for 90° field of view and 10 effective bits. Marker indicates desired system capabilities of ±2.5° accuracy and 40dB dynamic range. This system represents our current hardware setup.

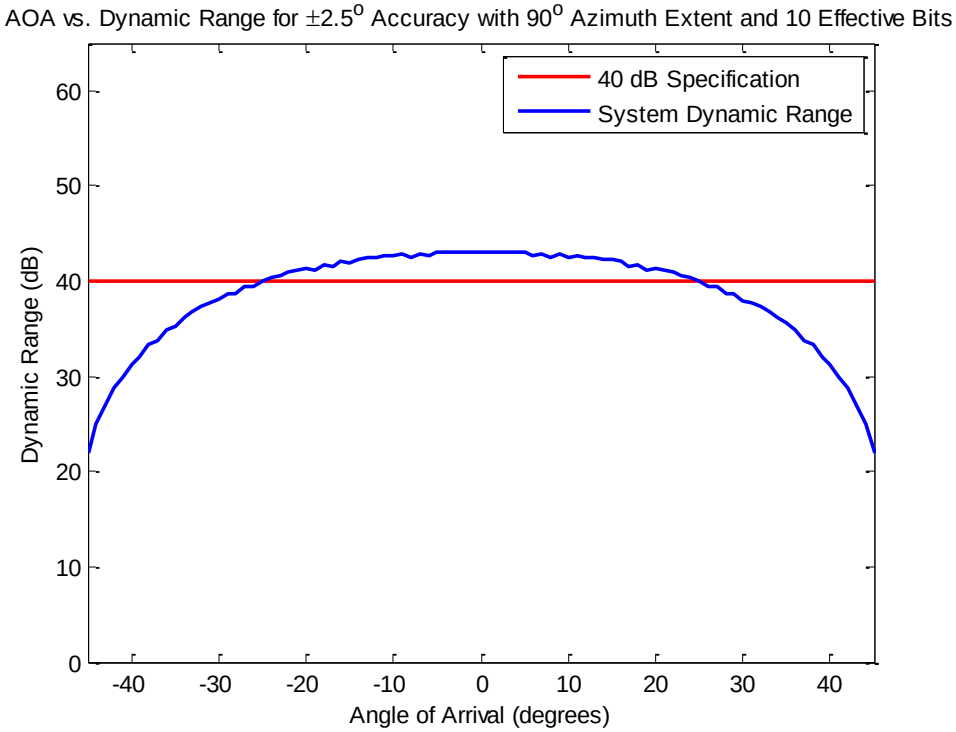

Figure 22. Angle of arrival vs. dynamic range for ±2.5° accuracy with 90° field of view and 10 effective bits. Solid line at 40dB shows the given dynamic range specification.

One method to increase the accuracy of a system at the edges of the field of view is to use antennas with a narrower beamwidth and restrict the field of view of the system. However, this method will require that multiple systems be combined to achieve the desired azimuth extent. The plots in Figures 23 and 24 demonstrate the behavior of a system with a 60° field of view and 10 effective bits. At +30° and -30° in this system, maintaining ±2.5° of accuracy will result in a minimum detectable input power of -38.65dBm and a dynamic range of 48.65dB, which is well within the specifications provided by Lincoln Laboratory. This achievement can be clearly seen by the fact that the red dot is within the blue area in Figure 23. Figure 24 shows that this dynamic range does not fluctuate greatly with angle of arrival and meets the specifications for any angle.

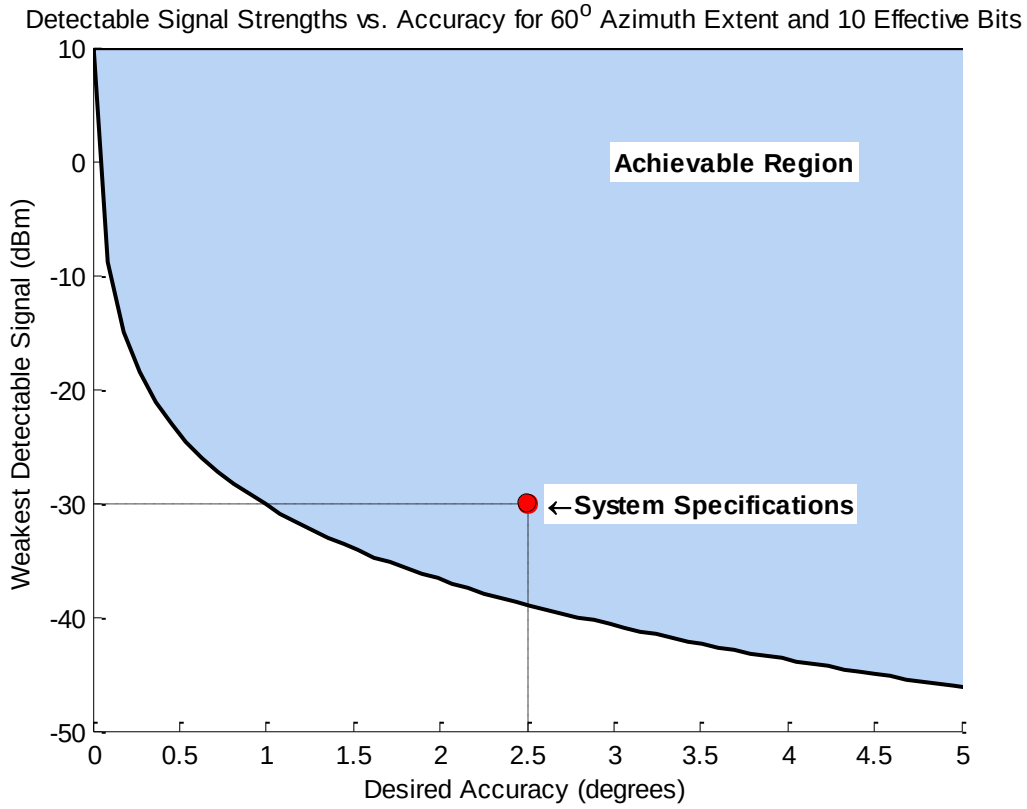

Figure 23. Solid line shows weakest detectable signal with a given accuracy for 60° field of view and 10 effective bits. Marker indicates desired system capabilities of ±2.5° accuracy and 40dB dynamic range.

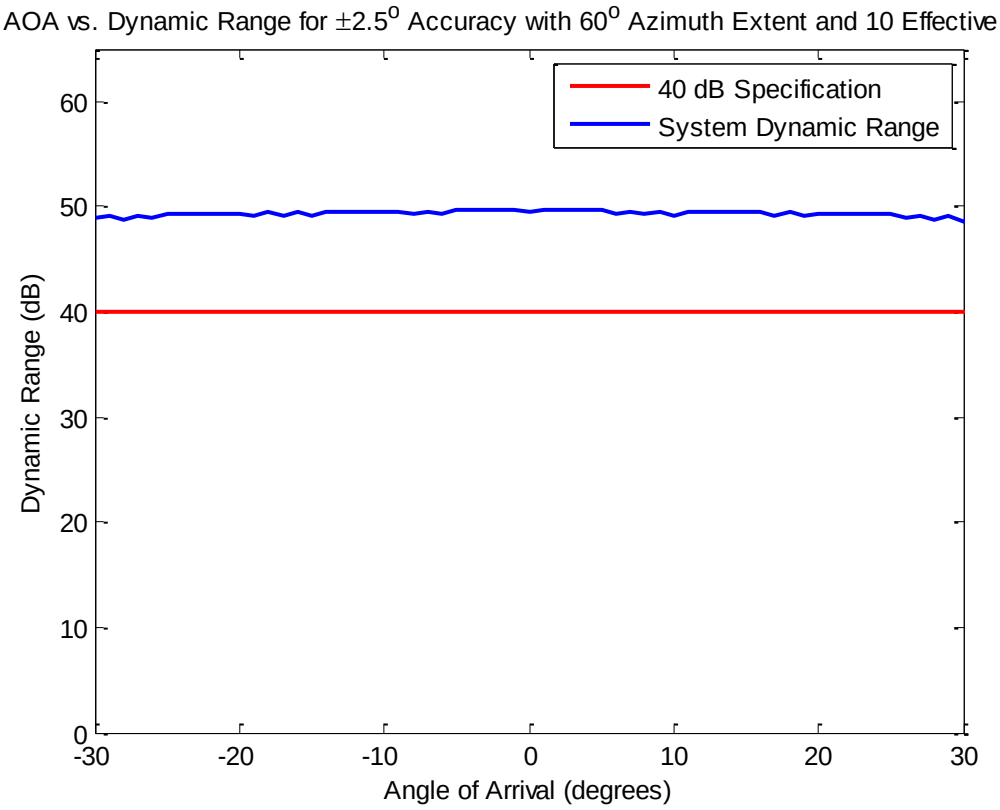

Figure 24. Angle of arrival vs. dynamic range for ±2.5° accuracy with 60° field of view and 10 effective bits. Solid line at 40dB shows the given dynamic range specification.

For the next test, the field of view was maintained at the original 90° and the effective number of bits was increased until the system reached at least 40dB of dynamic range. The resulting plots for 13 effective bits are shown in Figures 25 and 26 below. At -45° and +45° in this system, maintaining ±2.5° of accuracy will result in a minimum detectable input signal power of -29.92dBm and a dynamic range of 39.92dB, which is just below the given specifications. Similar to the first 90° field of view system, the dynamic range varies greatly with angle of arrival. However, due to the increase in the effective number of bits, the dynamic range for the entire system is increased, as can be seen in Figure 26.

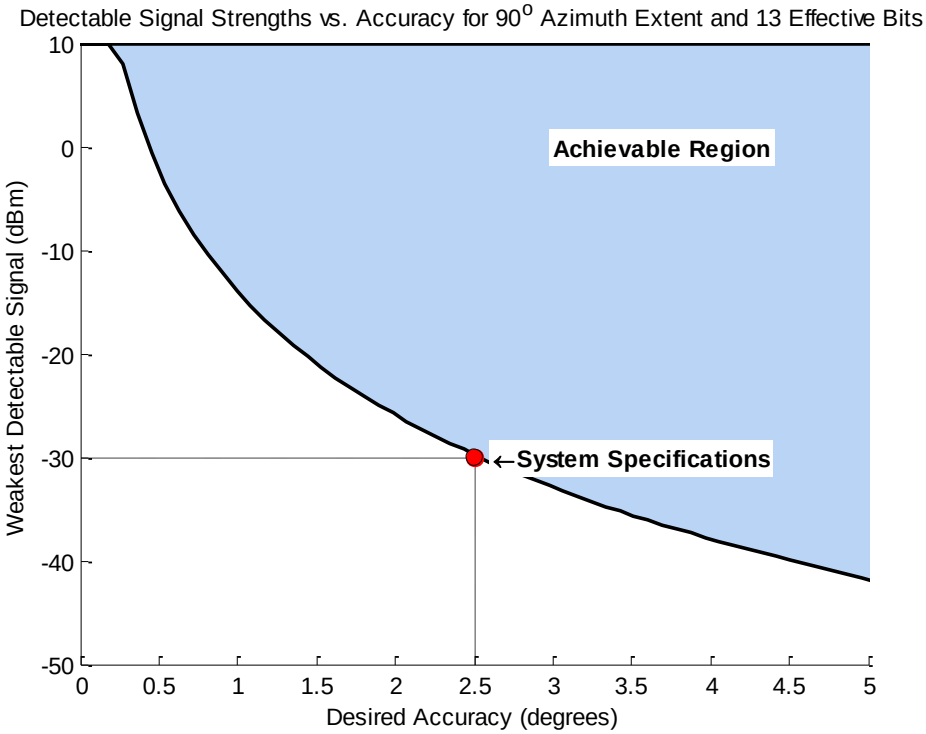

Figure 25. Solid line shows weakest detectable signal with a given accuracy for 90° field of view and 13 effective bits. Marker indicates desired system capabilities of ±2.5° accuracy and 40dB dynamic range

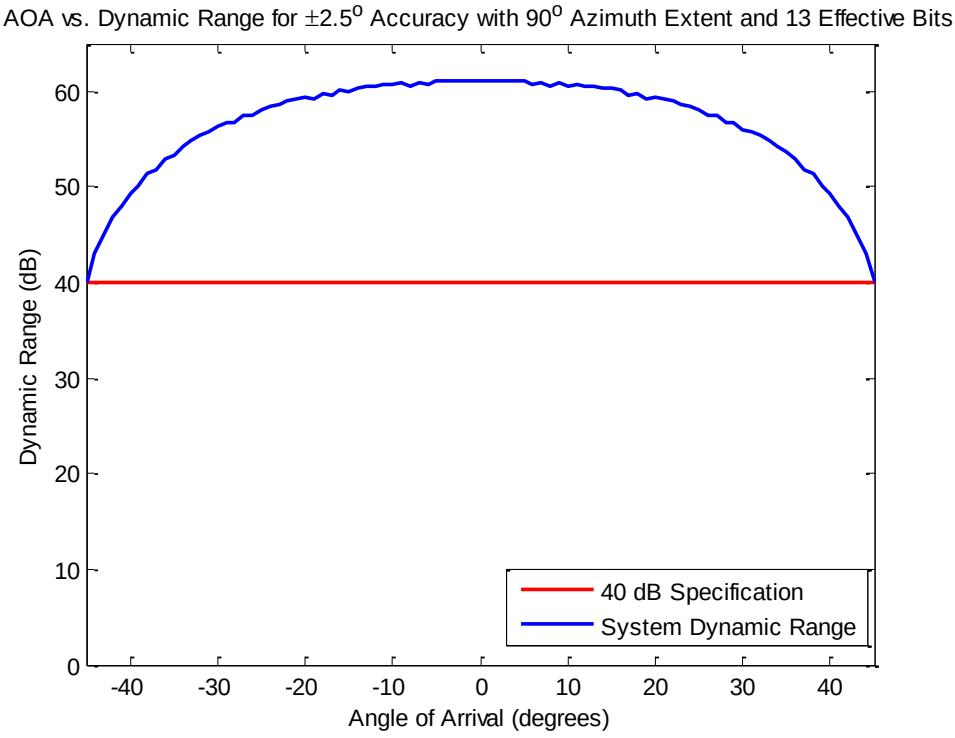

Figure 26. Angle of arrival vs. dynamic range for ±2.5° accuracy with 90° field of view and 13 effective bits. Solid line at 40dB shows the given dynamic range specification.

4. Simulation of Direction Finding Techniques

A major component of our project was to develop simulations of researched direction finding techniques using MATLAB software. The purpose of simulation was to analyze the predicted performance of several techniques in a virtual environment. Our sponsors could use the results of these simulations to determine the feasibility of implementing each direction finding technique in a practical system as well as to measure the theoretical system accuracy. Such information would be of importance to both the hardware portion of this project as well as any continuations of this project work in the future.

Our group attempted to provide simulations as realistic as we could manage, adhering to all specifications required of our prototype system, in order to produce results that could be safely used to estimate practical hardware system performance. To this end, we used a consistent flow of system specifications, signal generation, and algorithm implementation for the simulation of each direction finding technique (see Figure 27). Each simulation considers a user-configured set of parameters to define system specifications and source/receiver geometry. From these parameters, a set of signals are generated that simulate detected intermediate frequency beacon signals from the specified source location, and are used as input to the receivers of the direction finding system. The pulses from the input stream must then be detected and isolated by the system. Finally, each simulation utilizes a technique-specific algorithm to extract information from the detected signals and calculate an angle of arrival.

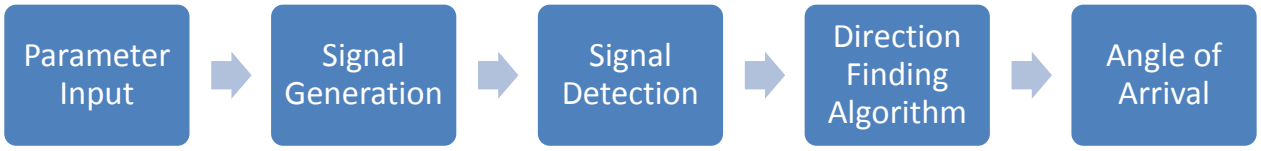

Figure 27. Block diagram of simulation flow. Parameters define a signal, which is then detected by a system and used to perform calculations to find an angle of arrival.

4.1 Parameters and Signal Generation

Initialization of the simulations begins with parameter input and signal generation. Various modifiable parameters are considered which define system specifications, source position, and signal characteristics. Configuration of these parameters allows for desired test scenarios to be created in order to test the system for performance and accuracy. Though each technique may use slightly different parameter sets due to the differences between their system geometries and algorithms, the basic functionality remains the same: the parameters are used to generate a set of signals for the input of the simulated direction finding system. The set of parameters used for simulation and the relevant direction finding methods are given in Table 2 below.

Parameter	Method		
	TDOA	Phase	Amplitude
Intermediate Frequency	●	●	●
Radio Frequency		●	
Received Signal Power	●	●	●
Pulse Width	●	●	●
Pulse Repetition Interval	●	●	●
Angle of Arrival		●	●
Receiver/Source Locations	●		
Distance between Antennas		●	
Sampling Frequency	●	●	●
Time Length / Number of Pulses	●	●	●
Noise Level		●	●
Interpolation Factor	●		

Table 2. Simulation parameters and the direction finding methods that utilize them.

Configuration parameters may be divided into several distinct categories, each serving its own purpose for simulation. The first of these categories is comprised of parameters that define the characteristics of pulsed emitter signals themselves, independent of system geometry. These parameters include intermediate frequency, radio frequency, received signal power, pulse width and pulse repetition interval. Such parameters define the characteristics of the signal as they are received by the system. As the direction finding device must be capable of operating on many types of received signals as defined by our sponsor, inclusion of these parameters allows the algorithm to be tested with a variety of input signals to ensure specifications are met.

The second category defines the overall system geometry and includes angle of arrival, receiver/source locations, and distance between antennas (see Figure 28). These parameters define the placement of the receiver system and the signal source, and determine the angle of arrival of the received signals. System geometry induces differences between signals recorded at different receivers, such as different arrival times due to different receiver distances or

different signal amplitudes due to intersection at different points on the antennas' beam patterns.

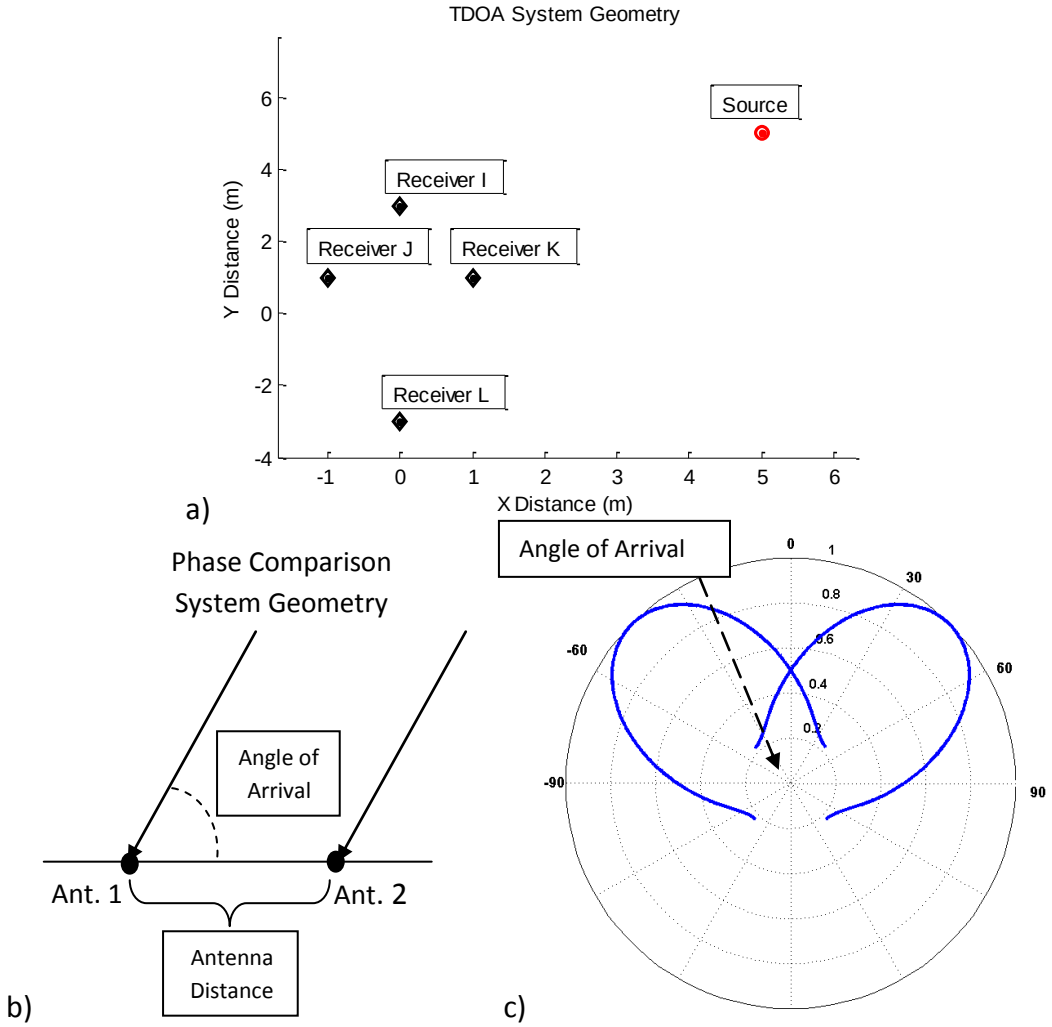

Figure 28. System geometries of the direction finding simulations: a) TDOA, showing the locations of four omnidirectional antennas b) Phase, showing the relative locations of two omnidirectional antennas c) Amplitude, showing the azimuth planar projections of the 45° overlapping beam patterns for two directional antennas.

The third and final category is comprised of system specifications and includes the remaining parameters: sampling frequency, time length or number of pulses, noise level, and interpolation factor. The values of these parameters are determined by the capabilities and specifications of the receivers and the direction finding hardware. A more realistic simulation of the system and its resulting accuracy can be made by incorporating such hardware capabilities as simulation parameters.

From these parameters, sets of input signals were generated. Each receiver was given its own signal set according to the parameter values defined within each simulation. At this point, signal detection began to isolate the portions of the input containing received pulses.

4.2 Signal Detection

After the input signals have been generated, the simulations must identify the portions of the input containing transmitted pulses. The ability to differentiate between transmitted signals and noise is an essential part of all radar systems and is frequently performed by a subsystem known as the signal detector. A common type of signal detector used in many receiver systems is the Cell Averaging Constant-False-Alarm Rate detector, or CA CFAR, as shown in Figure 29 below. [Skolnik, 2001] These systems measure the power of the input signal at each discrete sample and compare that value to an adaptive threshold value based on the noise level of the signal. If the power of the test sample exceeds the threshold, the signal detector will indicate that a signal is present. An outline of these calculations as performed on a single test sample is shown in Figure 29. The power at a test sample, or test cell, shown in red, is calculated using the in-phase and quadrature components of the signal. A threshold value can then be calculated from the average power of a series of reference cells, shown in green, before and after the test cell. In order to avoid contaminating the threshold calculations with samples where a signal is present, guard cells, shown in blue, are placed between the test cell and each reference cell. The guard cells cause the threshold calculations to ignore one pulse width of samples before and after the test cell, meaning that if a received pulse is present at the test cell, the pulse will not be mistaken for noise in the threshold calculations. After the average power of the reference cells is multiplied by a constant k to obtain the threshold value, the test cell power is compared to the threshold to determine if a signal is present.

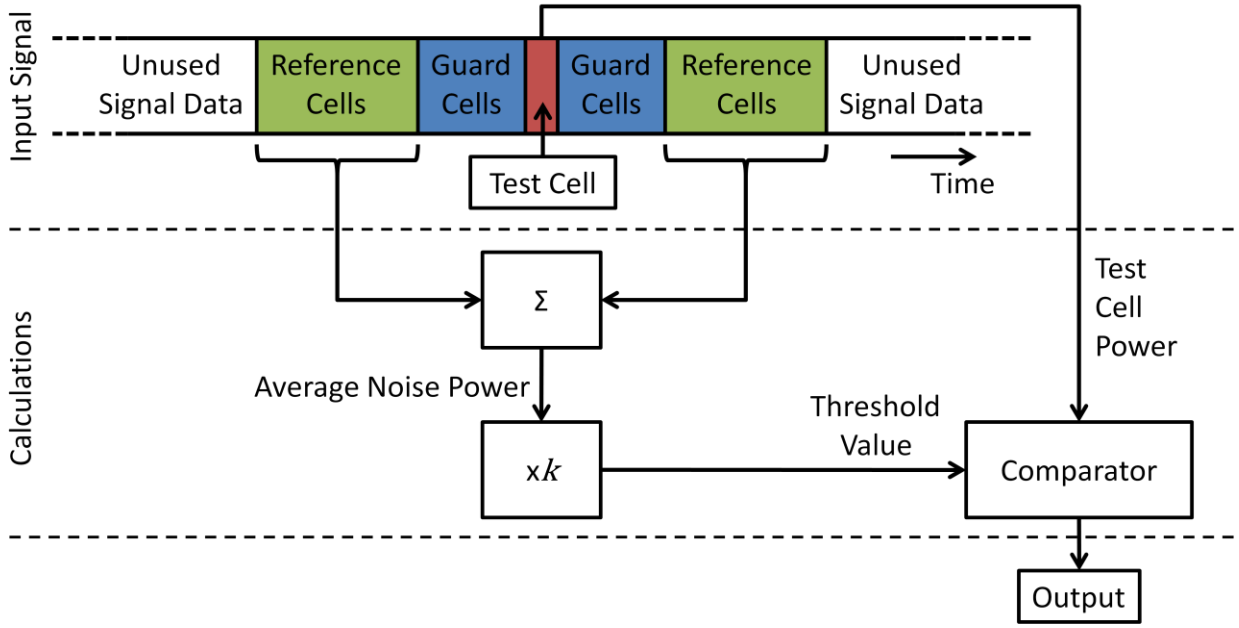

Figure 29. Diagram of a cell averaging constant-false-alarm rate (CA CFAR) detector performing calculations on a single test cell

Our MATLAB simulations can implement either one of two signal detection methods: a constant threshold detector, or a rudimentary CFAR using a moving average. With the constant threshold method, a single value is chosen at the start of the simulation as the noise threshold and is not changed to accommodate changes in noise level. The power level at each sample in the input signal is then compared to the threshold to identify the location of each pulse. The rudimentary CFAR essentially uses half of the CFAR method, only observing prior cells for reference calculations. The detector ignores a specified number of samples (currently 200 samples, which is just under 1 μs, the shortest expected pulse width) before the test cell as guard cells, then averages the next set of samples after the guard cells and multiplies the result by a constant k (currently 10, a value obtained through trial and error) to obtain a threshold value. The CFAR method requires significantly more calculations than the constant threshold method; however, the CFAR detector can also adapt to changing noise levels, whereas the constant threshold cannot. Since our simulations do not include variations in noise level, the constant threshold method of signal detection is sufficient for our purposes and was implemented in the simulations. Each method produces a binary vector that contains a value of 1 where the input signal exceeds the threshold value, indicating the presence of a pulse, and a 0 otherwise. This result can be seen graphically in Figure 30 below, where the binary output vector from the rudimentary CFAR signal detector is shown above the input signal being analyzed. In this diagram the detector measures the start of the pulse to within 1 sample and indicates the end of the pulse after approximately 230 samples to avoid including noise in later calculations. With the start and end time of the radar pulse known, the signal detector isolates the pulse samples and passes them to the next subsystem, where they are processed and the angle of arrival information calculated.

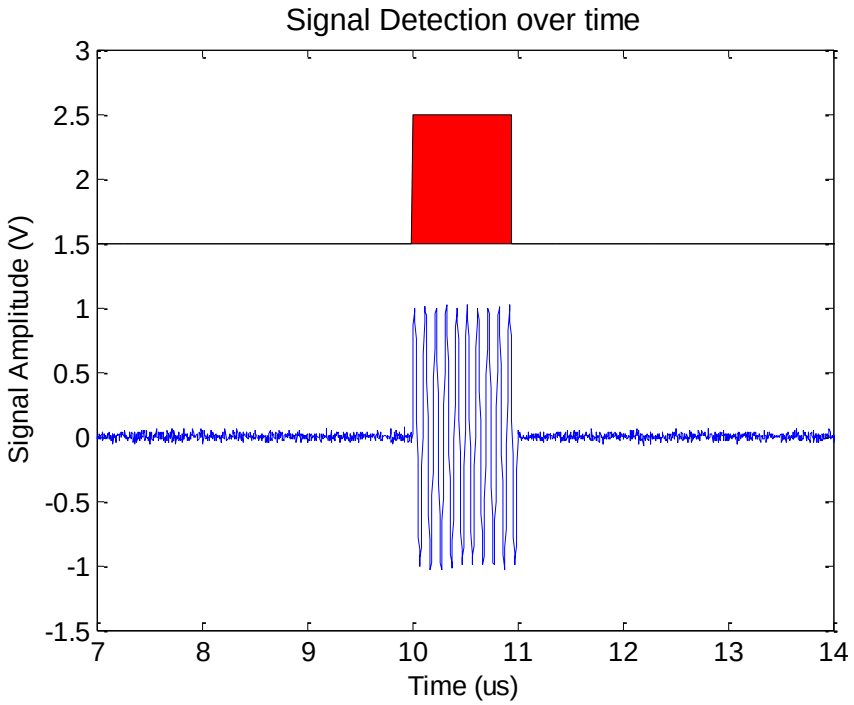

Figure 30. Overlay of the in-phase portion of an input signal (bottom) and output binary vector (top) for the rudimentary CFAR signal detector. The red area in the top plot indicates samples where a signal is detected.

4.3 Signal Processing

Once simulated radar beacon signals and signal detection information are generated for each receiver in a system, signal processing may begin to calculate the angle of arrival or source position. Each method handles this signal processing portion of the algorithm differently, depending on which signal characteristics are incorporated into calculations. In addition, each method requires a few of its own specific parameters in order to function. As such, though the initial portions of each simulation perform nearly the same functions, the latter portions deviate due to algorithm specifics.

4.3.1 TDOA Position Locating

The TDOA system simulation utilizes an existing algorithm from Bucher and Misra [2002] which calculates source position in 3D space from four TDOAs. The algorithm is a deterministic calculation of source location coordinates through the intersection of hyperboloids. Four receivers are required for this algorithm both to measure the four TDOAs and to perform coordinate calculations. As such, four different time delays are used as input to the algorithm. Signal processing for TDOA position is performed in three stages: input signal interpolation, cross-correlation between interpolated signals to determine TDOAs, and position location via the Bucher and Misra algorithm utilizing TDOAs and receiver coordinates (see Figure 31).

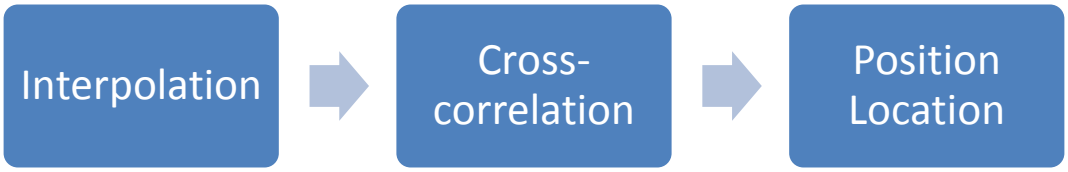

Figure 31. Block diagram of TDOA simulation processing. Input signals are interpolated for better resolution, then cross-correlated to determine TDOAs. An existing algorithm is used to calculate a location from the TDOAs and receiver locations.

Signal processing for this simulation begins with up-sampling of the input signals. Up-sampling increases the effective sampling rate used for calculation. Accuracy in determining the TDOAs could possibly be increased through such a method. The four input signals are up-sampled using both MATLAB's *interp* function with the interpolation factor specified as a simulation parameter. These signals are then used to calculate TDOAs.

Calculation of TDOAs in practical systems is performed through cross-correlations between input signals from pairs of antennas. Cross-correlation involves "sliding" two signals across each other and at each point calculating a value representative of how well the signals match. This value is calculated by multiplying the aligned samples of the two signals and summing the products. Figure 32 illustrates an example of two signals identical outside of a time delay and their cross-correlation results. The number of shifts that yields the peak output of the cross-correlation is the time delay between the two signals. By performing cross-correlations for four pairs of receivers (for the Bucher and Misra algorithm, using pairs 1-2, 1-3, 3-2, and 3-4), the four TDOAs necessary for position location can be calculated.

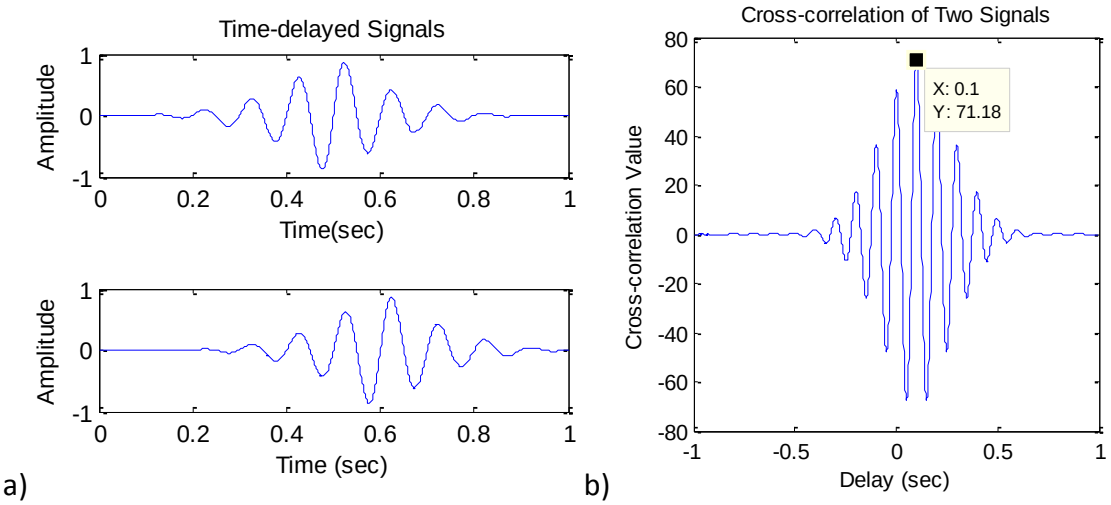

Figure 32. a) Two signals delayed in time by 1/10 second. b) Cross-correlation of the two signals. Peak cross-correlation output occurs at 1/10 second.

From the four TDOAs, the Bucher and Misra algorithm calculates positional data for the signal source location. It calculates sets of hyperboloids, finds their intersections, and extracts

numerical data for the coordinates of the source. As the algorithm provides only one hemisphere of unambiguous results, two possible locations are produced at the output: the source location, and an erroneous result. In a real application, this ambiguity could be resolved by including additional receivers and TDOA systems to use them, then comparing results between systems to determine the location at which the results converge. To simplify calculations of simulation accuracy, the correct hemisphere was assumed to have been determined, and the erroneous result was discarded. We calculated the distance between the simulation output and the real source location to determine the accuracy of the results. In addition, we also calculated an angle for the output location to better compare this simulation to the others.

4.3.2 Phase Comparison

Signal processing for phase comparison direction finding is comprised of four stages of signal measurement, manipulation and calculation, outlined below in Figure 33. First, a Hilbert filter is used to generate the in-phase and quadrature components of the input signals from the two receiving antennas. Second, these signal components are used to calculate the phase angle of the signals and their resulting phase difference. Third, the change in phase angle over time and the down conversion frequency are used to calculate the radio frequency of the signal. Fourth, the calculated radio frequency is used along with the average phase difference to calculate the angle of arrival.

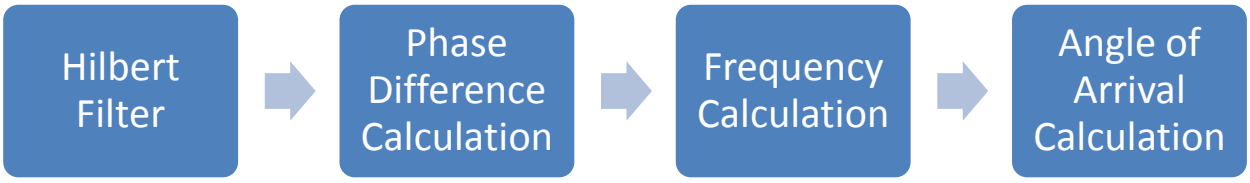

Figure 33. Block diagram of phase comparison direction finding simulation

In the first stage, a Hilbert filter, which introduces a 90° phase shift to a signal while ideally leaving the amplitude unaffected, is used to obtain the in-phase and quadrature components of the input signals. In the phase comparison direction finding method, the in-phase and quadrature components are used to calculate the phase angle at each point in time. The filter itself is a 30^{th} order linear-phase FIR filter designed with the Filter Design and Analysis Tool (*fdatool*) in MATLAB, which uses the Parks-McClellan algorithm. As can been seen in Figure 34 below, the filter has a magnitude response of roughly 0 dB over the normalized bandwidth of 0.05-0.95, which corresponds to 6.25-118.75 MHz at a sampling frequency of 250 MHz. This range covers the bandwidth requirements for the overall design of 12.5-112.5 MHz. Since the Hilbert filter is non-causal and therefore uses "future" data in its calculations, the quadrature output is delayed by half the order of the filter, or 15 samples. This delay is corrected in simulation by removing the first 15 samples from the vector representing the

quadrature component, and the last 15 samples from the vectors representing the in-phase component and elapsed time.

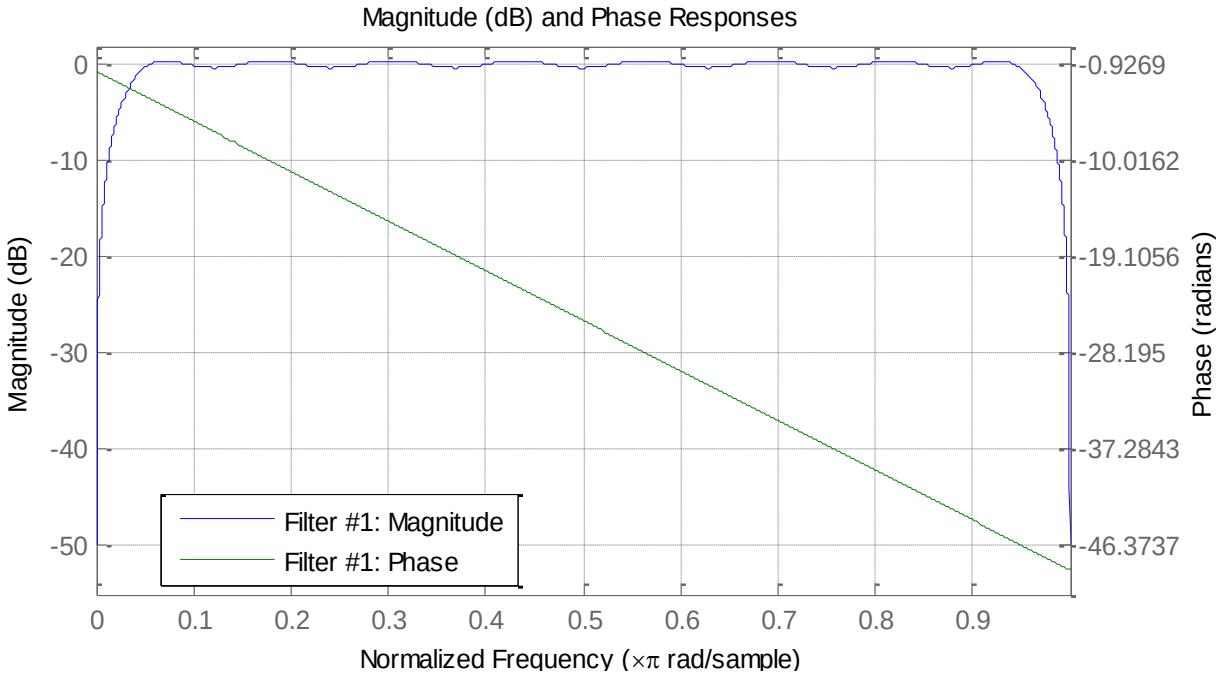

Figure 34. Magnitude response (blue line) and phase response (green line) of Hilbert filter

With the in-phase and quadrature components extracted, the next stage calculates the difference in phase angle between the two input signals over time. Due to the fact that the angle calculation is limited to the range [-π, π], ±2π phase shifts are periodically introduced to the phase difference signal as shown below in Figure 35a. Therefore, the MATLAB script uses a function called *unwrap* to eliminate the phase shifts and produce a smoother signal, as shown in Figure 35b. *Unwrap* iterates through the signal array, checks for differences between samples greater than π, and rectifies these by adding or subtracting multiples of 2π to the sample. Since the angle of arrival, and therefore the difference in phase angle, should not change significantly over the course of the pulse, all of the samples in a pulse can be averaged to obtain a single phase difference measurement and lessen the effect of noise. This averaged phase difference is plotted as a dotted red line in Figure 35 below, which also illustrates the effect of the *unwrap* function on its value. The averaged phase difference is stored and used in later calculations.

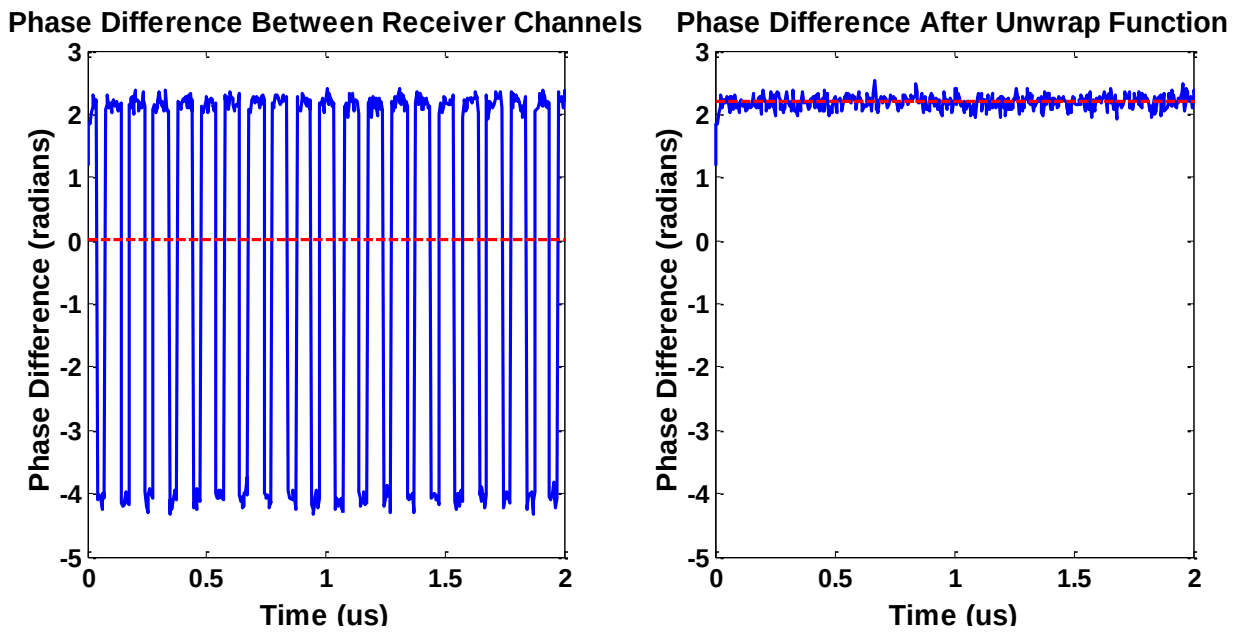

Figure 35. Phase difference between the two receiver channels vs. time (a) before and (b) after the MATLAB *unwrap* function is introduced, with the mean phase difference shown as a dotted red line.

Before the angle of arrival can be calculated from the phase difference between receivers, the DF system must determine the radio frequency at which the signal was transmitted. This frequency is obtained by adding the frequency of the local oscillator (LO) that was used to down-convert the signal with the measured intermediate frequency of the signal. First, the system must obtain the frequency of the LO that was used to convert the signal from the RF to the IF band. In a practical system, this information can be passed to the signal processor by setting up communication between the signal processor and the controller for the LO. For simulation, several variables are set to realistic values that represent settings in the receiver system. Second, the system must measure the frequency of the IF signal. This value can be calculated by measuring the change in phase of the signal over time. The system measures the phase of one receiver channel at a particular start time, and then waits a large number of samples (100 in the simulation) before measuring the phase again, while recording the number of times the phase rotates by 2π radians. Since the sampling rate is known, this measurement will give the system the change in phase over a known time period. Dividing this change in phase in revolutions by the elapsed time will produce the intermediate frequency of the signal, and adding that value to the frequency of the LO will give the radio frequency of the original signal.

Using the phase difference between receivers and the radio frequency of the transmitted signal, the system can calculate the angle of arrival. Equation 11, shown below, is used for this calculation, where *AOA* is the angle of arrival in radians, *d* is the distance between antennas in meters, $\Delta\theta$ is the phase difference between antennas in radians, *K* is any integer

value that produces a real solution for *AOA*, *c* is the speed of light in meters per second, and *f* is the radio frequency of the signal in Hertz. Evaluating Equation 11 with a *K* value of zero will provide one solution for the angle of arrival; however, due to the periodic nature of radar signals, there are often multiple possible angles of arrival for a given phase difference. These additional solutions are found by increasing and decreasing the value of *K* until Equation 11 produces solutions for cos(*AOA*) outside of [-1, 1], the range of the cosine function. Any of the angles calculated in this way could be the correct value for the angle of arrival. The phase method requires additional systems to remove these ambiguous solutions as discussed in section 4.6.2 Analysis of Phase Comparison Direction Finding.

$$\cos(AOA) = \frac{1}{d} * \left(\frac{\Delta\theta}{2\pi} + K\right) * \frac{c}{f}$$

Equation 11

4.3.3 Amplitude Comparison Method

The amplitude comparison direction finding algorithm designed for use in the project utilizes two receiving antennas to calculate the angle of arrival with one degree of freedom of an incoming signal. After the transmitted signal has been detected at both receivers, the voltage magnitude of the signal is measured at each receiver in order to compute the ratio of received powers. This ratio is then used to determine the angle of arrival of the incoming signal. The process used to implement amplitude comparison direction finding in simulation is illustrated in Figure 36 below. Sampled IF signals from each antenna are passed through Hilbert filters to extract the in-phase and quadrature components, from which the instantaneous voltage magnitudes can be calculated. The power ratio is then calculated and used to index into a lookup table of angles of arrival.

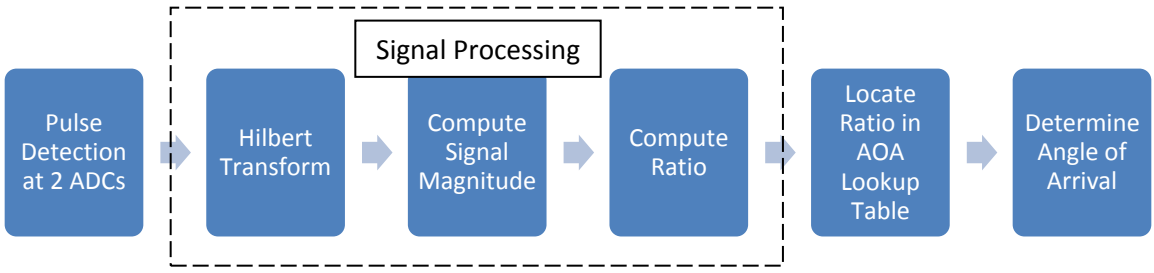

Figure 36. Block diagram of the algorithm for using amplitude comparison to determine angle of arrival.

The basis of the amplitude comparison algorithm involves computation of a ratio of magnitudes derived from the signals detected at each antenna. In order to determine the magnitude of the received signals, and eventually compute the ratio, a series of manipulations

must be performed on the detected signals. These manipulations can be simulated through the employment of predefined MATLAB functions and basic mathematical operations.

The first block of signal processing involves using a Hilbert filter to generate the quadrature component of the received signals. The functionality of the Hilbert filter is identical to that described in the algorithm for phase comparison direction finding: it produces a signal that is ideally identical to the original signal in terms of amplitude and frequency, but is shifted 90° out of phase from the original signal. For the amplitude comparison algorithm, the in-phase and quadrature components are used to calculate the magnitude of the received signals. The quadrature component of the signal is generated in simulation through the creation of a Hilbert filter using MATLAB's filter design and analysis tool, as described in the phase comparison section (4.2.3). Through the use of this filter, the algorithm generates the quadrature component of the in-phase signal as sampled by the ADC. The in-phase and quadrature components of two example signals are shown in Figure 37, below.

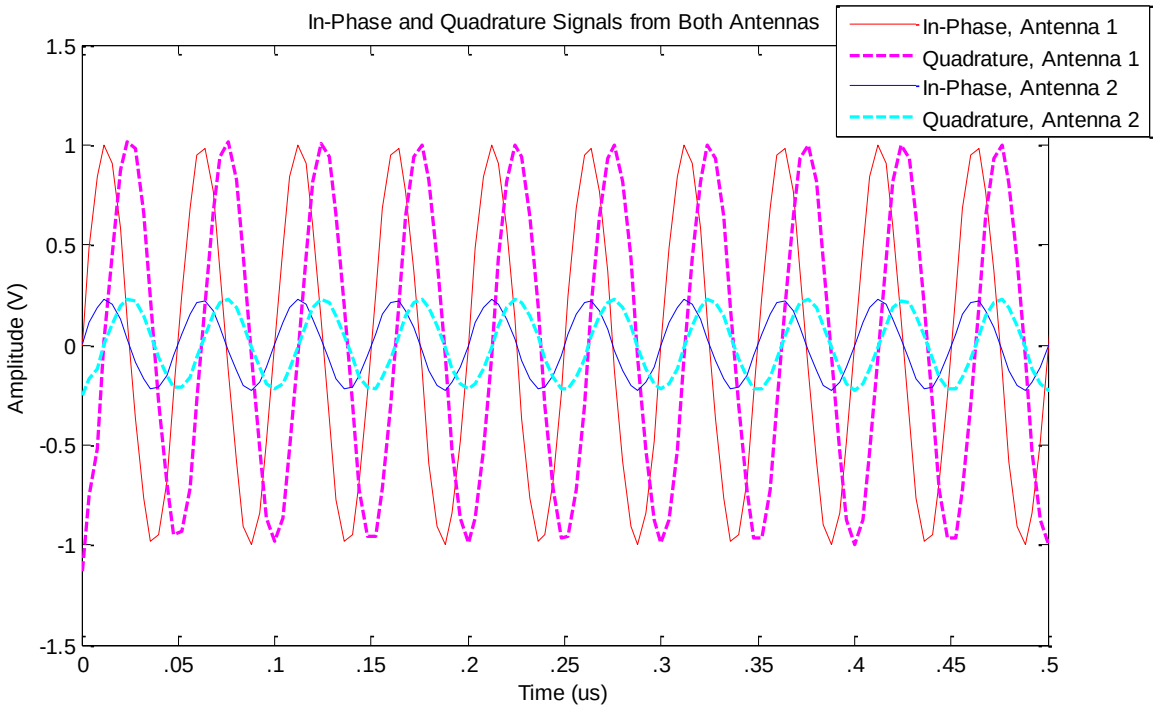

Figure 37. In-phase and quadrature components created through a Hilbert transform of two signals in MATLAB. The signals with greater amplitude are from Antenna 1, and the smaller signals are from Antenna 2.

The in-phase and quadrature components are then used to evaluate the voltage magnitude of the signal from each of the ADC channels. The instantaneous voltage magnitude can be computed from the equation $|V[n]| = \sqrt{I[n]^2 + Q[n]^2}$, where I and Q are the in-phase and quadrature signals, $|V|$ is the voltage magnitude, and n is the sample index. For a signal with no noise distortion, the resulting voltage magnitude is a constant value for all samples

containing transmitted data. The fact that the voltage magnitude is constant allows for simple comparison of the two signals, as opposed to the periodic nature of the voltages measured at the ADC which change with time.

Computation of the true voltage magnitude involves the square-root function, which is difficult to implement in hardware and time-consuming to process. However, since the amplitude comparison method for direction finding involves taking a ratio of power levels, this operation can be avoided. Power (P) is proportional to voltage (V^2), as stated in the equation $P = \frac{V^2}{R}$, where R represents a value of resistance. Therefore, a ratio of power levels is equivalent to a ratio of squared voltage magnitudes, where $\frac{P_1}{P_2} \sim \frac{V_1^2}{V_2^2}$. Thus, the ratio can be computed by dividing the squared voltage magnitudes of the two signals (Figure 38). Our simulation includes noise that is representative of the noise present in our hardware, as shown in the red and blue signal magnitudes in Figure 38. A continuous ratio computed over the transmitted signal will result in varying ratio values that fluctuate with respect to the noise on the channels, as shown in Figure 38 by the magenta waveform. Therefore, to accurately determine the ratio of voltage magnitudes as a constant value, our algorithm must first include calculation of the average of the magnitudes at each antenna. These averages can then be used to calculate the constant ratio of voltage magnitudes at the two antennas that is characteristic of a particular angle of arrival.

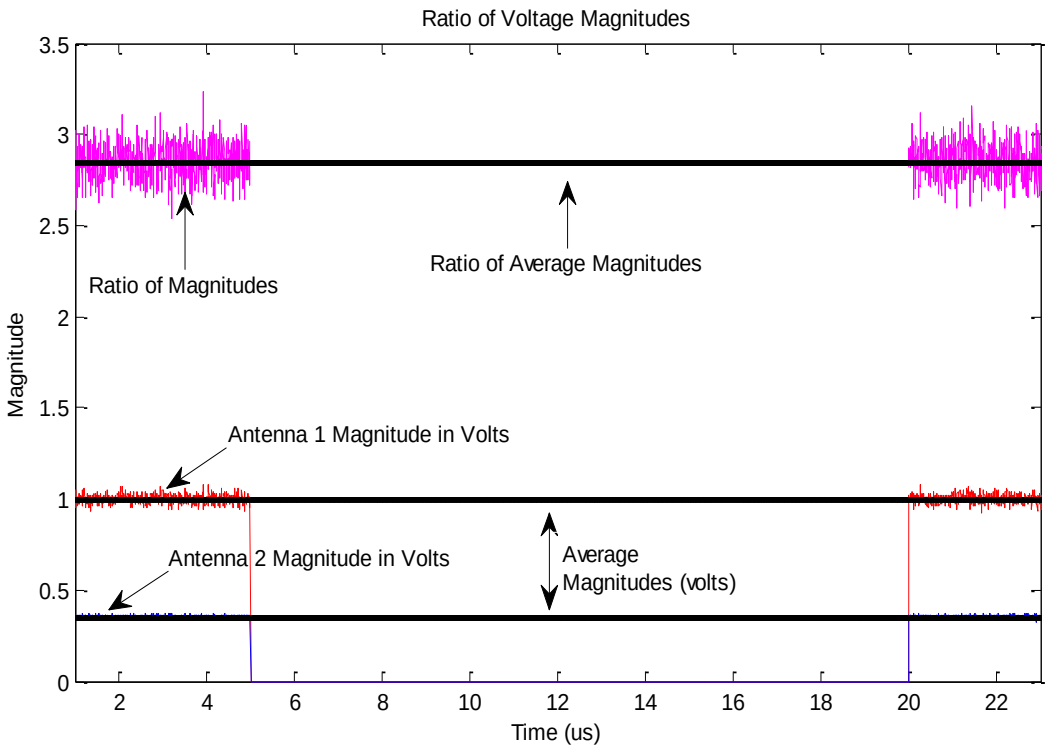

Figure 38. The ratio of voltage magnitudes can be calculated by dividing the larger magnitude by the smaller. This figure shows the voltage magnitude of Antenna 1 divided by the voltage magnitude of Antenna 2, resulting in an average ratio of 2.84 for times when the signal is on.

After calculating the average squared voltage magnitude of each of the respective pulsed signals, the ratio computation is performed by dividing the larger magnitude by the smaller. The purpose of dividing the larger voltage magnitude by the smaller is to obtain a resulting ratio greater than 1 over the entire azimuth extent. As shown in Figure 39, the calculated ratios range from a ratio of 1 when the target is located directly between the receivers to a ratio slightly less than 4.5 for a target that is located at either ±45° from the central median of the antenna array, or close to the boresight of one of the two antennas. Our method of dividing the larger voltage magnitude by the smaller reduces the necessary data resolution that arises from the fact that the ratio of a smaller value to a larger value always results in a ratio between 0 and 1. For example, over the azimuth range of -45° to 0° from the median of the antenna array, all computed ratios would numerically be very close in value, requiring more resolution to discern than ratios between 1 and 4.5. While MATLAB automatically uses floating point values for computation, a floating point implementation in hardware would be difficult to achieve and slow to process. Using fixed point values would limit our calculations to rounded ratio values that could result in erroneous angle of arrival determinations if the number of bits used to represent each number is too small. However, while using more bits to represent ratio values would improve accuracy, it would also increase

memory requirements and potentially slow processing speed. Therefore, our system uses the larger-to-smaller ratio calculations to increase the accuracy of the output as well as processing speed by reducing the number of decimal places necessary for accurate calculations of ratio.

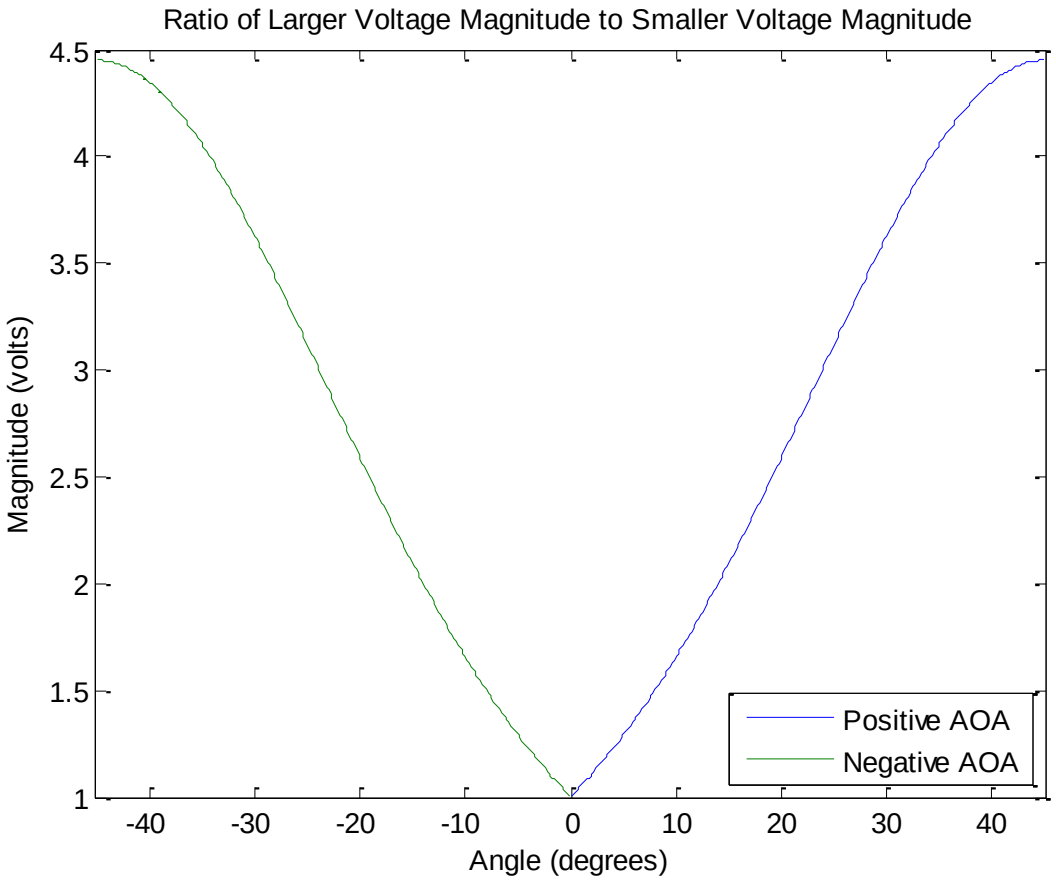

Figure 39. Symmetric ratio of voltage magnitudes achieved by dividing the larger magnitude by the smaller magnitude. Positive and negative angle of arrival is determined by identifying the signal with the larger magnitude.

The use of larger-to-smaller ratio calculations allows our system, both in simulation and in hardware, to perform ratio magnitude calculations more quickly and with greater accuracy than, for example, a calculation of the ratio of values from the right antenna to the left antenna over the 90° extent. However, this approach introduces an ambiguity of whether the signal arrived from an angle that was displaced positively or negatively from the central median of the antenna receiver system. This ambiguity can be resolved by the property of directional antennas that states a signal will induce a larger voltage magnitude at the antenna whose boresight it is closest to than it will at the antenna whose boresight is angled away from the source emitter. Due to the fact that the antennas are symmetrically displaced from the 0° central median, the plot of angles of arrival generated from computing the larger-to-smaller ratio will be symmetrical to reflect the identical gain characteristics of the two antennas, as

shown in Figure 39. Therefore, while only the half of the plot consisting of positive angles of arrival will be considered for calculation, the sign of the output can be set by determining which antenna has the higher signal gain.

The last block of signal processing in the amplitude comparison algorithm involves determining the angle of arrival of a signal through the employment of a lookup table. A lookup table of ratio values and corresponding angles of arrival between 0 and 45° can be derived from the known ratio pattern shown in Figure 39. The lookup table allows our hardware system to compare the calculated fixed point ratio value with a set of ratio values derived from the known antenna gain pattern. The lookup table for this system can be reduced in size due to the symmetric orientation of the antenna receiver system, and thus the symmetric property of the angle-to-ratio plot (Figure 39). By only using half of this plot, the size of the lookup table to be implemented in hardware is halved, allowing for significantly less memory to be used to achieve the required resolution than if we had included a lookup table for the full 90° extent.

4.4 Test Procedures

Software simulations of our system were tested for functionality through a variety of different methods. The tests we performed were designed to test the accuracy of each system for radar beacons varying in position over azimuth extent. Accuracies for the output of each system were recorded to determine how well the systems could meet our given project specifications.

To ensure that the results of our tests represented realistic system functionality as closely as possible, the antenna receiver geometry of each of the three systems was formatted to adhere to the specification for implementation on an airborne platform. The four antennas for TDOA were chosen to be located roughly on the nose, tail, and wings of an aircraft with 6m separating the receivers on the nose and tail, and 2m separating the receivers located on the wings. The two antennas required for phase comparison direction finding were chosen to be located 10cm apart to represent a realistic distance for implementation using omnidirectional antennas that are roughly the size of the horn antennas specified for this project. The two antennas used in the amplitude comparison method were chosen to be located adjacent to each other and offset from each other by 90° such that their 3dB points intersect.

In order to effectively compare the systems' accuracies, the three direction finding systems simulated the detection of the same distinct radar beacon. The beacon used for initial simulation exhibited 20MHz frequency, 5µs pulse width, 20µs pulse repetition interval, and 1mV (10dBm) amplitude as detected at the ADC to represent a nominal pulsed radar signal at an intermediate frequency that would be processed by our designed systems. The signals used for simulation also displayed properties determined by our hardware system, such as noise and sampling frequency. The noise on the signals was modeled through MATLAB's "add white

Gaussian noise" function, which overlays normally distributed white noise over the pulsed signal with a specified signal to noise ratio of 60dB to represent appropriate noise acquired through signal amplification in a radar system's front-end. All three simulations also used a 250MHz sampling frequency as specified by the clock on our development board. These common signal characteristics allowed our group to compare the results these tests for the three simulated direction finding methods.

Our group compared the results of each system for determining angle of arrival for simulated targets over the 90° azimuth extent to measure each system's accuracy for various angles of arrival. Each of the three simulated methods was tested to determine the accuracy of computed angles of arrival for target emitters over the ±45° extent in 0.1° increments to simulate the entire field of view of the system. By analyzing errors in the angle of arrival calculation for each of the three methods, our project group determined the accuracy of each of the methods over various ranges of azimuth extent, determined the limits of each simulation, and investigated ways the simulations could be improved to increase accuracy.

These tests were designed to verify the full functionality of each of the three simulated methods. The ability for each of the three methods to calculate angles of arrival over the full 90° azimuth extent within ±2.5° of accuracy would indicate that our designs met system specifications in simulation. These tests were also designed to identify areas of ambiguity for each of the three systems and to aid us in determining which aspects of the algorithms to modify to improve system accuracy.

4.5 Results

For each of the direction finding method simulations, our group first simulated a system that would be realistic for implementation according to our project specifications, including the capability for implementation on an airborne platform and adhering to all hardware limitations. We then explored modifications that could be made to each system beyond these specifications that could improve the accuracy of angle calculations.

4.5.1 Results of TDOA Simulation

The accuracy of the TDOA direction finding simulation is affected both by the distance between receivers and the sampling frequency used to measure detected signals. While retaining a receiver array geometry capable of implementation on an airborne platform, our project group determined the accuracy of the system using simulated noise levels characteristic of our design board with 10 effective ADC bits and a 250 MHz sampling frequency set by the resolution of our ADCs to simulate the accuracy of this system if it were to be implemented in our hardware (Figure 40). We also investigated the accuracy of this system geometry without the introduction of noise. Figure 41 shows that the effect of noise on the accuracy of angle calculations is negligible. However, the TDOA algorithm cannot resolve angles near the

boresight of the system as a result of a fault in the position location algorithm for closely spaced receiver geometries [Bucher and Misra, 2000]. The algorithm relies on the intersection of hyperboloids at a point to determine emitter position. With our chosen geometry, the algorithm resolves planes of possible sources locations along the X and Y axes instead of finding a point of intersection of hyperboloids. These planes exist at points equidistant from two receivers, where the time of arrival would be equivalent, and thus result in a TDOA of zero for all source positions on the plane. The algorithm cannot compare TDOAs of multiple sets of receivers when the emitter is equidistant from any of the receiver pairs because it encounters an error when dividing by zero, and therefore cannot resolve a source position. While retaining our receiver geometry selected for implementation on an airborne platform, this algorithm cannot resolve angles of arrival between ±5.1° using a sampling frequency of 250 MHz.

Figures 40-46 show the accuracy of angle calculations from the TDOA algorithm while varying select system parameters. These accuracies were determined by running the algorithm over the full 90° extent, and taking the difference between the calculated and expected angles of arrival. For example, Figure 40 shows the accuracy of angle calculations for the TDOA algorithm at a 250 MHz sampling frequency. In this example, the angle calculations at -25°, -13°, 13°, and 25° were the most accurate with only 0.02° error between the calculated and expected angle values, while angle calculations at -35°, -20°, 20°, and 35° were the least accurate. Figure 41 shows the same system with noise removed from the signals.

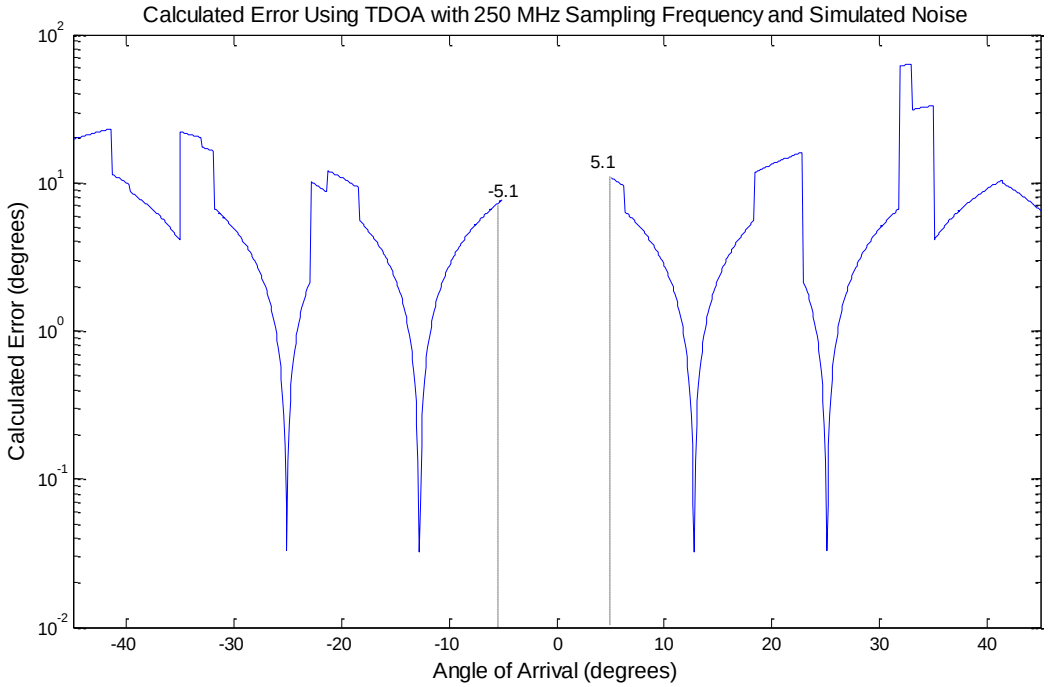

Figure 40. Error of calculations using TDOA direction finding with noise on the system to imitate our hardware and 250 MHz sampling frequency.

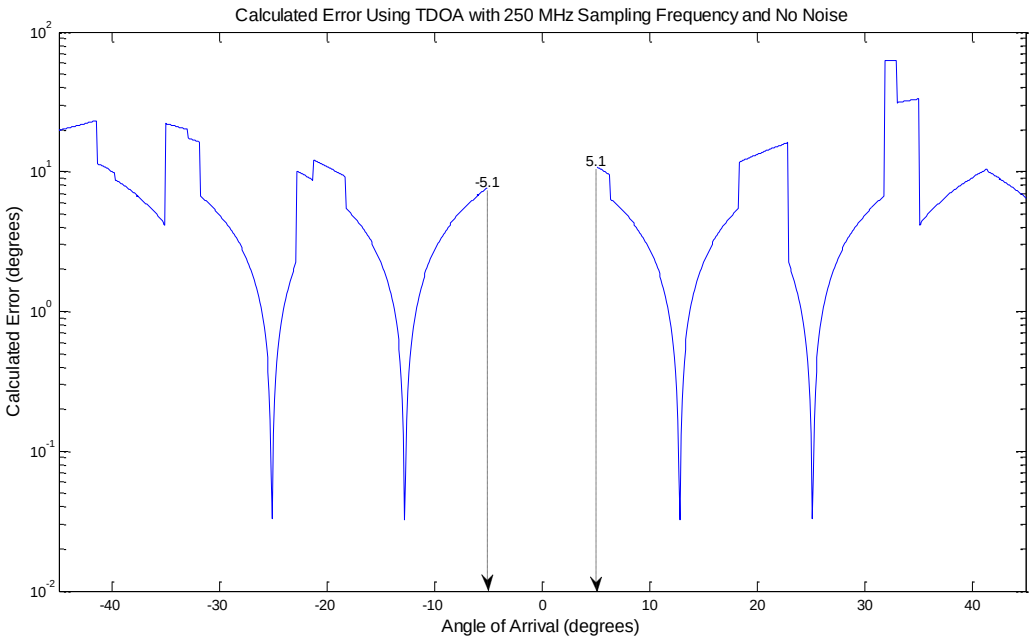

Figure 41. Error of calculations using TDOA direction finding with 250 MHz sampling frequency and no noise on the signals.

Our group then explored the impact of increasing the sampling frequency to 500 MHz and 750 MHz to determine if increasing the sampling frequency within the megahertz range would result in any significant improvement in the accuracy of the system. Figure 42 shows the errors calculated using the TDOA method with a sampling frequency of 500 MHz. This system is able to resolve angle calculations closer to the boresight of the system than the example using a sampling frequency of 250 MHz, though for some angles of arrival, such as around -35°, there is a significantly higher degree of error in calculations. Figure 43 shows the calculated error for the same TDOA system operating with a sampling frequency of 750 MHz. This system shows the greatest calculated errors around ±30°, and is only able to resolve angles greater than ±5.1° from the boresight of the system. This system also shows high error calculations around ±25°, whereas the system at 250 MHz was extremely accurate at these angles.

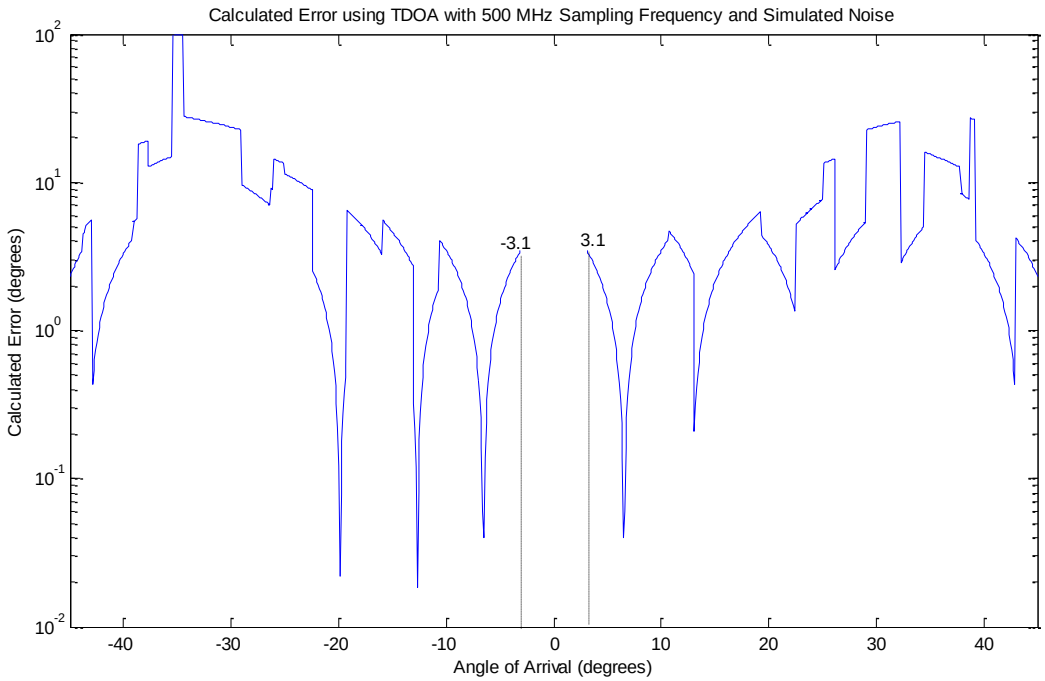

Figure 42. Error of calculations using TDOA direction finding with 500 MHz sampling frequency and simulated noise.

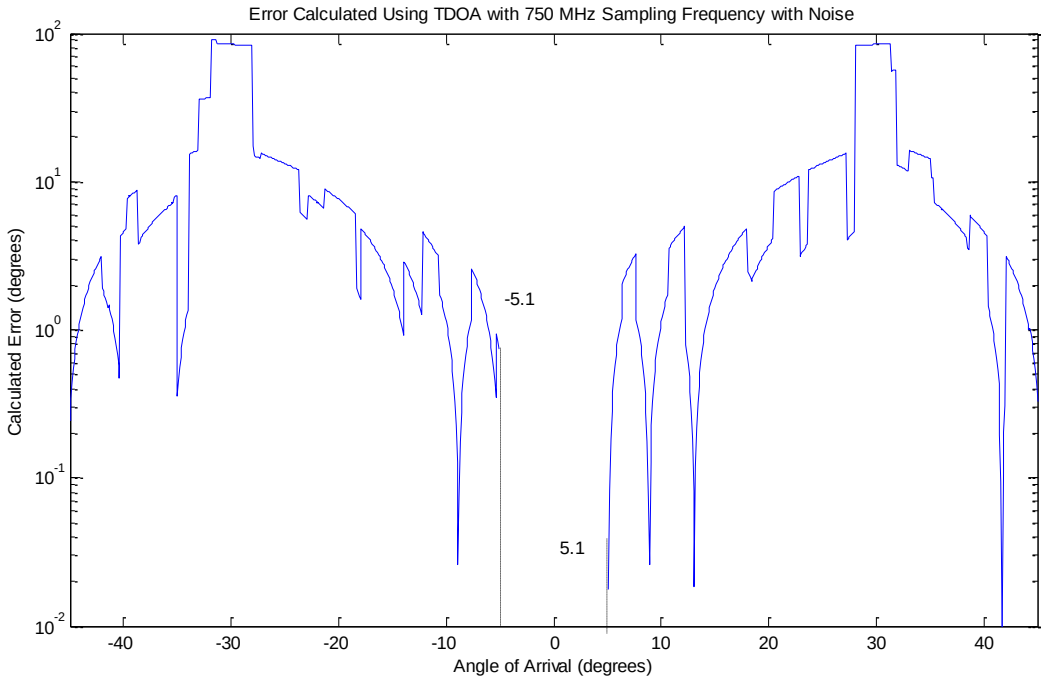

Figure 43. Error of calculations using TDOA direction finding with 750 MHz sampling frequency and simulated noise.

We then explored the impact of increasing the simulated ADC sampling frequency to 2.5 GHz, 25 GHz and 250 GHz. These calculations were also performed using an interpolation factor of 2. The resultant errors of angle of arrival calculations with these sampling frequencies are shown in Figure 44-Figure 46. As the sampling frequency increases from 2.5 GHz to 250 GHz, the simulation is able to resolve angles of arrival closer to the boresight of our system.

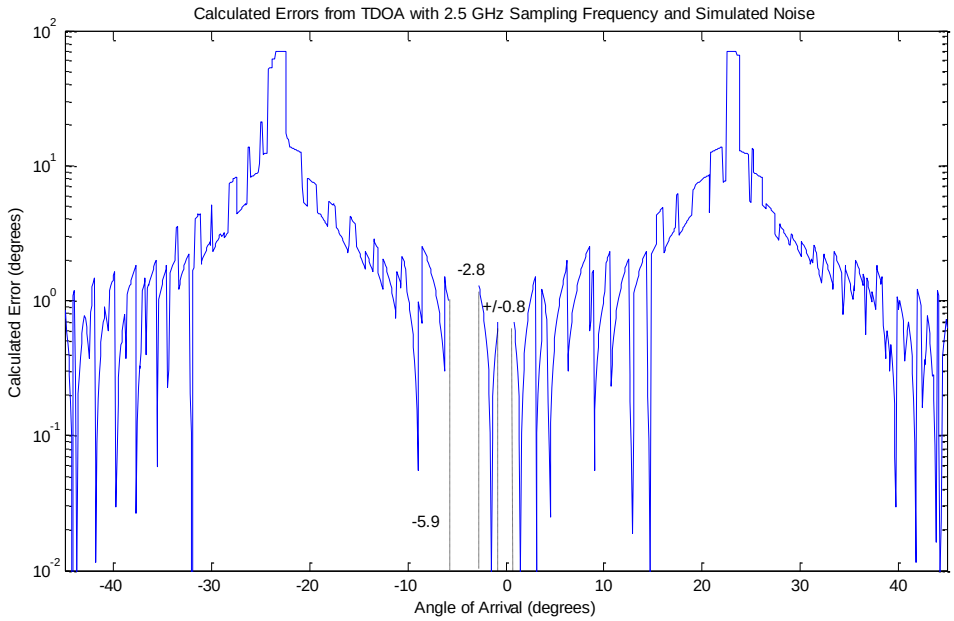

Figure 44. Error of calculations using TDOA direction finding with 2.5 GHz sampling frequency and simulated noise.

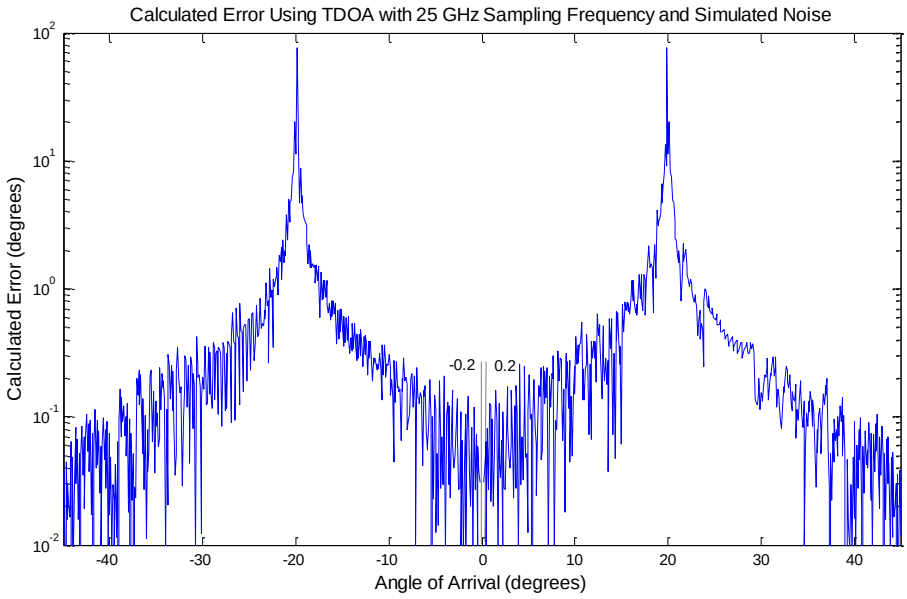

Figure 45. Error of calculations using TDOA direction finding with 25 GHz sampling frequency and simulated noise.

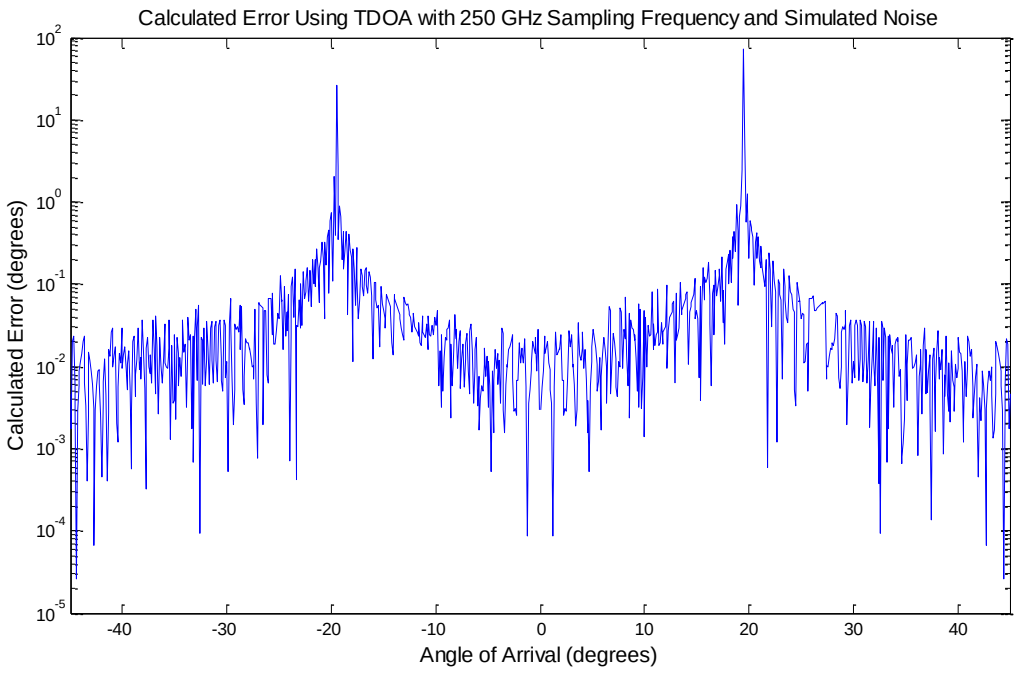

a)

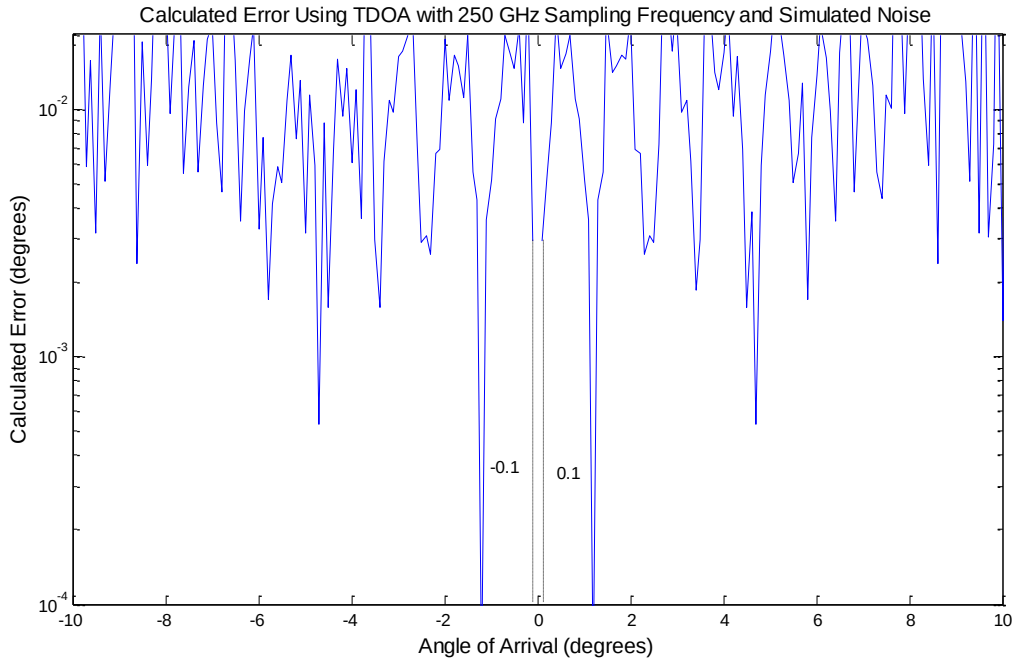

b)

Figure 46. Error of angle calculations using TDOA direction finding with 250 GHz sampling frequency and simulated noise, showing error trends over the entire azimuth extent (a) and the area near the boresight of the system where the TDOA algorithm could not resolve an angle of arrival (b).

4.5.1.1 Analysis of Cross Correlation within the TDOA Algorithm

An unfavorable characteristic of our TDOA algorithm is that there is a wide range of accuracies for angle calculations across the full azimuth extent. In an attempt to isolate the source of this inconsistency, we inspected the accuracy of the cross correlation function used for determining the time delay of received signals. To determine source location, our TDOA algorithm takes the cross correlation for four combinations of receiver pairs, , i-j, i-k, k-j, k-l, and then compares the results of each of the cross correlations. Our analysis was focused on the verification that the cross correlation calculations result in the correct time delays for all angles of arrival, and for all receiver pairs.

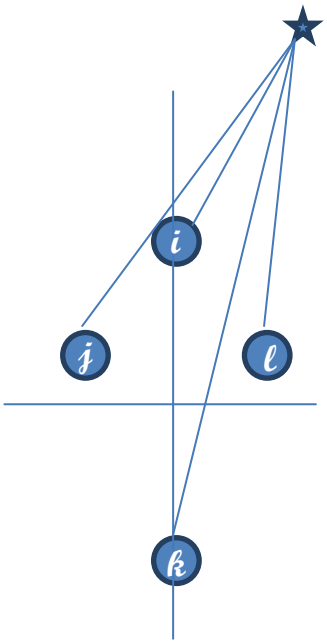

Figure 47. Signals from an emitter, denoted by the star, located at 25° from the boresight of the system intersecting each of the four receivers used for TDOA direction finding.

The first step in this analysis was to analyze the cross correlation results for a specified angle of arrival between each of the pairs of receivers. Using a receiver geometry as shown in Figure 47, we ran the cross correlation between signals from an emitter displaced 25° from the boresight of the system as detected at the specified pairs of receivers. The results of these cross correlations are shown in Figure 48. Since the signal travels a shorter distance to reach receiver i than receiver j, the peak of the cross correlation between receivers i and j shows a negative time delay (time to reach receiver i minus time to reach receiver j). Accordingly, since there is a greater difference in travel time between receivers i and k, the peak of the cross correlation shows a more negative time delay than the cross correlation between receivers i and j. This pattern is true for the other two pairs of receivers, which both resulted in positive time delays since the signal travelled a greater distance to reach receivers j and k than it did to

reach receiver l. These plots indicate that the cross correlation function at this angle is behaving as expected, and that the peak is clearly identifiable.

a)

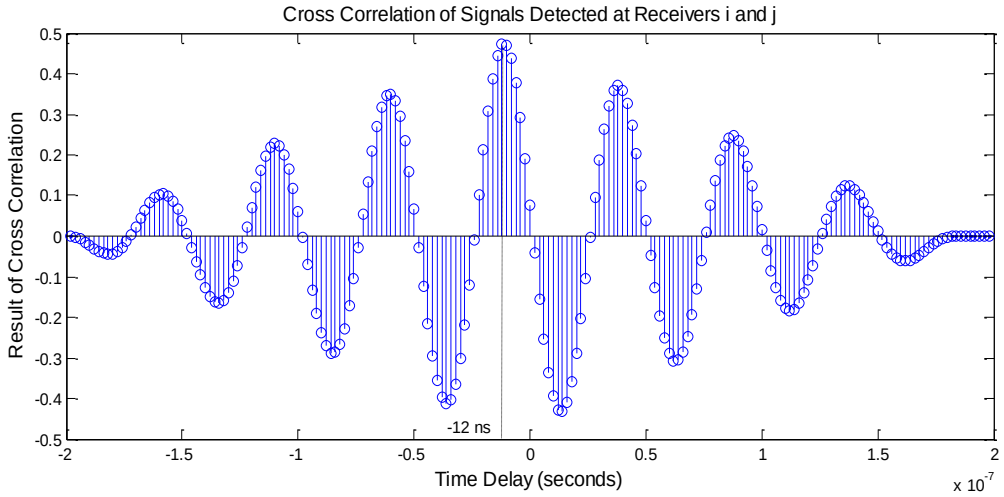

b)

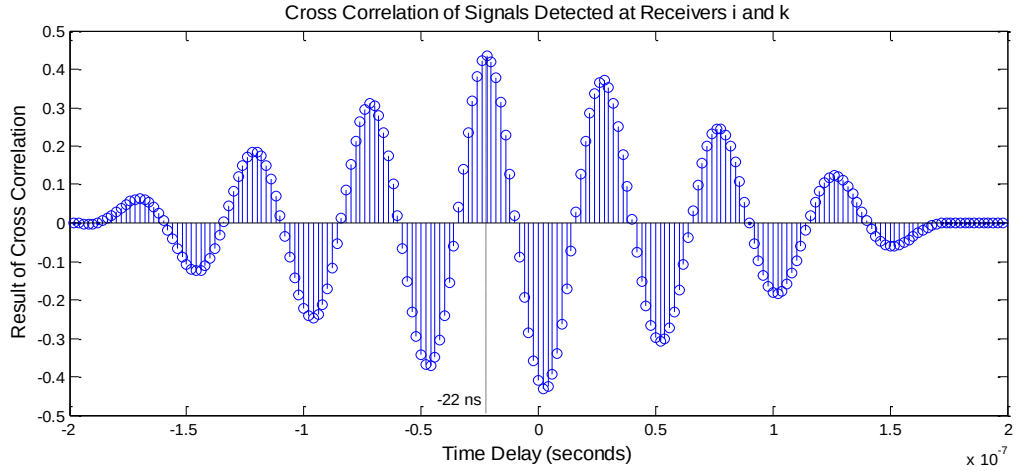

c)

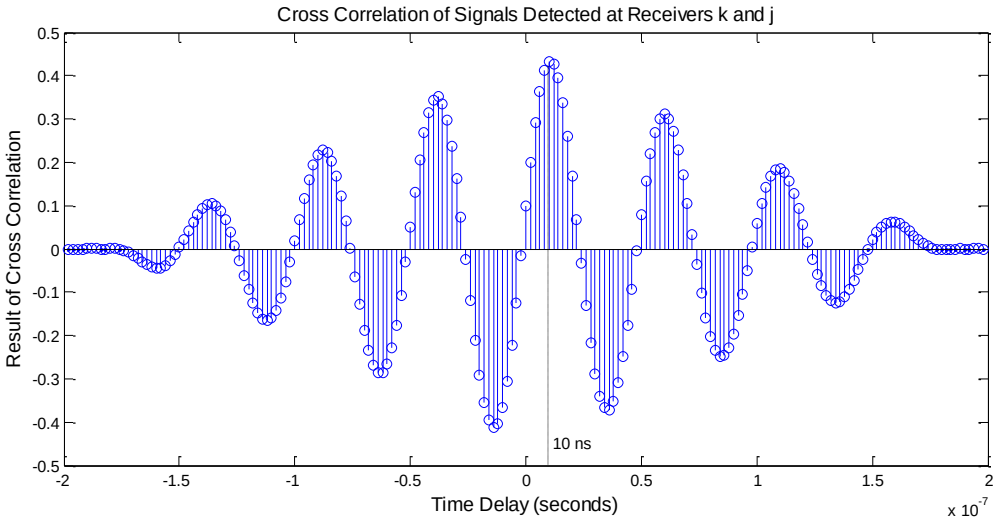

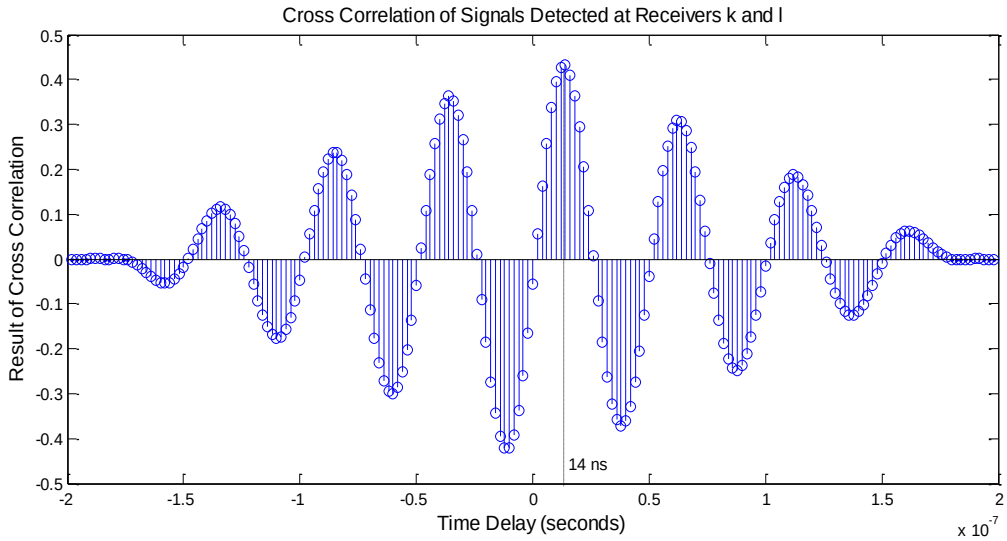

d)

Figure 48. Cross correlations for signals detected at the following receiver pairs: a) i-j, b) i-k, c) k-j, d) k-l.

The next step in our analysis involved determining the accuracy of the time delay calculation. To perform this analysis, we investigated the difference of the time delays calculated from the cross correlation and the true time delays as measured at the receivers. The calculated time delay was determined by locating the time at which the cross correlation function produced the peak result. The expected time delay was calculated by taking the difference between the signals' times of arrival at each of the two receivers. The maximum possible time delay (Max Delay) was calculated as an absolute value by using the distance formula to find the distance between receivers, and dividing by the speed of light to determine the time it would take light to travel between receivers. Using the same system geometry with an emitter located at +25° from the boresight of the system, we determined that each of the expected time delays were within the range of the calculated maximum possible time delay. We also computed the accuracy of the computed time delays resulting from the cross correlation function (Table 3), and determined that the calculated time delays were off by a factor of a few nanoseconds from the expected time delays. This calculation error could be attributed to the sampling frequency of 250 MHz, and would likely improve for higher sampling rates.

Receiver Pair	Calculated Delay	Expected Delay	Error	Max Delay
i-j	-1.20E-08	-7.46E-09	4.54E-09	7.46E-09
i-k	-2.20E-08	-1.81E-08	3.86E-09	2.00E-08
k-j	1.00E-08	1.07E-08	6.80E-10	1.37E-08
k-l	1.40E-08	1.35E-08	4.98E-10	1.37E-08
All values in seconds.				

Table 3. Accuracy of time delay calculations for signals arriving from 25° with a sampling frequency of 250 MHz using the cross correlation function.

We then investigated the accuracy of time delay calculations across the full azimuth extent. As shown in Figure 49, the time delays calculated through the cross correlation function are generally off by a factor of a few nanoseconds. The propagation of this error through the rest of the TDOA algorithm could potentially lead to wide variations in the accuracy of angle calculations across the full range of angles of arrival. Another observation is that the calculated time delays follow a step pattern defined by the sampling frequency across the azimuth extent. A sampling frequency of 250 MHz corresponds with a sampling period of 4ns, and the steps in the figure below show time delay calculations at intervals of 2ns. The time delays are calculated at intervals of half the sampling period as a result of the use of an interpolation factor of 2 in this algorithm. This step size can account for some of the error in calculated delay, since time delay is only measured once every 2 ns. Therefore, we can conclude that the time delays for a system with 250 MHz sampling frequency are being calculated as expected for our algorithm across the entire azimuth extent.

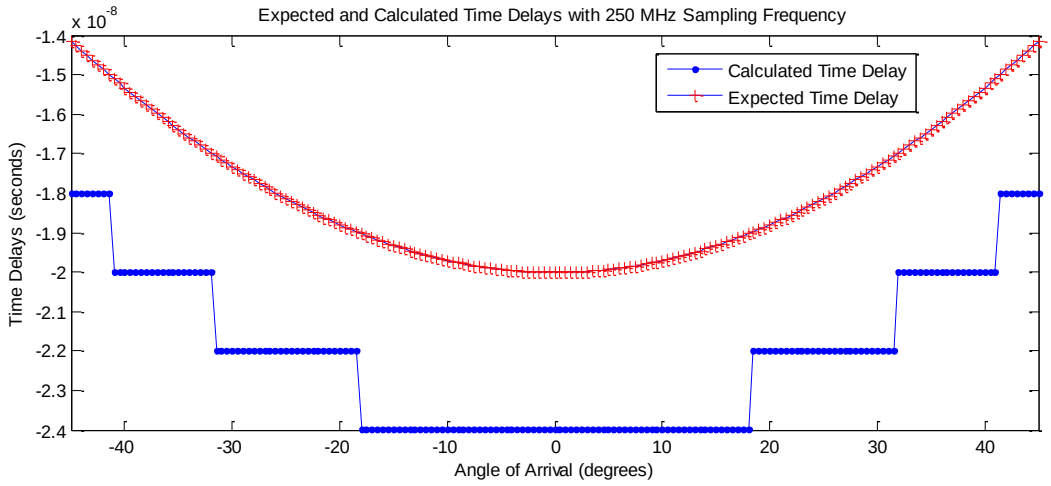

Figure 49. Calculated and expected time delays over 90° azimuth extent with 250 MHz sampling frequency.

We also analyzed the accuracy of the cross correlation function for higher sampling rates. The results of the cross correlation function with a sampling frequency of 2.5 GHz

yielded plots that followed the expected pattern that was seen with the 250 MHz sampling rate. However, the calculated time delays were more accurate at the higher sampling frequency, as seen in

Receiver Pair	Calculated Delay	Expected Delay	Error	Max Delay
i-j	-7.60E-09	-7.46E-09	1.44E-10	7.46E-09
i-k	-1.81E-08	-1.81E-08	0	2.00E-08
k-j	1.04E-08	1.07E-08	2.83E-10	1.37E-08
k-l	1.34E-08	1.35E-08	1.02E-10	1.37E-08
All values in seconds.				

Table 4. Since the expected delay and maximum possible delay are not dependent on sampling frequency, these values are the same the values used for error calculations at 250 MHz in Table 3.

Receiver Pair	Calculated Delay	Expected Delay	Error	Max Delay
i-j	-7.60E-09	-7.46E-09	1.44E-10	7.46E-09
i-k	-1.81E-08	-1.81E-08	0	2.00E-08
k-j	1.04E-08	1.07E-08	2.83E-10	1.37E-08
k-l	1.34E-08	1.35E-08	1.02E-10	1.37E-08
All values in seconds.				

Table 4. Accuracy of time delay calculations for signals arriving from 25° with a sampling frequency of 2.5 GHz using the cross correlation function.

This accuracy is evident over the full azimuth extent, as seen in Figure 50. In general, the calculated time delays are accurate to within less than a nanosecond of error. Calculating the TDOA between receiver pairs with greater accuracy would result in greater accuracy of source position calculations, which follows the trend of more accurate angle calculations with higher sampling frequencies as discussed earlier in this chapter. Also, the calculated time delays again follow a step pattern corresponding to an increased sampling frequency. A sampling frequency of 2.5 GHz corresponds with a sampling period of 0.4ns, and the steps in these error calculations occur at intervals of 0.2ns. This again follows the trend that time delays are calculated at intervals of half the sampling period as a result of the interpolation factor of 2.

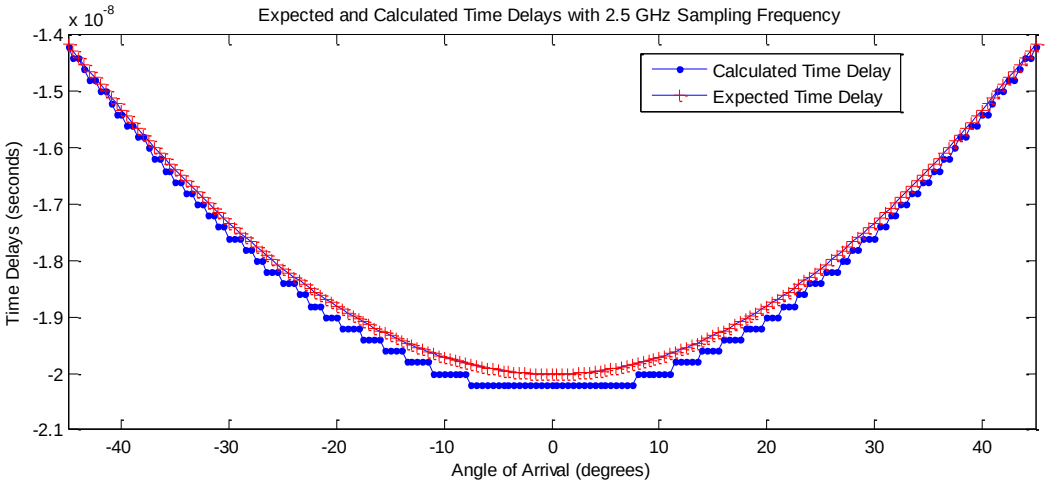

Figure 50. Calculated and expected time delays over 90° azimuth extent for 2.5 GHz sampling frequency.

Through these analyses, our group determined that the cross correlation portion of the TDOA algorithm is behaving as expected, with very small errors in time delay calculations. While these errors could lead to errors in source location calculations, we would expect these errors to be consistent across the full azimuth extent. As such, we don't believe the cross correlation is accountable for the wide variety of accuracies in TDOA angle calculations across the 90° extent.

4.5.2 Results of Phase Comparison Simulation

Due to the nature of the algorithm used for phase comparison direction finding, simulation of a 20 MHz IF signal with noise resulted in the calculation of several possible angles of arrival with the specified receiver geometry as described in the previous section with antennas separated by 10 cm. For most angle values in this simulation, the algorithm determined three possible angles of arrival, shown in Figure 51 as all points located on the blue lines. For example, for a true angle of arrival of -40°, the angles of arrival calculated by the phase comparison algorithm are approximately -40°, -5°, and 30°.

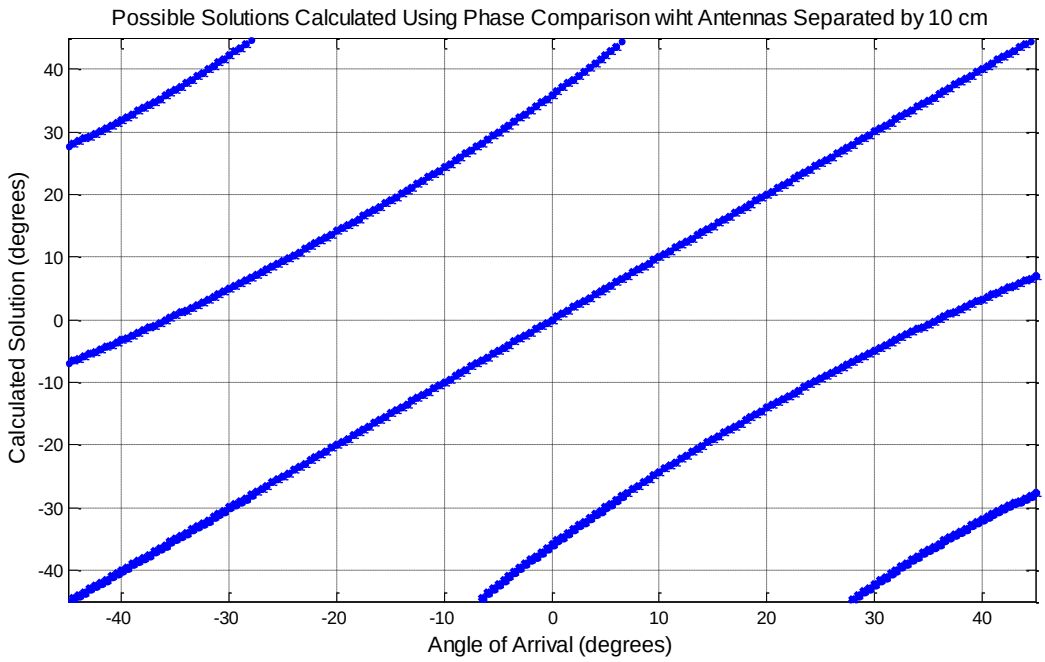

Figure 51. Possible angles of arrival calculated using the phase comparison method for direction finding.

The errors between the known angle of arrival and the returned ambiguous solutions are shown in Figure 52, below. These errors show that for each calculation of the phase comparison algorithm, one returned solution is very accurate, and that the others are several orders of magnitude in error. Without knowing the actual incident angle, the most accurate solution would be impossible to isolate from the ambiguities without the assistance of additional direction finding information.

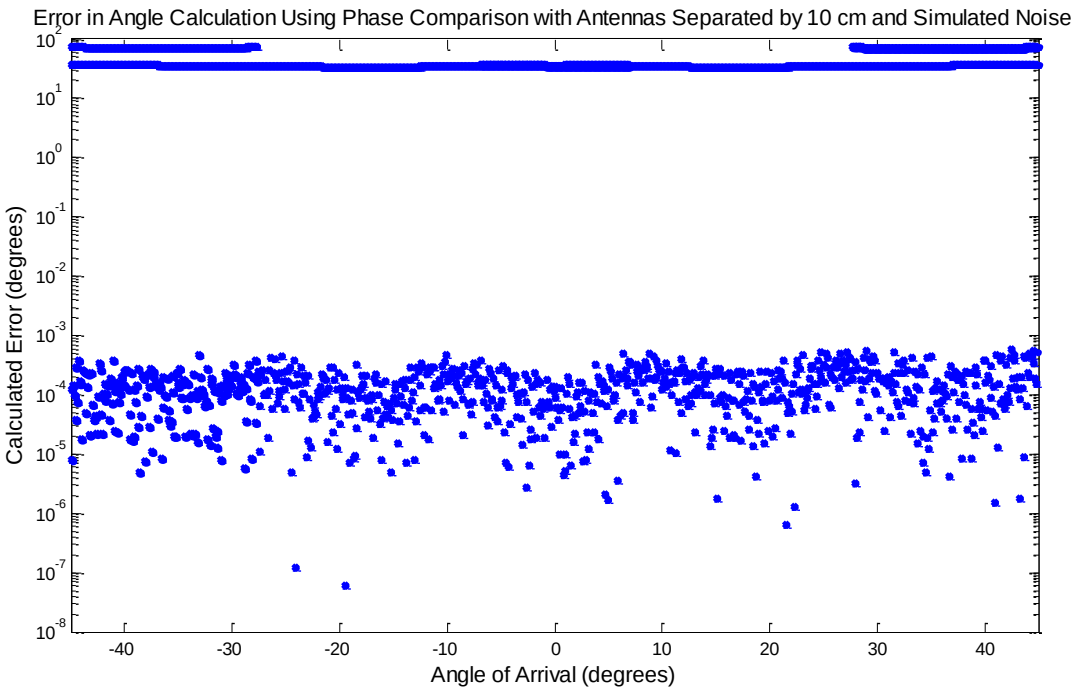

Figure 52. Calculated error using phase comparison with antennas separated by 10 cm. The calculations of error are assuming a known incident angle for comparison.

Our project group also explored modifications to this system that could be made to improve the accuracy of the overall direction finding algorithm. For the phase comparison simulation, the precision of the resolved angle of arrival could be improved by moving the antennas closer together so that the distance between the receiving antennas is less than or equal to one wavelength. Reducing the separation between the antennas to 5cm and 3cm resulted in less ambiguity in the calculated solutions (Figure 53). The resultant improvement in the phase comparison simulation's accuracy for a 20 MHz signal with a wavelength of approximately three cm is shown in Figure 54 for antennas separated by 3 cm. In this case, the phase comparison algorithm returns no ambiguity in angle calculations. Also, for this antenna geometry, the calculated solution is highly accurate (Figure 55), with an error less than 0.0008° over the entire ±45° extent.

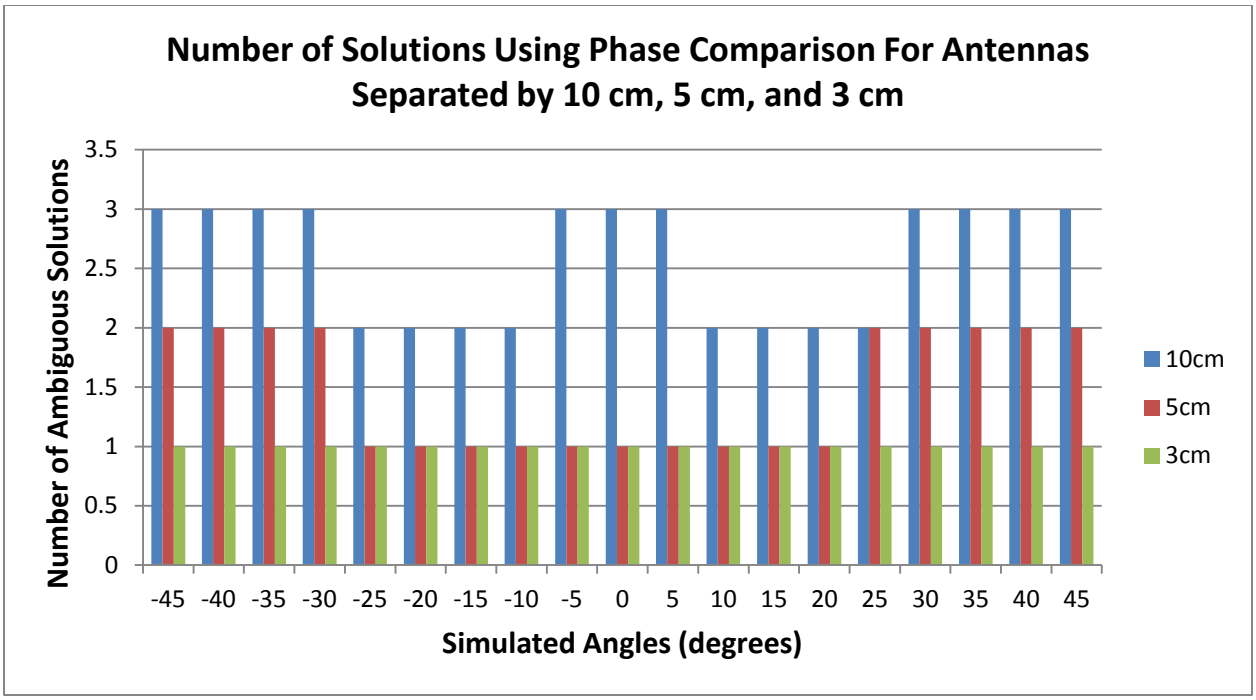

Figure 53. Number of solutions calculated over the full range of simulated angles of arrival calculated using the phase comparison with antennas that are separated by 10 cm, 5 cm, and 3 cm.

Figure 54. Angles calculated using the phase comparison algorithm with antennas that are separated by 3cm.

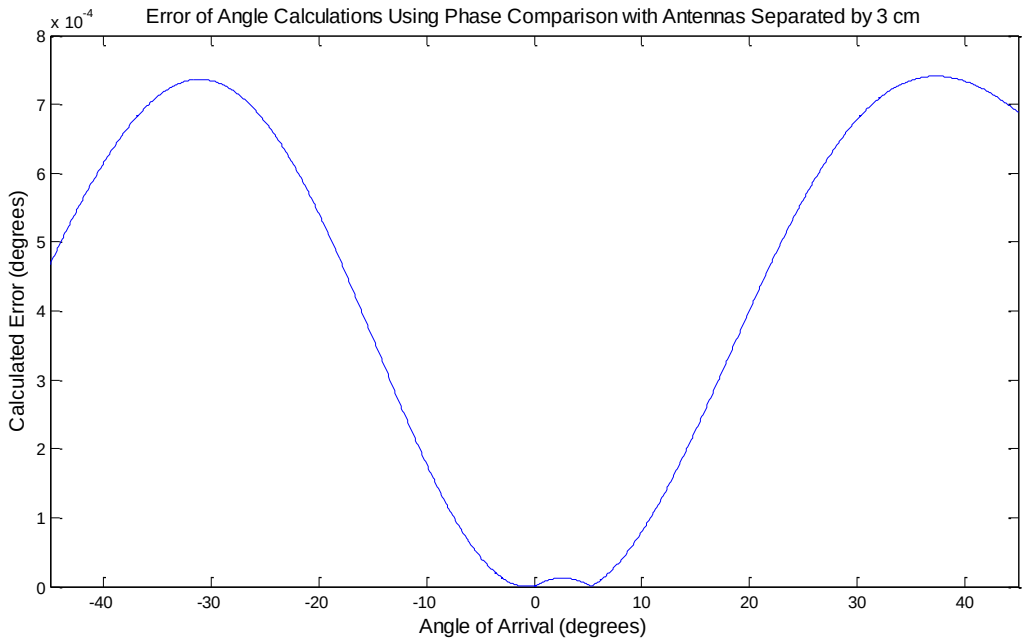

Figure 55. Calculated error using phase comparison with antennas separated by 3 cm.

4.5.3 Results of Amplitude Comparison Simulation

In the amplitude comparison direction finding simulation, two parameters that affect the accuracy of the resolved angle are the presence of noise on the system and the size of the lookup table used to determine the angle of arrival from the computed amplitude ratio. Our simulations include calculations both with and without noise distortion. Figure 56 shows the simulation that most closely corresponds with our hardware: the amplitude comparison method is used to calculate angles of arrival of noisy signals arriving over the entire ±45° azimuth extent using a lookup table of 25 elements with 1.8° resolution. Figure 57 shows the accuracy of angles calculated with the amplitude comparison algorithm using the same lookup table for ideal signals with no noise distortion, showing little impact on system accuracy through the removal or addition of noise on the signals. In both cases, the system is able to compute angle of arrival across the full 90° azimuth extent to within ±2.5° of accuracy. The fact that noise on the signals has such little impact on angle calculations is a result of the inherent rounding in angle calculations due to the small lookup table. While any amount of noise on the signals results in errors in voltage magnitude and ratio calculations, these errors are mitigated through the use of the lookup table. The calculated ratios are used to index into a lookup table of pre-calculated ratio values, and the closest ratio value from the table is used to determine angle of arrival, therefore lessening the impact of calculation errors due to noise.

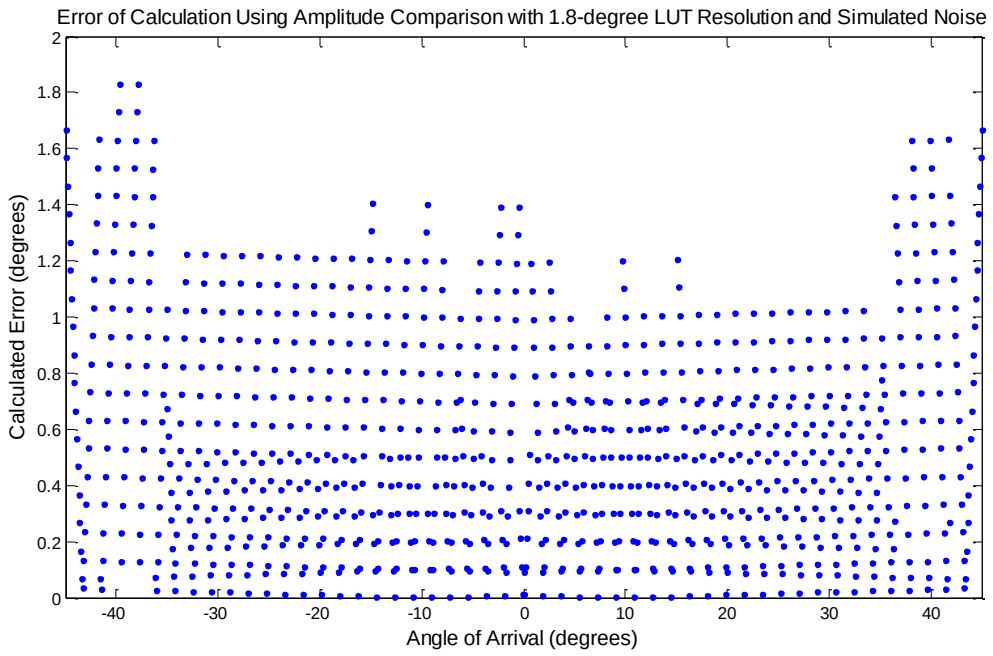

Figure 56. Error of angles calculated through amplitude comparison using a lookup table of 25 values. All angles are resolved within the desired ±2.5° accuracy.

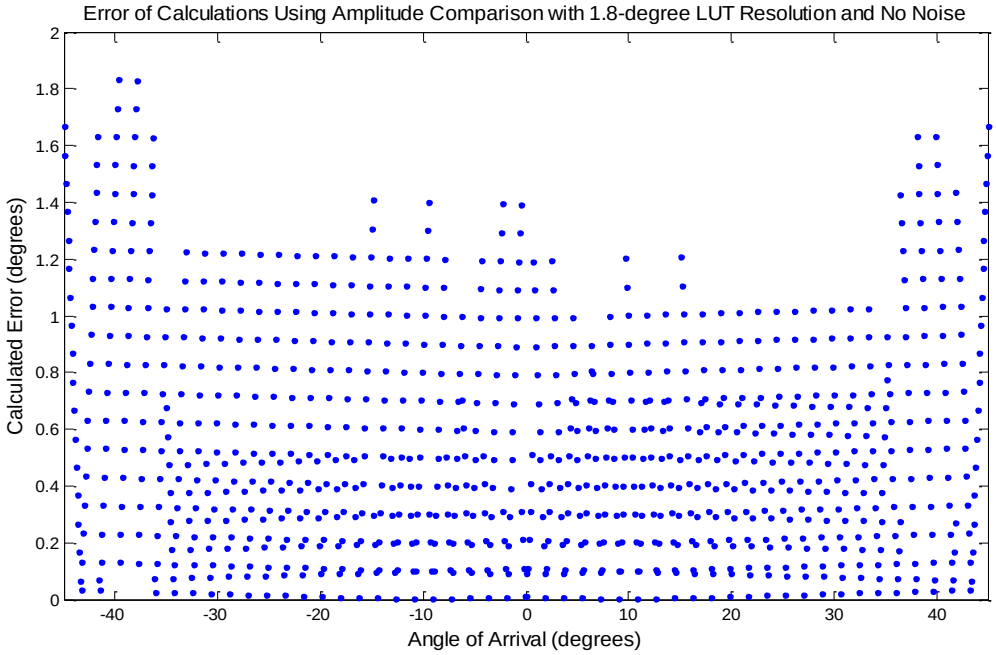

Figure 57. Error of angle calculations from the amplitude comparison method using a lookup table of 25 values with no noise on the signals.

Our group also investigated the impact of increasing the size of the ratio lookup table. Figure 58 shows the accuracy of angle calculations derived from the amplitude comparison

algorithm for signals with simulated noise using a lookup table of 250 values. Figure 59 shows the same calculation with no noise on the signals. Again, both systems are able to calculate angles of arrival across the full azimuth extent within the required degrees of accuracy.

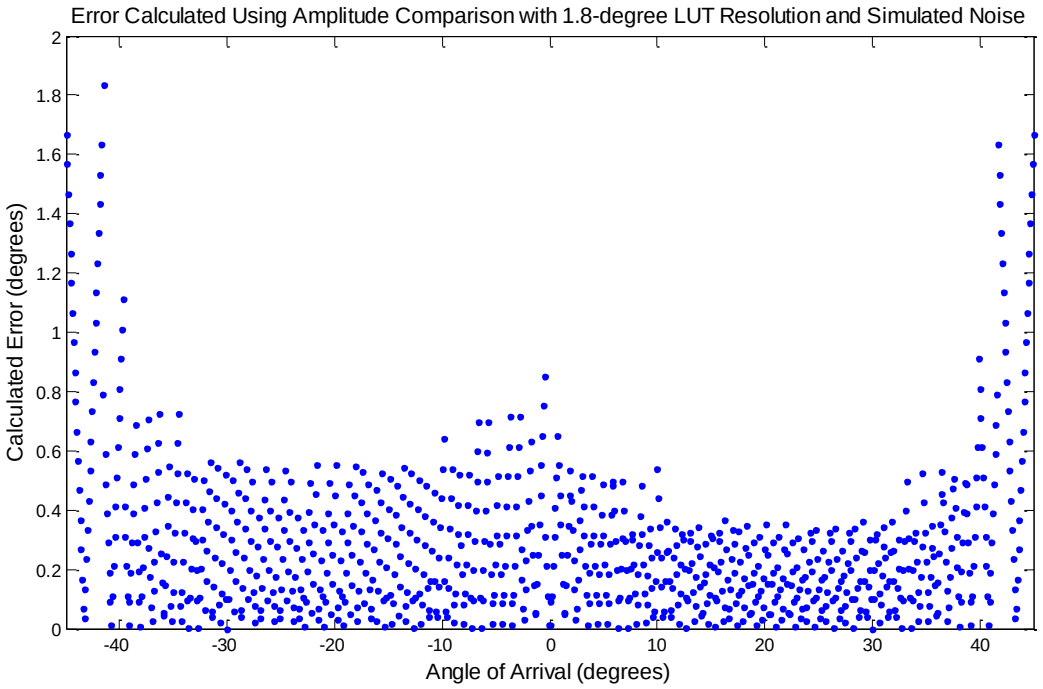

Figure 58. Error of angle calculations using amplitude comparison with a lookup table of 250 values.

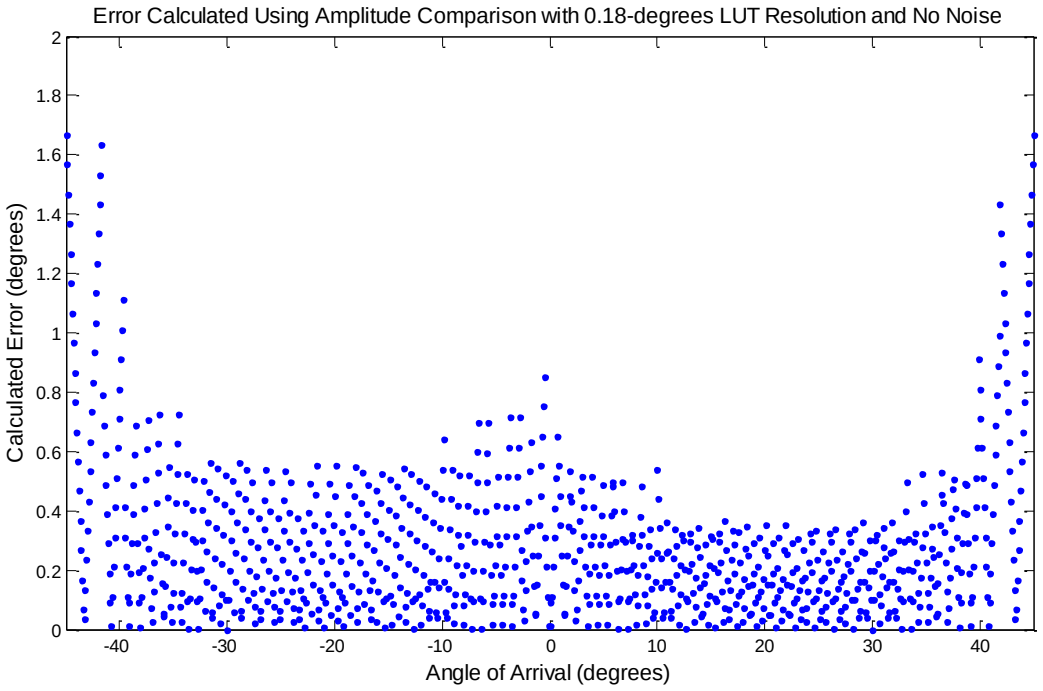

Figure 59. Error of angle calculations using the amplitude comparison algorithm with a lookup table of 250 values and no noise on the signals.

Our group increased the size of the lookup table to 2500 and 25000 values to determine the benefit of continuing to increase the number of ratio values within the lookup table. The accuracies of these systems are shown in Figure 60 and Figure 61, respectively. These calculations include fixed point ratio values that are computed by multiplying the calculated floating point ratio in MATLAB by 24 and then truncating the value to create an integer. However, we determined that solely increasing the size of the lookup table cannot increase the accuracy of angle calculations unless we also increase the number of bits used to represent the fixed point ratio values in the table. The accuracy of the amplitude comparison algorithm using lookup tables of this magnitude requires an increased number of bits to represent such a large number of ratio values. Therefore, Figure 62 and Figure 63 show the accuracy of the amplitude comparison direction finding algorithm using lookup tables of 2500 and 25000 values, which require 16-bits and 32-bits, respectively, to represent the ratio values. As shown in these figures, a lookup table with 0.018° or 0.0018° resolution is no more accurate than a smaller table with 0.18° resolution if the ratios in the table are only represented with four bits. By increasing the number of bits used to represent these values, the systems shown in Figure 62 and Figure 63 can resolve angles to within 0.25° of accuracy over the entire azimuth extent.

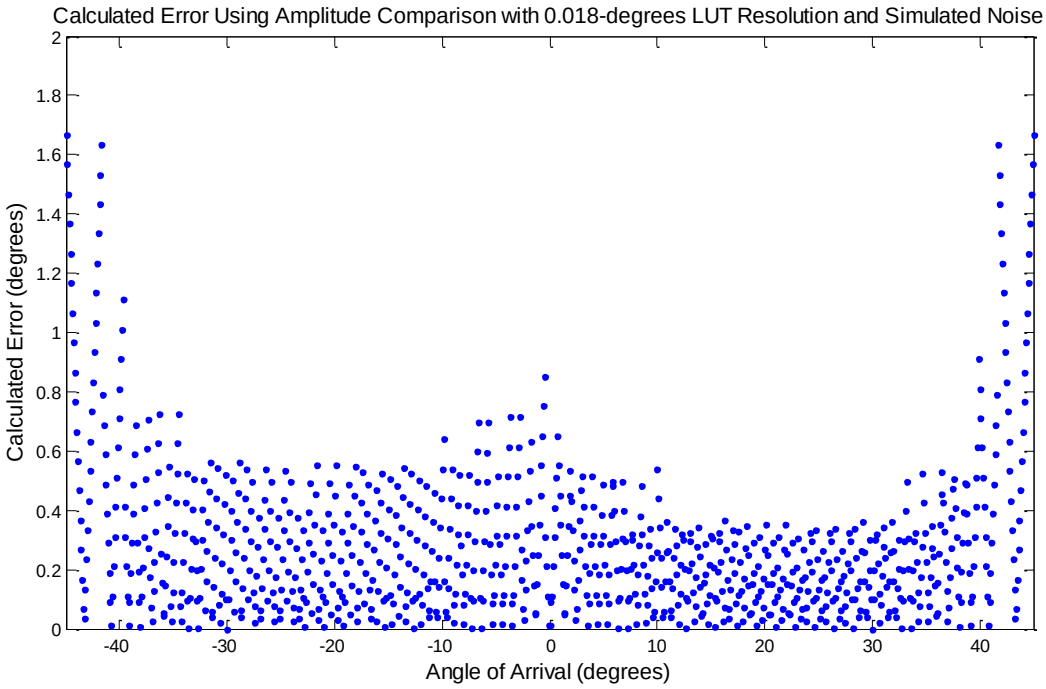

Figure 60. Error of angle calculations using the amplitude comparison with a lookup table of 2500 values and simulated noise.

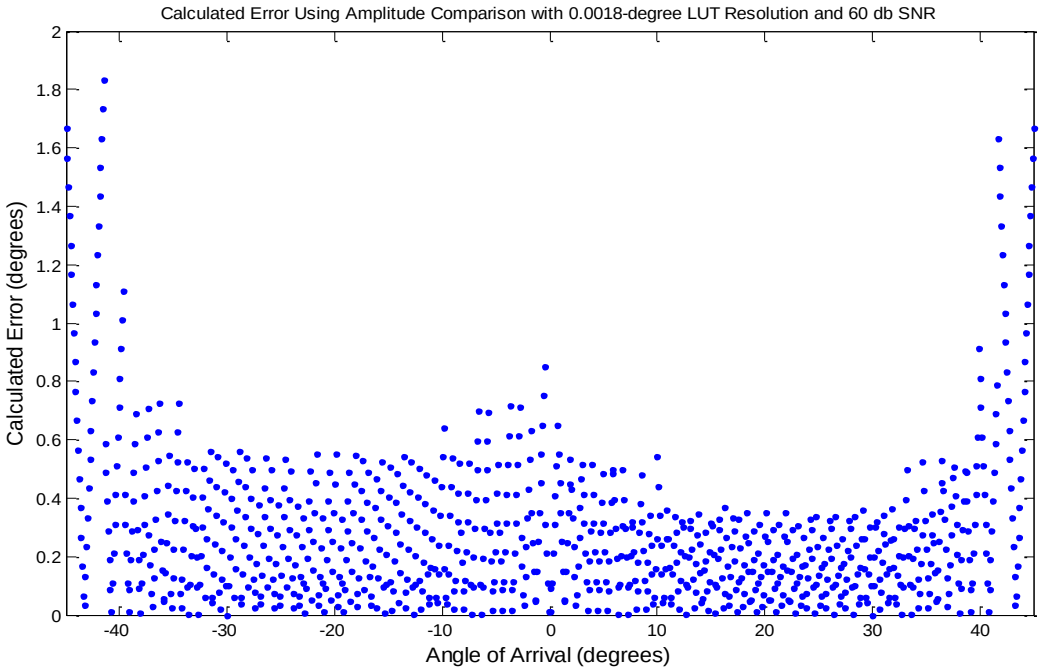

Figure 61. Error of angle calculations using the amplitude comparison algorithm with a lookup table of 25000 values and simulated noise.

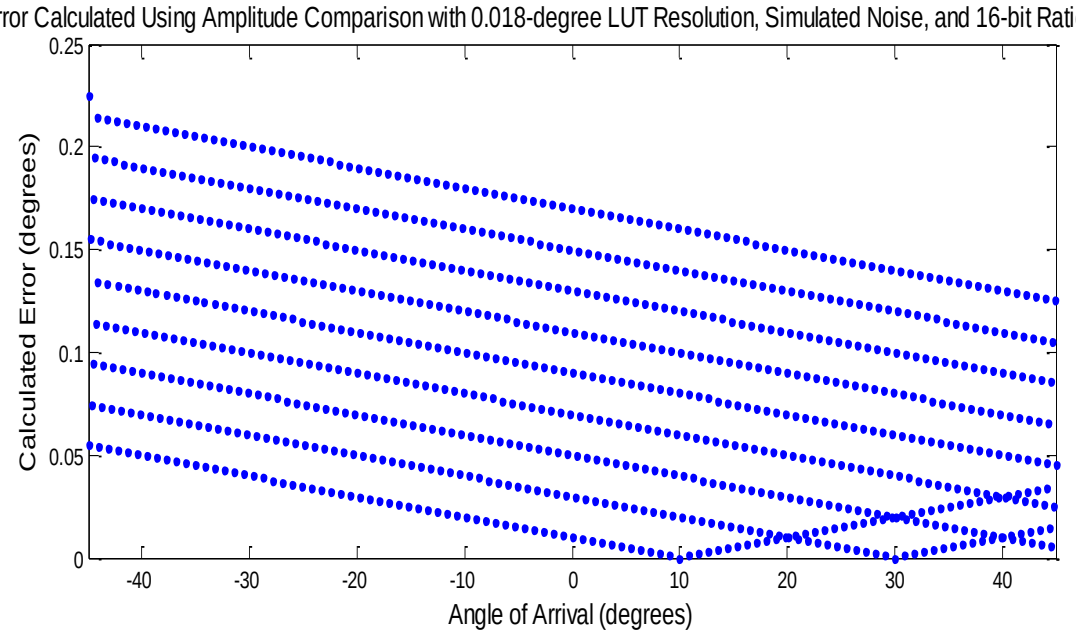

Figure 62. Calculated error using amplitude comparison with a lookup table of 2500 values, using 16 bits to represent each of the ratio values.

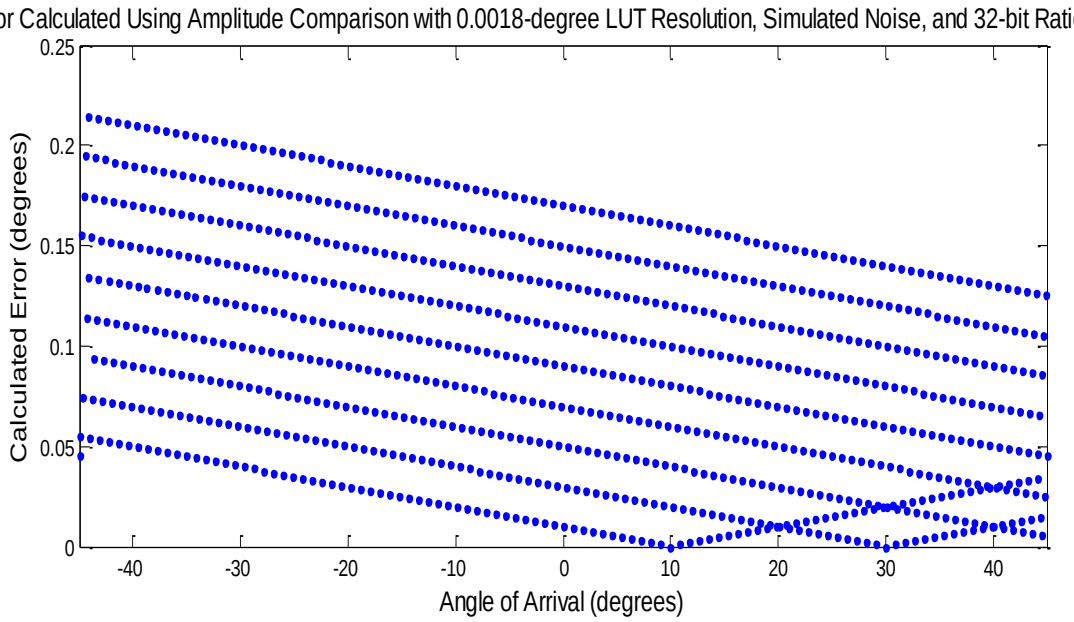

Figure 63. Calculated error using amplitude comparison with a lookup table of 25000 values, using 32 bits to represent each of the ratio values.

4.6 Discussion

Through analysis of our results from the previous section, our group was able to estimate the accuracy of each of the three direction finding methods as designed for implementation on an airborne platform and adhering to the specifications of our hardware.

We were also able to explore the benefits of changing certain parameters in each of the systems to improve the accuracy of the overall systems, and investigated areas for future research.

4.6.1 Analysis of TDOA Direction Finding

The TDOA method for direction finding is greatly influenced by both antenna geometry and sampling frequency. Most TDOA direction finding systems implemented for use with radar signals utilize antennas mounted on cell phone or radio towers for calculations, with separation between towers on the order of kilometers. As this magnitude of separation is impossible for antennas mounted on an airborne platform, our group restricted our analysis to the impact of changes in sampling frequency on the accuracy of the system, since this parameter could be modified to improve functionality.

When considering the ability for TDOA to be used to meet the specifications of this project, the sampling frequency of 250 MHz defined by our ADCs proves to be inadequate for the TDOA direction finding algorithm with the specified antenna geometry capable of implementation on an airborne platform. For certain angles of arrival, the algorithm was able to calculate the direction of the detected beacon well within the required ±2.5° azimuth accuracy. Areas of highly accurate calculations occurred around the regions of ±12° and ±26° from the boresight of the system. This accuracy is a result of the detected signal intersecting the antenna array in line with two of the receivers, as shown in Figure 64, resulting in highly accurate angle calculations at those receivers using TDOA.

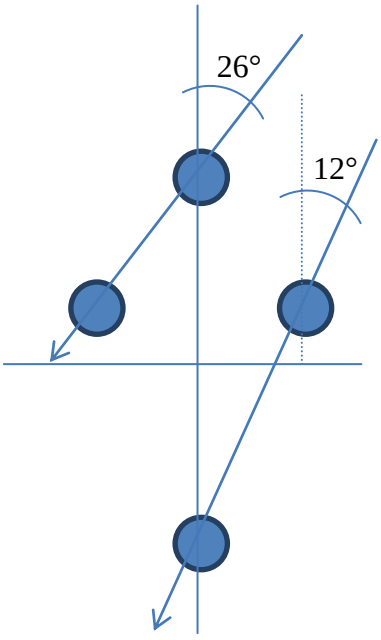

Figure 64. Signals that intersect the TDOA antenna array at approximately 12° and 26° from the boresight of the system will be in line with a pair of receivers, resulting in greater accuracy of angle calculation.

Additionally, using a 250 MHz sampling frequency, our designed TDOA system was able to resolve an angle of arrival within the required ±2.5° accuracy over about 22% of the full azimuth range (Figure 65). However, for most angles, the algorithm was not able to calculate angles of arrival within the specified range of accuracy. Peaks of inaccurate calculations occurred around ±20° and ±35°, ranging up to 70° of error. Additionally, at this sampling frequency, the algorithm was unable to resolve angles of arrival between ±5.1° from the boresight of the system. Our group determined that the problem was inherent to the deterministic algorithm from Bucher and Misra that we had used for simulation. Additionally, using a 250 MHz sampling frequency, our designed TDOA system was able to resolve an angle of arrival within the required ±2.5° accuracy over about 22% of the full azimuth range (Figure 65). However, for most angles, the algorithm was not able to calculate angles of arrival within the specified range of accuracy. Peaks of inaccurate calculations occurred around ±20° and ±35°, ranging up to 70° of error. Additionally, at this sampling frequency, the algorithm was unable to resolve angles of arrival between ±5.1° from the boresight of the system. For this algorithm to resolve angles across the full azimuth extent, angles around the system's boresight could be assigned a value of 0°, which would result in an error of up to 5.1°. Our group determined that the problem was inherent to the deterministic algorithm from Bucher and Misra that we had used for simulation. The algorithm depends on the intersection of hyperboloids at a point for its output. However, there exist source positions in space such that the calculated hyperboloids do not intersect at a single point. In our particular simulation, with the geometry we used, there exist planes of possible source locations along the X and Y axes rather than hyperboloids. Source locations on these planes lie directly between two receivers, resulting in a TDOA of zero for all source positions within the plane. The Bucher and Misra algorithm thus encounters a geometry it cannot handle, resulting in various internal calculations canceling out and leaving the simulation unable to calculate a source position.

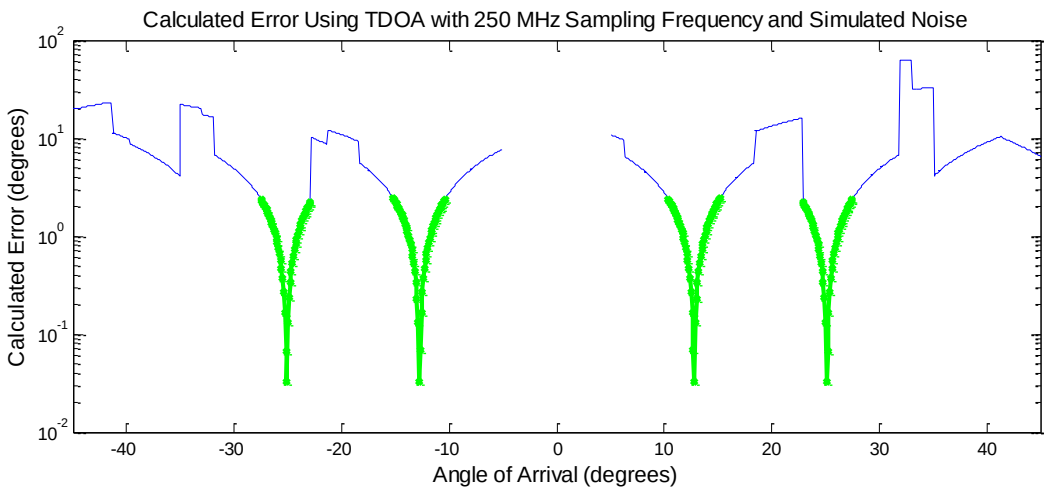

Figure 65. Accuracy of angle calculations using TDOA direction finding with 250 MHz sampling frequency and simulated noise. The areas with green dots show the angles that were calculated by this system within ±2.5° of accuracy, which amounts to 22% of the total field of view.

The next step in our analysis involved exploring modifications that could be made to our TDOA system, using our designed algorithm, to improve the accuracy of angle calculations. The first modification we explored involved effectively increasing the sampling frequency by means of an interpolation factor. By methodically increasing the sampling frequency, our group was able to make additional observations regarding the trends of the system. We determined that if provided with faster hardware, specifically an ADC with greater sampling frequency capabilities, a TDOA system using our specified antenna geometry would be able to determine angle of arrival with accuracies that generally improve as the sampling frequency increases.

Our first observations included analyses of increased sampling frequencies in the megahertz range. Initially, increasing the sampling frequency from 250 MHz to 500 MHz resulted in better angle calculations closer to the boresight of the system by shrinking the set of angles near boresight for which the algorithm could not resolve angles, and even increased the percent of angle calculations that met our specification of ±2.5° of accuracy to about 26% (Figure 66). However, increasing the sampling frequency from 500 MHz to 750 MHz resulted in a wider range of angles around the boresight of the system for which the algorithm could not resolve angle of arrival. The increase from 500 MHz to 750 MHz sampling frequency again increased the percent of angles that were calculated to within ±2.5° of accuracy to about 29% (Figure 67).

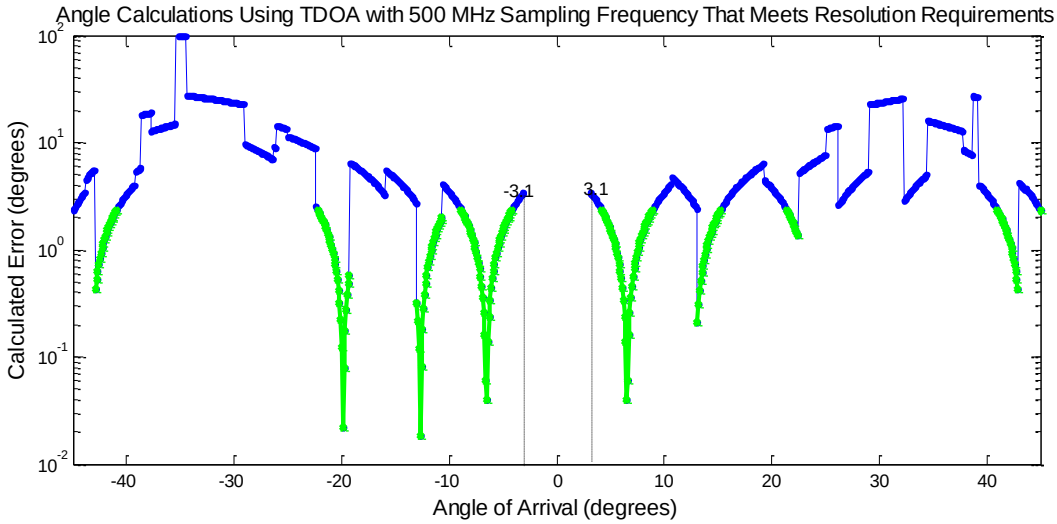

Figure 66. Angles calculated with the TDOA algorithm with a 500 MHz sampling frequency and simulated noise that met our requirement of ±2.5° of accuracy are shown in green.

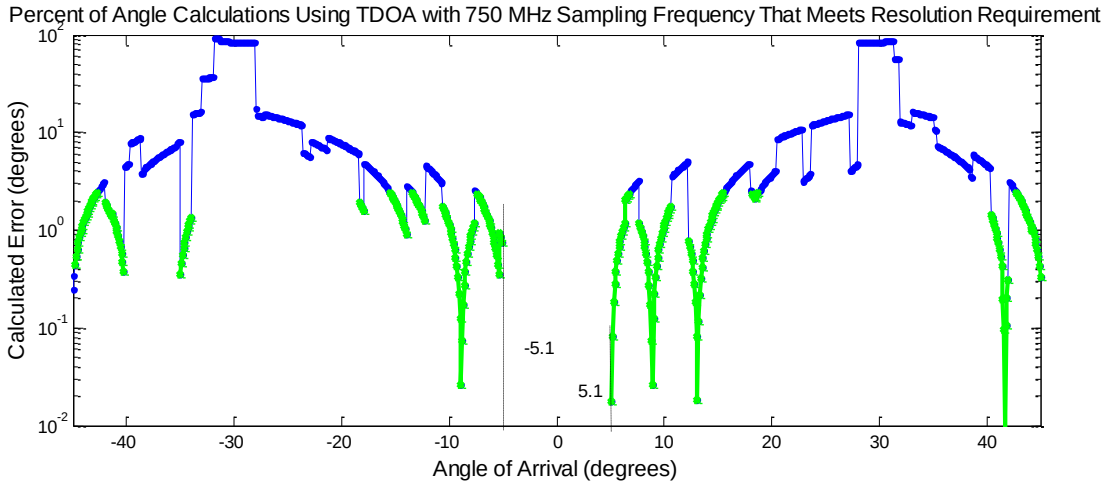

Figure 67. Angles calculated using TDOA with a 750 MHz sampling frequency and simulated noise that met our requirement of ±2.5° of accuracy are shown in green.

After increasing the sampling frequency to 2.5 GHz, the baseline of the system improved from around 10° of error to 3-4° of error. Peak inaccuracies in angle calculation occurred at approximately ±22° from the boresight of the system with up to about 80° of error (Figure 68). Using this increased sampling frequency, the TDOA system was able to resolve angle calculations for all values across the ±45° azimuth extent except for angles within ±0.8° from the boresight of the system, and for angles between -2.8° and -5.9°. While the angular ambiguity for angles between -2.8° and -5.9° seems random, the ability for this algorithm to calculate angles close to the boresight of the system improved from ambiguities between ±5.1° to only having ambiguity between ±0.8° from the boresight of the system. As such, if we allotted a value of 0° for irresolvable angles around system boresight, there would only be an

error of up to 0.8°. Also, the inability for the TDOA algorithm at 2.5 GHz sampling frequency to calculate angles between -2.8° and -5.9° remained true with no noise on the signals.

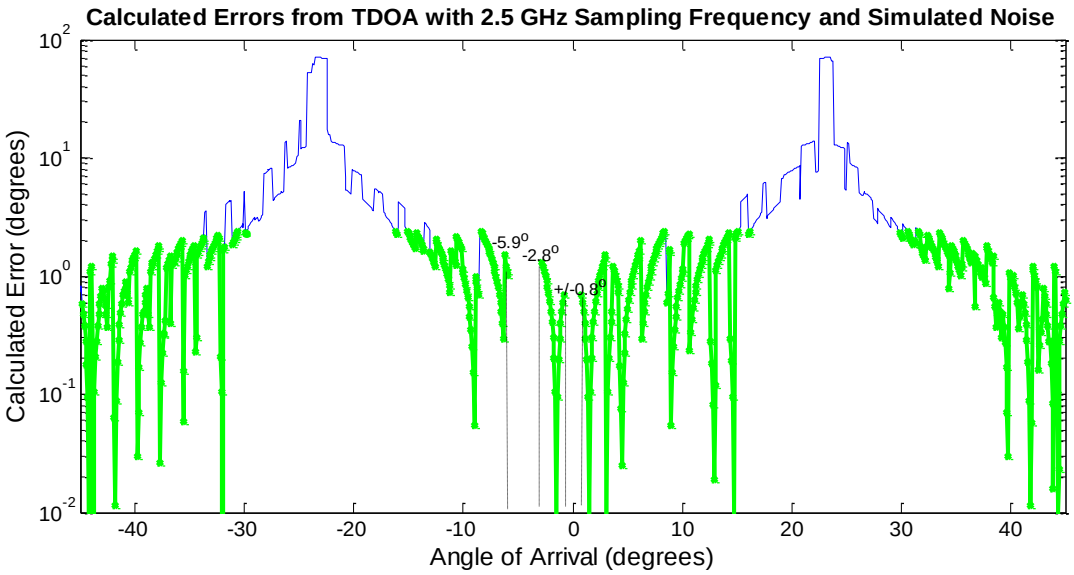

Figure 68. Errors in angle calculations using TDOA with 2.5 GHz sampling frequency and simulated noise. Angles that meet our specified accuracy are shown with green dots.

Increasing the sampling frequency to 25 GHz, while maintaining the same antenna geometry, improved the overall accuracy of angle calculations for this system, where about 95.5% of the calculations were within the desired ±2.5° of accuracy (Figure 69). At this sampling frequency, peak errors in angle calculations occurred around ±20° from the boresight of the system, where the only calculated errors that exceeded ±2.5° occurred from -21° to -19° and from 18.8° to 20.8°, with a maximum of 76.27° of error in these areas. Additionally, this system exhibited a greater range for angle calculations since it was only unable to calculate angles between ±0.2° from the boresight of the system. Finally, we simulated a TDOA system operating at a 250 GHz sampling frequency and employing our specified antenna geometry. While this system exhibited similar peak errors to the system operating with 25 GHz sampling frequency, where angles at ±20° from the boresight of the system were calculated with a maximum of 71.34° of error, the system using a sampling frequency of 250 GHz displayed greater overall accuracy than the system using 25 GHz sampling frequency. The system was able to resolve angle calculations for all values greater than ±0.1° from the boresight of the system.

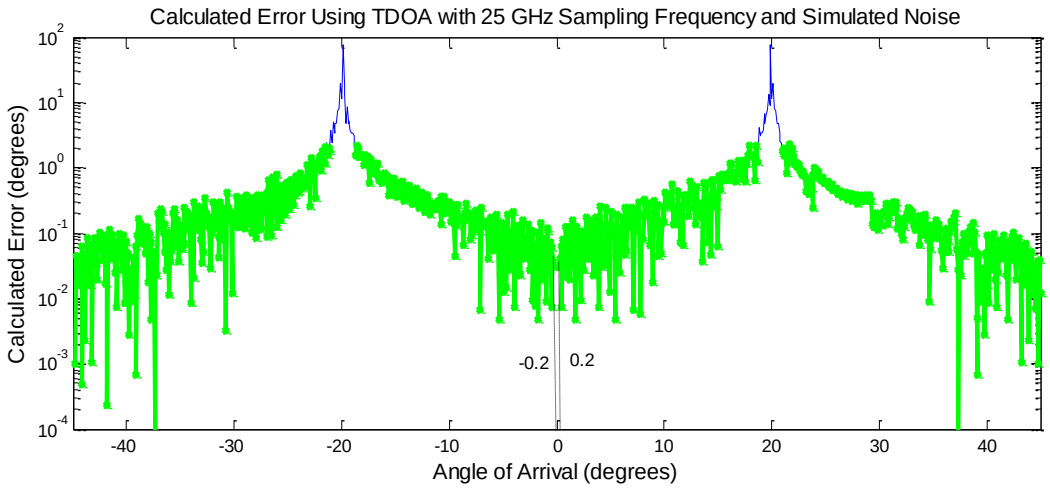

Figure 69. Angles calculated using TDOA with 25 GHz sampling frequency and simulated noise that met the requirement for ±2.5° of accuracy.

Our project group determined that increasing the sampling frequency at the ADC resulted in overall improved system accuracy (Figure 70). As the sampling frequency increased, the system was able to take more measurements at smaller angular intervals over the entire azimuth extent. Also, we determined that the consistent inaccuracy around ±20° is a result of the signal arriving at the antenna array at an angle directly between the four receivers. As stated earlier in the paper, angles of arrival of ±12° and ±26° resulted in extremely accurate angle calculations at 250 MHz because the angles intersected the antenna array in line with a pair of receivers, resulting in highly accurate TDOA measurements, and therefore accurate angle of arrival calculations. Similarly, at higher sampling frequencies, the inaccuracy of angle calculations around ±20° can be explained by the fact that a signal arriving at this angle will intersect the antenna array between receivers, resulting in less accurate TDOA calculations.

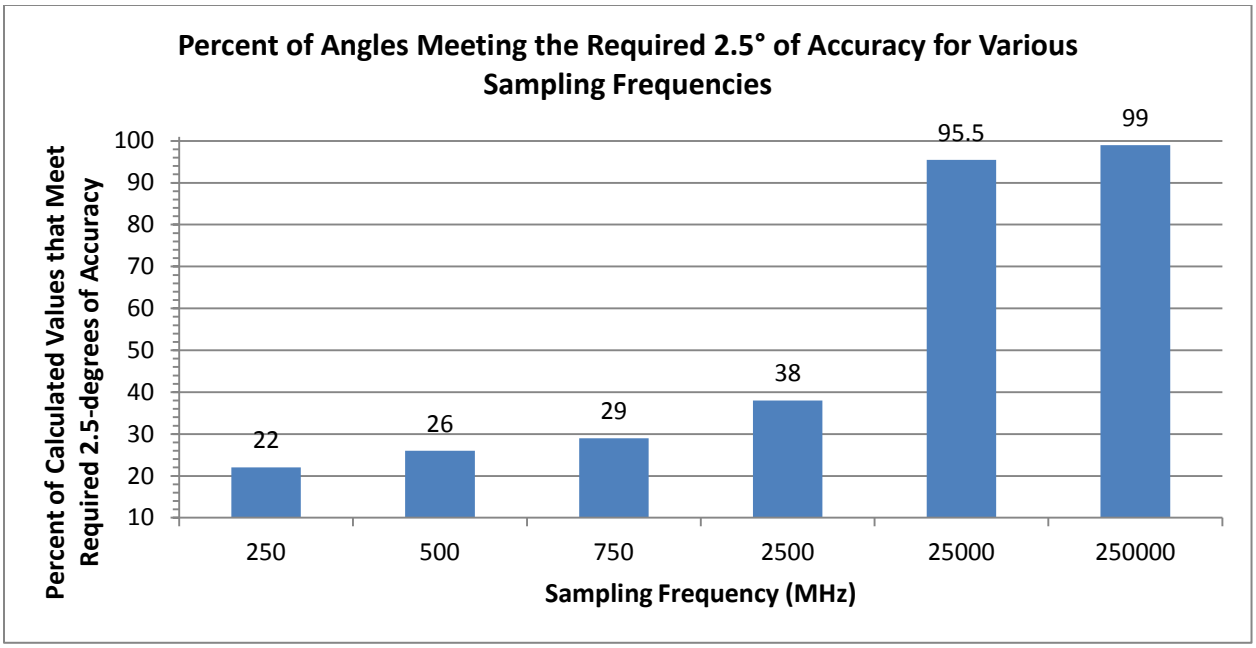

Figure 70. Percent of angle calculations for various sampling frequencies that meets the requirement of 2.5° of accuracy.

While the antenna geometry chosen for our calculations plays a large role in the accuracy of our system, due to time constraints of our project, we were unable to compare the effectiveness of various antenna setups. However, we recognize that there are several factors of the chosen geometry that could be modified to improve system accuracy. A geometry to be considered by future groups could include four antennas spaced linearly equidistant across the axis of an aircraft's wings, providing the system with a full 90° azimuth range and eliminating ambiguity that could result from a signal intersecting only a portion of the antennas in the array. Another option could include using a geometry similar to the one implemented in this project, but offsetting one of the antennas on the wings to make the array asymmetrical to reduce the possibility of multiple antennas receiving a signal at the same time.

Through the analysis of these system modifications, our group determined that while the TDOA method did not prove to be the most useful for implementation in this project, there are several means by which this method could be altered to meet the specifications of slightly different project applications. While our group has hypothesized about the accuracies of various different antenna geometries, due to the time constraints on this project, the analysis of changing antenna geometries is beyond the scope of this project. Another means of modifying this system could include exploring the benefits of using a different hardware platform. For example, with the employment of more advanced hardware and ADCs with higher resolution, this TDOA algorithm can resolve angles of arrival to within very high degrees of accuracy over the majority of the 90° extent.

4.6.2 Analysis of Phase Comparison Direction Finding

According to our simulations, this project group determined that the phase comparison direction finding algorithm was predominantly influenced by the separation distance of the omnidirectional antennas used for signal detection and by the presence of noise on the signals. Though this particular method for direction finding is additionally influenced by the radio frequency of the detected signal, our analysis was focused to adhere to the limited scope of this project involving the processing of IF signals for the purpose of direction finding. As such, the simulations for this direction finding method investigated the accuracy of angle calculations using antennas separated by 10 cm to imitate a reasonable antenna geometry for airborne implementation. We additionally explored the effects of reducing the separation between antennas.

Through the analysis of these simulations, our group determined that the phase comparison algorithm, using antennas separated by 10 cm, would not be able to determine the angle of arrival of a beacon signal on its own since this system calculates multiple ambiguous solutions for a signal at any angle over the required azimuth extent. However, as shown in Figure 51, since there is a difference of at least 15° between each of the ambiguous solutions for any given angle of arrival, the appropriate solution could be extracted from the ambiguous calculations if the azimuth extent was first reduced from ±45° from the boresight of the system to ±15° from the angle of arrival of the target. If an additional direction finding method were first used to narrow down the range of detection to within ±15° of the detected signal, the phase comparison algorithm could be used to determine the angle of arrival with extraordinary accuracy (Figure 51).

Our project group investigated the effect of reducing the separation of the antennas from 10 cm to 5 cm and 3 cm. We determined that as the distance between antennas decreases, the ambiguity due to multiple angle calculations is lost (Figure 53). If the separation distance between antennas is equal to or less than the wavelength of the signals detected at that antenna, only one angle of arrival will be calculated. Additionally, for antenna geometries that yield only one solution, the algorithm calculated the angle of arrival to within ±.0008° of accuracy over the entire ±45° azimuth extent. Though reducing the antenna separation to a distance of one wavelength greatly improved the accuracy of the system in simulation, this separation may not be realistic for most omnidirectional antennas due to the fact that closely spaced antennas are more susceptible to timing errors as a result of the difficulty for a system to resolve differences in phase over small distances with noise on a signal. With a separation of 3 cm, the time difference to travel between the two antennas is 0.1ns, which imposes very strict time constraints for accurate calculations.

Also, we took into account that our results from simulation only reflect the accuracy of the system with 20 MHz IF signals. The requirements for our project indicate the ability for our direction finding system to operate over 100 MHz bandwidth, from 12.5-112.5 MHz. A 112.5

MHz signal would be very close to the Nyquist frequency of 125 MHz for our system. As the frequency of a signal approaches the Nyquist frequency, the ability for the phase comparison algorithm to resolve angle calculations would not be affected because the measurement of incident phase is taken instantaneously per sample. Reducing the samples taken per period of the sinusoid would still allow the algorithm to accurately compare instantaneous phase measurements for signals detected at the two receivers. Through simulation, we determined that increasing the frequency of the incoming signal to approach the Nyquist frequency resulted in angle of arrival calculations that were as accurate as calculations of a 20 MHz IF signal, with the same level of ambiguity. Through these analyses, our group determined that although the phase comparison direction finding method was able to produce extremely accurate angle of arrival computations, our designed system with antennas separated by 10 cm required the assistance of an additional direction finding method to initially narrow down the field of view before a reasonably accurate angle of arrival could be calculated. For the purposes of this project, the investigation and implementation of two individual direction finding systems would have been impractical and unnecessarily time consuming. However, this phase comparison algorithm would be ideal for implementation in an existing system which utilizes a direction finding technique with the capability of determining angle of arrival to within a few degrees of a detected signal. The use of the phase comparison algorithm combined with the less accurate direction finding method would dramatically improve the overall accuracy of the system.

4.6.3 Analysis of Amplitude Comparison Direction Finding

Through the analysis of our simulations, we determined that the accuracy of the amplitude comparison direction finding method was predominantly influenced by the resolution of the AOA lookup table. Since our designed amplitude comparison algorithm involved the use of a lookup table, the accuracy of the system was dependent on the number of ratio calculations included in this table. A perfectly accurate amplitude comparison system would include a lookup table that contained every possible ratio value for all angles of arrival over the entire ±45° azimuth extent. However, this lookup table size, and therefore this level of accuracy, would be impossible to implement in any hardware system. Accordingly, our algorithm was designed to compute a ratio of voltage magnitudes and find the closest ratio within the provided lookup table to determine the corresponding angle of arrival. This process of finding the closest table value intrinsically required using an approximate, pre-calculated ratio value to determine the angle of arrival of the detected signal. The accuracy of the resolved angle of arrival depended on the magnitude of difference between the ratio calculated with our algorithm and the ratio provided in the lookup table. The resolution of the lookup table improves as the size of the table is expanded and the angle calculations were more accurate with larger lookup tables. However, since large lookup tables are undesirable for

implementation in hardware because they occupy unnecessary amounts of space that could be used for additional signal processing, our group investigated the tradeoff in accuracy of our amplitude comparison system using lookup tables of various resolutions.

Our first analysis involved simulations of the amplitude comparison direction finding system as implemented in hardware. This simulation included using a lookup table of 25 values, with 1.8° resolution, and simulated white Gaussian noise on the signal. Over the entire ±45° azimuth extent, this simulation was able to resolve angle calculations within the required ±2.5° of accuracy for 1 mW (+10 dB) signals. The lookup table of 25 values provided enough accuracy to resolve angles of arrival within the required accuracy while maintaining a relatively small lookup table size for fast signal processing in hardware. We then investigated the effects of noise on the signal on the system's ability to determine angle of arrival from the lookup table. After removing noise from the simulation, we determined that the accuracy of this system was relatively unaffected due to the fact that this system only uses a lookup table of 25 values. Even if the presence of noise on the signals caused a slight error in ratio calculation, the calculated ratio would index to the lookup table location of pre-calculated ratio values. Since the algorithm chooses the pre-calculated ratio lookup table value that is closest to the calculated value, the resultant angle of arrival would usually be the same for small variations in calculated ratios caused by noise on a signal.

We then analyzed the effect of increasing the size of the lookup table to improve the resolution of computed angles of arrival. Increasing the lookup table to include 250 pre-calculated ratio values across the 90° range yielded a resolution of 0.18°. Our group first examined the accuracy of angle calculations for ideal signals (no noise). With the increased lookup table resolution, angles were able to be calculated more precisely than when using the smaller lookup table. Through the employment of the lookup table with 0.18° resolution, most angle calculations over the 90° extent were calculated within 0.6° of error, not only meeting but surpassing our accuracy requirement. After adding noise to the system, the overall accuracy of the angles still remained within 0.6° of error, with the exception of angles greater than ±40°, which were about 0.2° less accurate when calculated with noise on the signals, but still met our requirements for ±2.5° resolution.

Our group explored the benefits to increasing the size of the lookup table further. When increasing the lookup table to 2500 and 25000 values, without changing the number of bits used to represent ratio values, there was very little improvement in the accuracy of calculations. The accuracy of angle calculations did not improve because there were not enough bits to represent each number individually, and several ratio values were being represented by the same fixed point integer values. This problem was addressed by increasing the number of bits used to represent the ratio values in the lookup tables. The table of 2500 values required 16 bits to represent the ratios, and the table of 25000 values required 32 bits to ensure that each ratio was represented by a different integer value.

Additionally, we recognized that the performance of our designed amplitude comparison algorithm would decrease as signal power decreased. As stated earlier in this paper, our designed system does not meet both requirement of degree of accuracy and dynamic range. As signal power decreases, the difference between induced voltages at the two directional antennas decreases, making the comparison of these voltage magnitudes more difficult and the overall ratio calculation less accurate. However, we also recognized that the amplitude comparison system was not dependent the frequency of the received signal. Our system was able to resolve the same degree of accuracy for signals that approach Nyquist frequency as it was for 20 MHz signals.

5. Hardware Methodology

The final component of our project was the development of a hardware device capable of performing the signal processing necessary to determine an angle of arrival for IF signals. This device included a hardware implementation of the amplitude comparison direction finding method as well as a software graphical user interface (GUI) to render system output in an intuitive graphical format. A commercial off-the-shelf FPGA development board was used as the platform for project development. Existing tools at MIT Lincoln Laboratory were leveraged to develop the direction finding system, and the final design was synthesized and tested on the FPGA.

5.1 Selection of the Amplitude Comparison Method

Our group was able to complete a hardware implementation of one of the researched direction finding methods. We selected the amplitude comparison direction finding method based on information gathered from background research as well as results from simulation. Background research revealed that in terms of algorithm complexity, amplitude comparison was the most intuitive and far less complex than TDOA position location. Since our group was responsible for the development of other components, such as ensuring signal detection at the ADCs and fabrication of a GUI, in addition to the implementation of the direction finding algorithm, we felt that we could develop a far more robust amplitude comparison device in our project timeframe than with any of the other methods. In terms of algorithm accuracy, simulation results revealed that amplitude comparison and phase comparison could produce results that either met or were reasonably close to our sponsors' specifications, whereas the results of TDOA simulation were very inaccurate while using realistic system specifications and geometry. However, in order for the phase comparison algorithm to achieve system accuracy comparable with our sponsor's specifications, the receiver geometry required antennas that were placed closer than would be possible given realistic antenna widths. These results indicated that, given our sponsors' system specifications, amplitude comparison would be the most appropriate algorithm to implement for our direction finding device.

5.2 Selection of the FPGA

Of the devices considered for project development (see section 2.4), the FPGA was chosen for its low processing latency and its ease of use. The requirement of real-time processing favored the specialized devices for their decreased latency and placed the FPGA above the rest in that regard. The ability to integrate our design with other systems on the same FPGA also added merit as our sponsors would like to integrate direction finding with other systems they are developing. In addition, Lincoln Laboratory provided a comprehensive set of tools for working with an FPGA. The tools provided include a generic hardware shell for rapid development, debugging tools, and an FPGA-to-PC communication program. The

availability of these tools helped reduce the inherent development time requirements of using an FPGA for project development, thereby increasing its appeal. With all factors considered, it appeared that the FPGA would be the most suitable platform for this project.

5.3 Development Platform and Tools

Project development was done using a commercial off-the-shelf development board, the Innovative Integration X5-400M (see Figure 71), along with relevant software and hardware tools and a radar signal emulator for testing. The development board was built with a Xilinx Virtex-5 FPGA for its processing core. In addition to the FPGA, the board contained two 14-bit ADCs operating on a 250 MHz system clock which could be used for signal input. This development board was connected to a PC running a Linux operating system through a PCI Express card slot. Communication between the PC and the FPGA could be performed through this slot. Utilizing this functionality, we were able to develop a direction finding device on the FPGA and a graphical software interface on the PC, then forward data from the device to the software.

Figure 71. Commercial off-the-shelf development board used for this project. It contains a Xilinx Virtex 5 FPGA for hardware synthesis as well as two ADCs clocked at 250 MHz with 10 effective bits of resolution.

To develop the direction finding hardware, several software and hardware tools were utilized. Xilinx ISE was used to write and synthesize VHDL descriptions of the hardware design. Contained within this software was the Xilinx Core Generator which automated development of components such as the Hilbert filter and the divider used to calculate a power ratio. Our system design was simulated for testing using ModelSim along with existing scripts and VHDL test benches provided by our sponsors. A generic hardware shell developed at MIT Lincoln Laboratory was leveraged to simplify hardware design and gain access to PCI Express communication. Finally, an accompanying communication program was used in conjunction

with this hardware shell to allow data to be transferred back and forth between the PC and FPGA.

Once the system was developed and tested in simulation, the device was synthesized and tested with physical signals. Since our project work does not include the RF receiver frontend, IF input signals were simulated for testing using a hardware radar signal emulator designed for use in this project. This device receives user input that specifies various pulsed sinusoidal emitter signal characteristics to define a desired signal waveform. In addition, it allows for a schedule of signals that change in characteristics over time in order to better simulate realistic radar waveforms. The emulator utilizes two DACs which can produce two simultaneous signals, one for each simulated antenna. By varying the amplitude ratio of signals at both DACs over time, a target signal moving across the mainlobes of the antennas can be simulated. Though this project relies on simulated signals, the emulator is designed to produce high fidelity signals in hardware which are representative of true IF signals that would be present at the front end of a radar system. Therefore, the emulator was deemed by our group and our sponsors as an appropriate and accurate solution for testing the direction finding system within a lab environment.

5.4 Analysis of System Throughput

One of the hardware components to be tested was the PCI Express communication port between the FPGA and the CPU. It is important to know the data transfer rates between these systems because the rates define the speed at which the output display can be updated. These rates also indicate how much internal information about the FPGA can be passed to the CPU during the debugging process, at which point we will want to know as much as we can about what is happening inside the FPGA.

Data throughput was calculated by polling the hardware for data and recording the time taken. For this test, the hardware was polled 140,000 times in blocks of 10,000 polls. Each poll requests 4 bytes of data, corresponding to a total of approximately 560 KB of data polled in 40 KB blocks. The time taken for each block was recorded and used to calculate 14 separate data rates (see Table 5), which were then averaged to produce a single data rate estimate of 2.4 MB/s. If the highest precision format available (double-precision floating point) is used to represent angles of arrival, 8 bytes will need to be read for every angle, resulting in a throughput of 300 angles of arrival per millisecond. For a graphical user interface refresh rate of 30 Hz, a standard refresh rate, it is possible to read 104 angles of arrival per frame. This throughput far surpasses our needs, enabling us to select sample sets and average them to produce more accurate results on the display.

Poll Block #	Data Rate (MB/s)	Poll Block #	Data Rate (MB/s)
1	2.3985	**8**	2.4030
2	2.3979	**9**	2.4020
3	2.4004	**10**	2.4008
4	2.4010	**11**	2.4013
5	2.4018	**12**	2.3965
6	2.4037	**13**	2.3906
7	2.4028	**14**	2.3649
Average: 2.4 MB/s		**Standard Deviation: 0.01 MB/s**	

Table 5. Data rates calculated from polling the hardware. Each block is 10,000 polls, and the data rate is an average for the entire block.

5.5 System Overview and Block Diagram

The block diagram for the full system is shown below in Figure 72, and system processes closely follow the algorithm used for the amplitude comparison simulation (see section 2.3.4). Operation begins with signal acquisition using two ADCs located on the development board. The input signals from the emulator are representative of the IF signals from the two receivers. Digitized signals from the ADCs are then passed through separate Hilbert filters to produce in-phase and quadrature components for each signal. The resulting components are squared and summed to produce values for squared voltage. The ratio of the squared voltage values is then used to index into a lookup table of angles of arrival. A proper index is found by searching through a list of pre-calculated ratios and selecting the closest match. The accompanying index value for the pre-calculated ratio is used to retrieve an angle of arrival from the lookup table. Angles of arrival are then forwarded to the Linux PC using the existing PCI Express interface, averaged over time, and transmitted across the local network to another PC running a graphical user interface we designed for the device. This user interface then renders the angle of arrival in a simple graphical format.

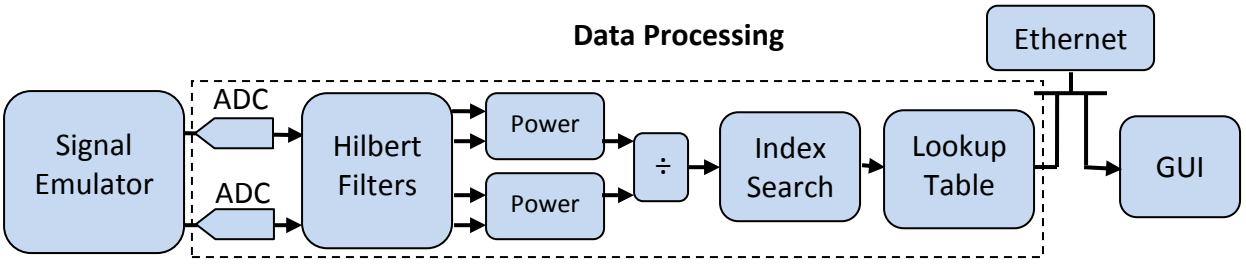

Figure 72. Block diagram of the amplitude comparison direction finding hardware, which consists of acquiring signals, performing the algorithm, and providing a graphical output.

5.5.1 Signal Input

Two analog IF input signals from the emulator were digitized for calculations using the two 14-bit ADCs on the provided development board. Digitization of the input signals allowed for algorithm implementation and computations using digital components and associated development tools. With the given hardware, our group used these digitized signals for comparison and calculation to execute the amplitude comparison algorithm.

5.5.2 Power Calculation

Once the two input signals were digitized, values for their squared amplitudes were calculated using the quadrature signal components extracted using Hilbert filters. The filters were generated with the Xilinx Core Generator using 31 digital finite impulse response filter taps with 16-bit fixed-point coefficients. The filter was designed to be identical to that used in simulation (see section 4.3.2 for frequency response). As the magnitude response of the filter is not perfectly flat across the passband, the bit width required to accurately represent the resulting quadrature component was increased to 16 bits from the 14-bit input signal. For proper calculations, the delayed in-phase signal was sign-extended to match the quadrature width. The in-phase and quadrature signals were then squared at each sample using signed-input hardware multipliers built into the FPGA. Normally, multiplication of two 16-bit integers results in a 32-bit result; however, as squared numbers always result in positive values, the multiplication result could be accurately represented with an unsigned 31-bit integer. The squared in-phase and quadrature samples were then added to produce an unsigned 32-bit value for the squared input signal amplitude.

5.5.3 Determination of an Angle of Arrival

Deviating from the process flow outlined previously, the next components developed were the lookup table and an accompanying index list search. An index list search was developed similar to the implementation in simulation in order to account for the fact that the ratios calculated would likely not directly match any value within the lookup table. The index list search would remedy this matching issue by finding the pre-calculated ratio closest in value to the ratio calculated in hardware, and then using an accompanying index value to index into a lookup table of corresponding angles of arrival. These components were developed ahead of the ratio calculation due to the fact that the number of ratio bits needed is determined by the number of angles of arrival in the lookup table. The values in the lookup table require accompanying pre-calculated ratios, resulting in an equal number of angles of arrival and pre-calculated ratios. Following this fact, the number of ratios used for the index list search would directly correlate to the bit resolution needed to distinguish between these ratios. This resolution must be at least matched by the calculated ratio in order to properly select an angle of arrival.

A lookup table containing eighteen angles of arrival was generated for the device (see Table 6). Capitalizing on the symmetrical placement of the receiver antennas, we designed the table to cover only the 45° field of view corresponding to amplitude ratios greater than one. Such a design reduces the table size to half of the full field of view size. In addition, less resolution is needed for the ratio due to the fact that the set of ratio values between 0 and 1 are inherently more closely spaced than the same number of values greater than 1. Calculations stemming from the amplitude comparison simulation revealed that a table of eighteen angles of arrival would meet the ±2.5° accuracy specification from our sponsors while minimizing hardware complexity and associated calculation delays. Rather than implementing a fixed lookup table of values, a set of registers was connected to the PCI Express hardware interface to allow values to be written. Such an implementation would allow different antenna beam patterns to be represented in the device, adding a level of flexibility for future projects. The registers used were 32-bits wide, and the representation (fixed point, floating point, etc.) could be determined by the program writing and reading the values. For our testing, we used 32-bit fixed-point values to represent the angles of arrival.

Integer Ratio	Angle of Arrival (Degrees)	Integer Ratio	Angle of Arrival (Degrees)
16	0.0901	**46**	22.7930
18	2.6126	**50**	25.3150
20	5.1351	**54**	27.8380
23	7.6577	**58**	30.3600
26	10.1800	**62**	32.8830
30	12.7030	**65**	35.4050
33	15.2250	**67**	37.9280
37	17.7480	**69**	40.4500
41	20.2700	**70**	42.9730

Table 6. Lookup table of 18 angles of arrival and integer ratios (decimal ratio multiplied by 2^4 and rounded) for hardware implementation.

To index into the lookup table, a searching function was implemented to compare the ratios calculated in hardware to a set of pre-calculated ratios and select an index value. Searching was done by first calculating the differences between the calculated ratio and each pre-calculated value in parallel. These differences were then compared with each other to find the smallest calculated difference. The index value associated with the pre-calculated ratio resulting in this difference was then used to index into the lookup table. For a lookup table of twenty five values for angles of arrival, twenty five pre-calculated ratios were used. As floating point numbers would greatly increase hardware complexity and calculation time, these ratios were each bit shifted and rounded to produce integer values. Calculation revealed that a shift

of four bits (multiplication by 24, refer back to Table 6) would provide enough resolution to differentiate between the pre-calculated ratios. These ratios could then be represented using registers of only 7 bits. Similar to the lookup table, these registers were connected to the PCI Express hardware interface to allow configuration of the pre-calculated ratios according to the antenna beam pattern used.

5.5.4 Ratio Calculation

Once the specifications for the lookup table were finalized, the ratio calculation component was developed. The main component in the ratio calculation was a 32-bit divider generated using the Xilinx Core Generator. This divider operated on the two squared amplitudes calculated from the input signals. Divider output included both an integer component and a fractional component. By combining the integer and fractional components into a single output, we in essence shifted the divide result by 24, resulting in the integer ratios used for the lookup table. The divider was configured to produce a 7-bit ratio for use in determining angle of arrival. Due to the fact that the lookup table contained values only for ratios greater than one, a comparison between the squared amplitudes was made before they were input to the divider. The comparison selected the larger of the two values to be divided by the smaller to ensure that the ratio remained greater than one. The logical result of this comparison was then stored for use after retrieving a value from the lookup table. Using this comparison result, the angle of arrival could be determined to be either positive or negative depending on which antenna had the higher amplitude.

5.5.5 Display

Finally, the angle of arrival determined by the system was output to an external graphical display, which we designed and developed in the Java programming language. Our display is designed to retrieve angles of arrival from our system and display them on a polar plot (see Figure 73). Data retrieval is performed using a transmission control protocol (TCP) connection over Ethernet. As such, any PC connected to the same LAN as our direction finding device will be able to utilize the display.

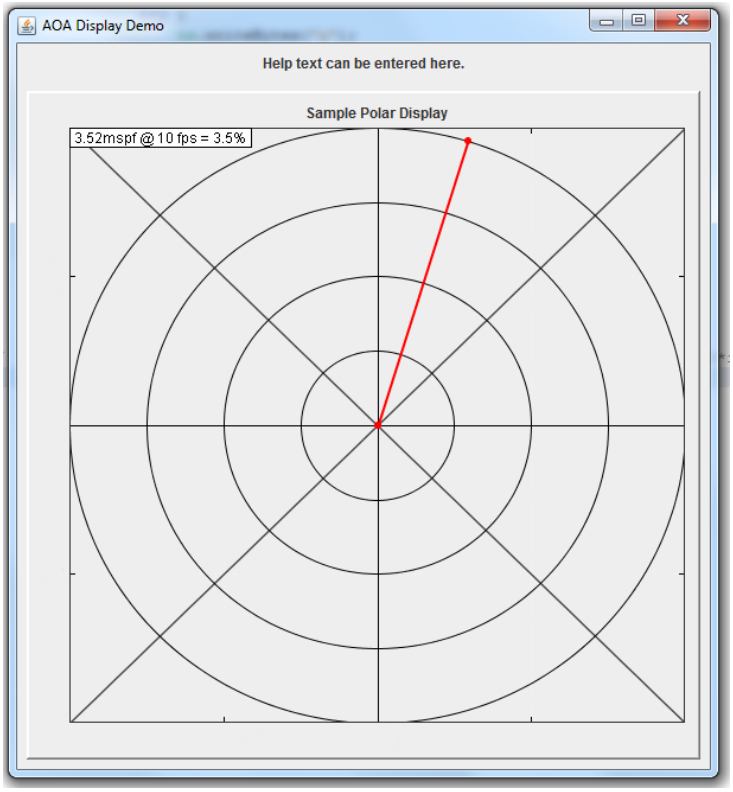

Figure 73. Graphical display for angles of arrival output from our system. It receives angles of arrival through a TCP connection with the direction finding hardware and uses them to indicate emitter direction with a red line on a polar plot.

Our system forwards data recorded from the hardware and averaged over time to the graphical display. Raw angles of arrival are first retrieved from the system using the PCI Express communication interface software. These angles of arrival are then averaged over approximately 500 µs, the result of which is stored as a double-precision floating-point value. This averaged angle of arrival is then forwarded across the TCP connection to the graphical display. Once it receives data, the display program draws a red line at the received angle of arrival on the polar plot.

5.6 FPGA Resource Usage

Once we had completed each component and connected them all together, we analyzed the amount of FPGA resources our project consumed. We recorded two sets of resource usage information: one set for the core direction finding hardware developed in this project, and another set for the full system containing the PCI Express hardware provided by our sponsors. Both sets are given in Table 7 below. Included in this table are only the four significant utilizations of FPGA resources by our direction finding hardware. From this information, it appears that slice registers are by far the most necessary resource for the hardware. Other resource utilizations, while significant, are less than half the magnitude of the

slice register utilization. Assuming the same development board is used to generate multiple instances of our hardware to handle separate beacon channels, the FPGA will be able to synthesize 7 instances of our direction finding hardware alone, or 6 instances when including the PCI Express hardware.

	Direction Finding Hardware			Full System with PCI Express		
Resource	**Used**	**Available**	**% Utilized**	**Used**	**Available**	**% Utilized**
Slice Regs	8025	58880	13.63%	14463	58880	24.56%
Total LUTs	3049	58880	5.18%	6814	58880	11.57%
LUTRAMs	231	24320	0.95%	459	24320	1.89%
DSP48E	22	640	3.44%	22	640	3.44%

Table 7. FPGA resource utilization of the beacon locator system. Data is available for both the direction finding hardware alone as well as the full test system wtih the PCI Express hardware.

5.7 Hardware Test Procedures

In order to verify that the resulting synthesized hardware functioned properly, each component was independently tested for correct operation. Isolating the components required test inputs and test points to be set up before and after each system block in the design. Several of the hardware components were tested for functionality within simulation. The results of simulation testing revealed whether the block was properly designed to produce its desired function. In addition, all components were tested on the FPGA using real input signals in order to determine their realistic performance. This latter setup was achieved by separating the inputs and outputs of each logical block within VHDL and connecting them to external ports on the FPGA board such as the ADCs/DACs or PCI slot.

5.7.1 Signal Acquisition

The first stage of testing involved verifying that data could be recorded at the ADCs and propagated to the PC display without performing any processing. Doing so verified that fundamental components of the development board, namely the ADC and PCI Express interface, work properly and contain no faults that could cause difficult problems later in the design process. The test involved placing a known DC voltage at the input of the ADC, propagating the ADC output through the PCI Express interface, and retrieving the data on the PC using the communication program. The retrieved value was compared to the input voltage amplitude to ensure that they were the same.

We were able to record data from the ADCs within hardware and retrieve the data with the communication program on the attached PC. Our successful retrieval of data verified that

the PCI Express connection between the FPGA and the PC was indeed working. The input voltages and the recorded results are given below in Table 8. Data values recorded from ADC1 are close in value to the input with an average error of only -3 mV, indicating that ADC1 is functioning and accurate within datasheet specifications. However, data values recorded from ADC0 show a constant DC error of approximately +30 mV. This DC component can be mitigated by subtracting an equal magnitude value from the digitized ADC output. Performing this subtraction results in ADC0 accuracy similar to that of ADC1, indicating that both ADCs are able to function accurately.

Input Voltage	ADC0 Recorded Voltage	Error		ADC1 Recorded Voltage	Error
-973	-941	32		-973	0
-728	-698	30		-732	-4
-485	-456	29		-489	-4
-241	-213	28		-246	-5
-1	29	31		-3	-2
244	273	29		240	-4
485	516	31		483	-2
727	759	32		726	-1
970	1000	30		968	-2
All values in millivolts.					

Table 8. Recorded DC voltages from the two ADCs on the development board, and the DC offset errors from the actual input voltages.

5.7.2 Hilbert Filter

Before we performed the hardware testing of the Hilbert filter, we simulated its functionality in MATLAB. Simulation of the Hilbert filter predicted accurate functionality within our IF band. MATLAB was used to filter several signals over a range of frequencies using a filter model with the same coefficients as in hardware. Each signal encountered a 90° phase shift, and amplitude changes were in accordance with the theoretical magnitude response of the filter.

After verifying functionality using simulation, we implemented the component in hardware and performed another test. Hardware testing of the Hilbert filter verified that it introduced a 90 degree phase shift for all frequencies over the input bandwidth while adhering to the theoretical magnitude response. To set up the test, the input of the Hilbert filter was connected to an ADC, which was in turn connected to a signal generator. The output of the filter was connected to a DAC, which then output the phase-shifted signal on an oscilloscope for visual analysis (see Figure 74). In addition, several periods of each Hilbert filter output were

recorded and imported into MATLAB to calculate an exact numerical measurement of phase difference. The signal generator was used to create a series of signals of constant amplitude with frequencies ranging from 12.5 MHz to 112.5 MHz, the minimum and maximum frequencies that the system was required to process. By comparing recorded numerical values from the input and output waveforms, we were able to verify the amplitude and phase response for the filter.

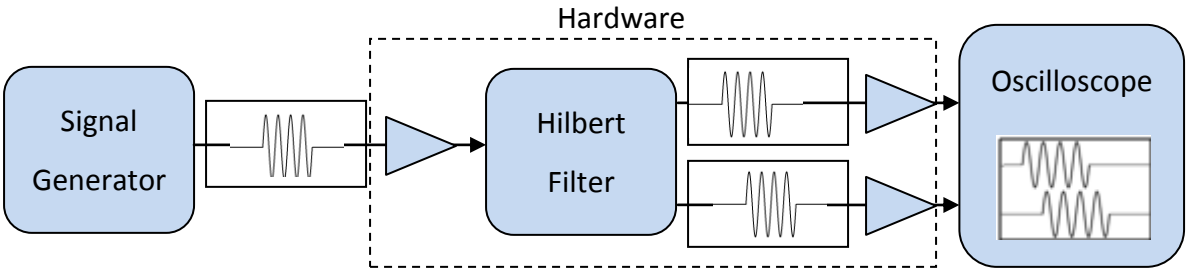

Figure 74. Test setup for Hilbert filter testing. Signals are digitized and input into the Hilbert filter. The filter outputs are converted back to analog and viewed on a scope.

Several signal frequencies over the IF bandwidth of the system were used to test the Hilbert filter. Visually, each output appeared to be correct to our group (see Figure 75). Once we determined that the filter appeared to be working correctly with no major faults, we recorded in-phase and quadrature signal data and calculated their phase differences. Phase differences were calculated using the same method utilized for the phase comparison direction finding simulation (see section 4.3.2). Each frequency and its resulting phase difference are given in Table 9 below. The quadrature signal consistently exhibited an approximate 90° phase shift throughout the input bandwidth. Calculated values remained within ±0.4° from the ideal phase shift. Causes for the inaccuracies in the phase difference calculation include noise present on the in-phase and quadrature signals as well as the non-ideal frequency response of the Hilbert filter.

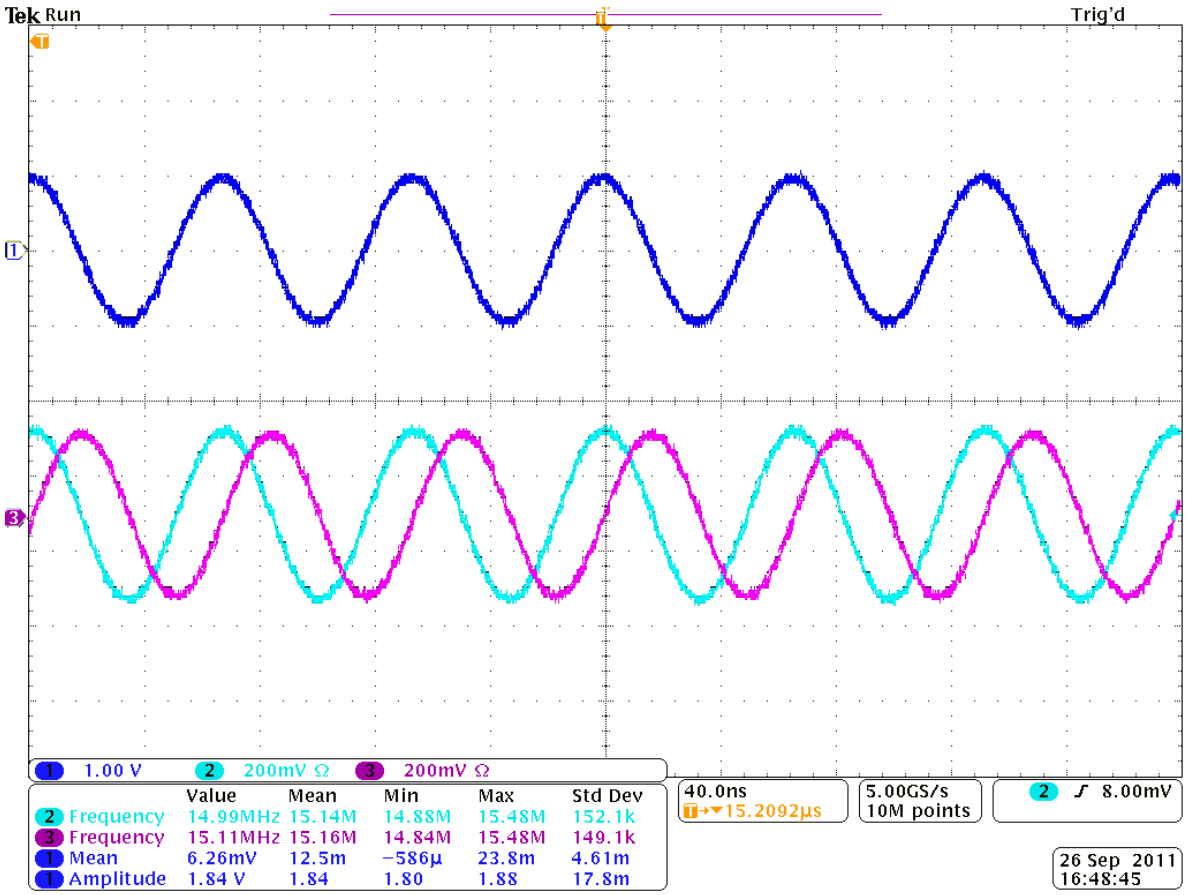

Figure 75. Oscilloscope screen capture of Hilbert filter output. Top signal is the input to the system, the bottom two signals are the in-phase (blue) and quadrature (magenta) Hilbert filter outputs. The bottom two signals appear to have a phase difference of 90°, the desired filter result.

Input Frequency (MHz)	Phase Difference (°)
12.5	89.7784
15	89.6679
20	89.9767
38	90.0595
45	90.1388
63	89.9856
71	90.2431
88	90.1461
112.5	90.2458

Table 9. Phase differences calculated between in-phase and quadrature signals from the Hilbert filter for several frequencies in the system IF bandwidth.

In addition to verifying phase difference, the extent of the magnitude ripple in the Hilbert filter frequency response was measured. The maximum gain was measured using the 38 MHz signal, while the maximum attenuation was measured using the 15 MHz signal. We found that the 15 MHz input signal resulted in a -0.3702 dB magnitude change in the quadrature amplitude. This attenuation is close to the theoretical value of -0.3771 dB. We then found that the 38 MHz signal resulted in a gain of 0.3231 dB. The theoretical gain for a 38 MHz signal is 0.3625 dB, indicating an approximate error of 0.04 dB. However, this error is likely due to the limited resolution available when measuring the magnitudes of the signals. From these calculated magnitude differences and phase differences, we concluded that the Hilbert filter performed its function correctly.

5.7.3 Power Calculation

Power calculation was tested by applying input signals of variable amplitude to the system. The input signal was split into in-phase and quadrature components by the Hilbert filter, and power calculation was performed on these components. The calculated power value was then output through a DAC for viewing on an oscilloscope. In addition, the power values were recorded over multiple input signal periods for analysis in MATLAB. Our MATLAB calculations involved calculating values for signal amplitude from the recorded signal power values. We then compared these calculated amplitudes to the respective input amplitudes in order to determine the accuracy of the power calculation block of our system.

Viewing the DAC output on an oscilloscope allowed our group to quickly recognize that the power would oscillate at the same frequency as the signal. Theory suggests that, for perfect in-phase and quadrature signals, the power level should be flat at a single value for each point in time. However, due to small magnitude changes on the quadrature signal resulting from the Hilbert filter's frequency response, the in-phase and quadrature signals do not have the exact same magnitude. The result from this slight magnitude mismatch is the oscillation of the calculated power value around the true power value.

To determine the accuracy of the power calculation, we recorded sample sets of the oscillating power calculation values over several signal periods, calculated values for amplitude, and averaged their values (see Table 10). For most input signal amplitudes, the average calculated amplitude was within a few millivolts of the actual value. Averaging the calculated power values over a set period of time should therefore provide good accuracy. However, at roughly 19 mV input signal amplitude, near the bottom of our dynamic range, the error of the average calculated amplitude grew to approximately 18 mV. Viewing the input signal on an oscilloscope, we found that there was a +13 mV DC offset at the ADC input. In this particular case, the DC offset shifted the signal up by roughly 2/3 of its amplitude. The resulting power calculations from such a signal would be noticeably skewed by this DC offset. In the same method explained for signal acquisition, the DC component could be eliminated by subtracting

an equal magnitude value from the digitized signal. Alternatively, a high-pass filter after ADC signal acquisition may also eliminate this DC component. Performing either method would eliminate the power calculation skew.

Input Signal Amplitude	Calculated Amplitude	Error
940	946	6
700	711	11
470	477	7
235	242	7
94	98	4
47	54	7
19	37	18
All values in millivolts.		

Table 10. Signal amplitudes calculated from in-phase and quadrature components of signals with varying amplitude, and the resulting calculation error.

5.7.4 Ratio Calculation

The ratio calculation block was initially tested for functionality within simulation. To test the ratio calculation, various ratios were chosen which would test different features of the block, such as fraction calculation and input comparison. The test set included ratios of value 1.0, 2.0, 5.0, and 2.5. We iterated through these sets of values and viewed the output using a VHDL test bench in ModelSim to verify that the block produced correct ratios at the proper resolution.

An annotated screen capture of our test results is provided in Figure 76. Note that there exists a 43-cycle propagation delay between input and output. This delay is due primarily to the divider core, which needs a long pipeline to calculate a division result. In addition, the calculated ratios have been left with fractional components for easier illustration of the results. Viewing all seven ratio bits as a single integer produces the 24-shifted integer ratios used for the lookup table. In the first test case, both simulated antenna received signal powers had the value of 1, resulting in a calculated ratio of 1.0. The power value for the right antenna was then increased to 2 and then 5, which produced proper results at the output. Next, the signal power from the left antenna was increased to 2, testing the ability to calculate the fractional ratio component. The correct ratio value of 2.5 was produced at the output, indicating that the ratio calculation block was indeed able to calculate fractions. The final test case used a power value of 5 for the left antenna and a value of 2 for the right antenna in order to test the comparison result. A value of 2.5 was output for this case, indicating that the input comparison was performed correctly and that the block indeed divided the larger value by the smaller. In addition, the logical result of the comparison was output from the system at the same time as

the associated ratio, indicating that the comparison result was correctly stored for the exact time delay needed to compute the ratio.

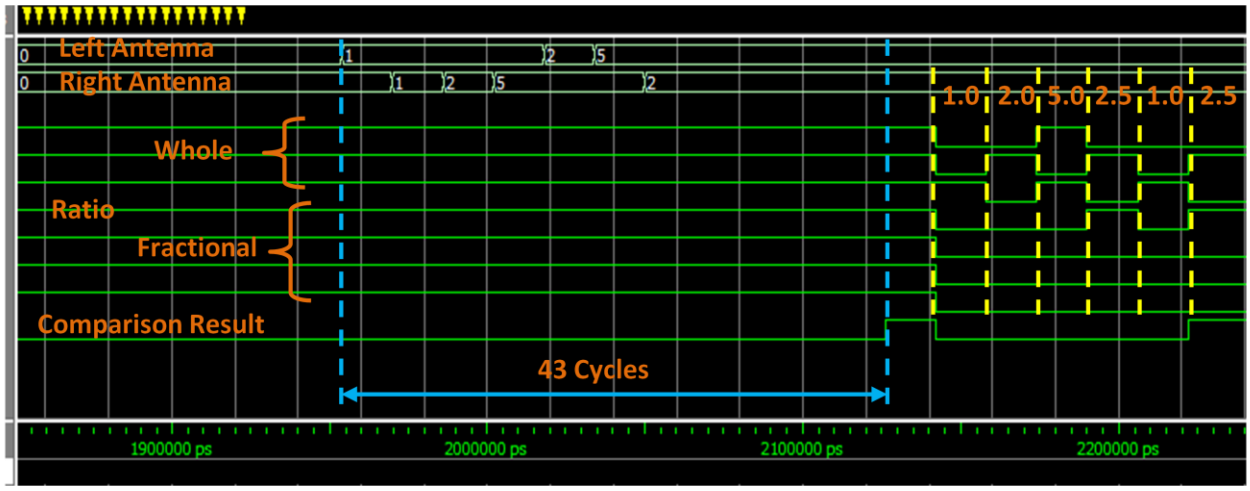

Figure 76. ModelSim capture of simulated ratio calculation from two simulated antenna signal power values (left and right antennas). Each input produces the correct ratio at the output after a 43-cycle delay to due division. Logical result of input comparison is output at the same time as the division result (for left=5, right=2).

In addition to simulation testing, we synthesized the divider block along with the processing blocks needed to calculate signal power in order to test the system with real signals. Several different ratios that the system would typically encounter were selected to test the ratio calculation. The ratios chosen were 1.0, 2.0, 3.0, 4.0, and 4.5, which extend over the whole range of valid signal ratios. We then produced input signals to the system with amplitudes that would produce the desired ratios.

Each signal set was input to the system, and the resulting ratio calculations were recorded and averaged. The results of our test are given below in Table 11. In each case, the system was able to calculate a ratio near in value to the input ratio. Though the magnitude of the errors enlarged for greater ratios, the percent error for each remained roughly between -3.6-5.3%. This error may be due to the imprecise nature of the calculated power signals. As described earlier, the power calculations fluctuate due to the non-ideal Hilbert filter response. It is possible that these fluctuations occur around a power value that is not equal to the true signal power value, causing an error in ratio calculations. Another factor that may have affected our results is DC voltage at the ADC inputs, as this would have also caused errors in calculated power values as discussed earlier.

Ratio	Actual Ratio	Calculated Ratio	Magnitude Error	% Error
1.0	1.000	0.958	-0.042	-4.164
2.0	2.011	1.921	-0.089	-4.431
3.0	2.984	2.874	-0.110	-3.677
4.0	4.086	3.869	-0.216	-5.294
5.0	4.558	4.332	-0.226	-4.953

Table 11. Results of hardware ratio calculation. Input signal magnitudes were recorded and used to calculate the actual input ratios. Error magnitudes grew with input ratio, but percent error stayed roughly between -3.6% and -5.3%

5.7.5 Index List Search

Testing of the index list search block was performed by sweeping over the full range of possible ratios from minimum to maximum. The resulting index output was then observed to ensure that it incremented from zero up to the index value for the last item in the list. For analysis, we used these output indices to determine which pre-calculated ratios the search block had selected. Doing so allowed us to ensure that the index list search was indeed selecting the pre-calculated ratio closest in value to the input ratio.

The pre-calculated ratios selected by this block for every possible input ratio were graphed to depict the functionality (see Figure 77). As we incremented the input ratio from minimum to maximum, the selected ratio followed. In addition, the pre-calculated ratio selected by the search function was always the closest pre-calculated ratio in value to the input. These results indicated to our group that the index search block was indeed operating properly. As such, angles of arrival stored in a lookup table could be correctly retrieved by this system block.

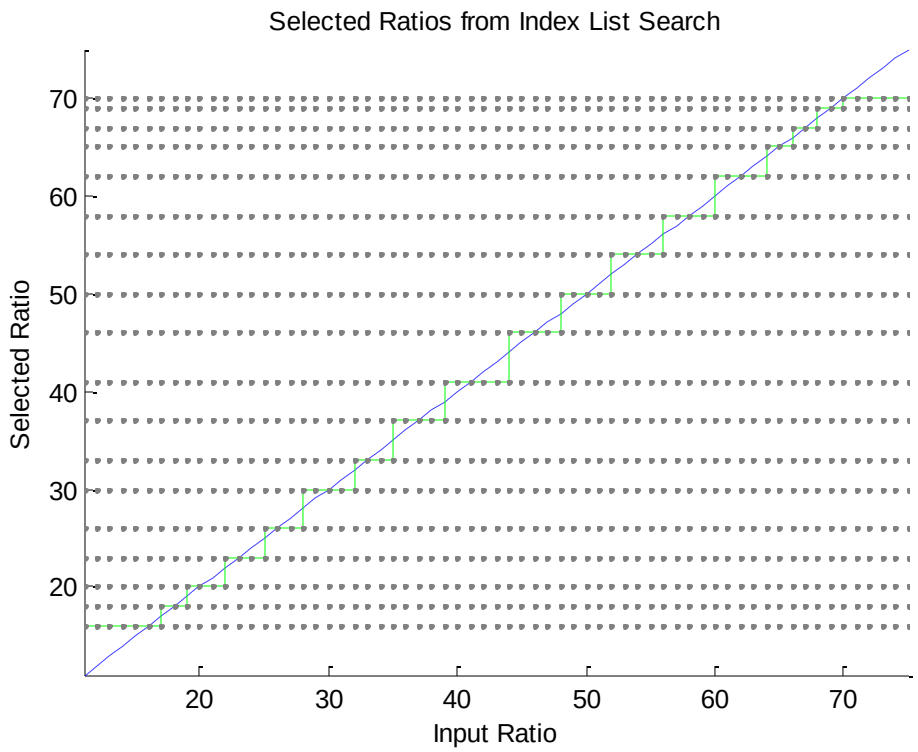

Figure 77. Ratios selected by the index list search in hardware from given input ratios. The dashed line indicates every possible calculated ratio. The stepped line is the ratio selection of the search block. Horizontal dotted lines mark the pre-calculated ratios stored in hardware, which were used by the search block to compare to the input ratio.

5.7.6 Display Testing

The final component of our system that we tested was our graphical display. To test our display, we first connected our hardware device and a PC with the display program to the same LAN. The hardware device was setup to listen for TCP connections from the display and to send its output across those connections, and the display was configured to connect to our hardware device in order to receive angles of arrival. We then generated input signals from which our device could calculate angles of arrival. These angles of arrival were displayed on screen both before and after the TCP network transfer in order to verify correct functionality.

Our test indicated that the display was indeed working correctly. Both ends of our system displayed the same angles of arrival, indicating that data was being correctly transmitted using TCP connections. In addition, the display was able to graphically indicate the received angle of arrival with a red arrow on its polar plot. We visually inspected this arrow and determined that it was being drawn at the correct angle on the display.

5.8 Complete System Testing

Once we developed and tested each hardware component, we assembled the full system and tested it. The tests we performed were designed to determine whether the system would be able to meet its accuracy specifications for the full 90° azimuth extent. To do so, we selected input signal amplitudes that would represent several angles of arrival from roughly -45° to 45°. We then configured our signal emulator to produce analog signals with these amplitudes. Our system received these signals as input, and its output for each input angle was recorded over approximately 500µs and averaged.

The results of our test are given below in Table 12. The data in this table also include the error from the calculated angle of arrival to the true input. According to these results, the system appears to be able to meet our ±2.5° accuracy specification for most of the azimuth extent. However, our error values vary with no immediately apparent pattern, angles at the extremes of our field of view see large increases in error, and we were not able to meet specification for the maximum input angle of 44.6°.

Input Angle	Calculated Angle	Error
-44.6	-42.5	2.2
-40.5	-40.8	-0.4
-30.4	-31.0	-0.7
-20.3	-22.1	-1.8
-10.2	-10.2	-0.1
0.1	0.1	0.0
10.2	10.3	0.1
20.3	20.3	0.0
30.4	30.8	0.5
40.5	39.1	-1.4
44.6	40.7	-3.9
All values in degrees.		

Table 12. Average calculated angles of arrival from the direction finding hardware and the errors from the true value.

We investigated possible causes for the behavior of our error values and determined two likely problems, both of which we have discussed previously. First, one of the ADCs on our development board appeared to have a DC voltage bias. This bias caused errors of varying value in our ratio calculations, noted in our test of the ratio calculation block. Though we attempted to take biasing into account when generating signals, our calculations may have been off. Therefore, we believe that ADC biasing (along with noise and other physical signal inaccuracies) is the primary cause of our erratic error values. Second, our calculations fluctuate over time. As

such, the angle of arrival output from the system also fluctuates. Our measurements take this into account by averaging our results. However, due to the finite number of elements in our lookup table, angles at the edge of our azimuth extent will have their fluctuations clipped. Any calculated ratios higher than the maximum in our table will be clipped down to the maximum angle of arrival in the table, thereby biasing the results toward a lower angle of arrival. The cause of this fluctuation has been previously determined to be non-idealities of the Hilbert filter, though the biasing of the ADC may have also played a role. To mitigate clipping due to fluctuation, a portion of the averaging may be done in hardware, thereby reducing the extent of the fluctuation ideally within the bounds of the lookup table.

5.9 Discussion

We were successfully able to design and assemble a hardware implementation of the amplitude comparison direction finding method. Our device is capable of receiving two IF signals, as would be produced by a receiver array with two directional antennas, and using them to determine angles of arrival. In addition, our device is capable of transferring data through a TCP connection to a graphical display that we have designed. Each component of our system was tested, followed by a test of our complete system. The results of our tests indicate that our hardware is functionally correct.

Some issues were encountered which hinder the ability of the device to meet accuracy specifications. Such issues included ADC voltage biasing and clipping of fluctuating angles of arrival. As such, though our system would theoretically be able to meet accuracy specifications for a limited bandwidth as discussed in section 3, we were not able to make a complete and accurate measurement of system performance as these issues induced noticeable errors. Fortunately, additional hardware should be able to mitigate these issues and improve system performance. The DC voltage bias on the ADC could be resolved using an internal bias with an equal and opposite magnitude. Alternatively, a high-pass filter placed after the ADCs would strip their output of any DC components. The clipping of angles of arrival could be solved by performing averaging within the system, thereby reducing the extent of the calculation fluctuations and, as a result, the degree of clipping.

Finally, our work could be expanded upon to provide useful features for a direction finding system. One such feature would be the ability to detect pulses on the input signal. Currently, our system only works with continuous wave IF signals. We originally intended for the device to function on pulsed signals as these would likely comprise the majority of the system's practical input. Indeed, we had begun work on implementing a signal detector in hardware similar to that described in section 3.3, but we were unable to complete this work due to time constraints. Another useful functionality expansion would be multiple emitter tracking. In a practical application, the system may encounter multiple emitter signals simultaneously at its input. The ability to separate these signals and perform direction finding

for each would be highly desirable in these situations. Though our system currently operates on a single beacon only, we designed the hardware to be modular, allowing it to be duplicated to produce additional operation channels in a straightforward manner. By duplicating our system and developing signal tracking components, the system could be expanded to operate on multiple simultaneous beacons.

6. Summary

There were several accomplishments, as well as recommendations for future work, that resulted from this project, which can be categorized as derivative of the following investigations: specification analysis, simulation analysis, and hardware analysis.

6.1 Specification Analysis

The current hardware setup with the amplitude direction finding system is unable to meet the specifications provided by Lincoln Laboratory that the system should be able to detect beacon locations to within ±2.5° over 40 dB of dynamic range for the full 90° azimuth extent. There are several methods through which this could potentially be corrected. If different antennas were used, providing a 60° field of view rather than 90°, signals detected at the edges of the field of view would be well within the specifications. However, if maintaining the 90° field of view is considered essential, multiple systems will need to be combined, requiring additional antennas and hardware. Another approach, if better hardware is available, is to replace the current ADCs with ones with a greater number of effective bits. The ADC is a limiting component for the design, so improving its capabilities would increase the dynamic range of the system, which would be especially noticeable at the edges of the azimuth extent. Alternatively, if the accuracy of locating weak signals near the edge of the field of view is not essential, the design could be accepted as is.

6.2 Simulation Analysis

Simulating each of the three direction finding methods in MATLAB allowed our group to assess the accuracy of each of the systems, as well as modifications to each system that could increase the accuracy. The TDOA algorithm was relatively inaccurate for the purposes of this project when using a sampling frequency of 250 MHz and the specified antenna geometry, with only 22% of angle calculations achieving the required ±2.5° of accuracy. However, throughout the duration of this project, we determined several ways to improve the accuracy of the TDOA method that could be used for future projects. Our group determined that by using ADC's with greater sampling frequency, or by digitally upsampling the signals, the accuracy of the TDOA system in the given geometry would improve. Through simulation, we determined that a sampling frequency of 25 GHz would result in about 95% of the calculated angles to be within ±2.5° of accuracy. Using a sampling frequency of 250 GHz would result in close to 100% of the calculated angles to be accurate to within ±2.5°. Though this system would be more expensive as a result of ADC's with significantly greater sampling frequencies, these levels of accuracy would be possible if required to meet the specifications for a future project.

Through simulation of the phase comparison technique, our group determined that exclusive implementation of this direction finding method would likely be inaccurate for most applications due to ambiguous solutions, unless the antennas were separated by a distance less

than or equal to the wavelength of the detected signals. To resolve this issue, we believe that a combination of amplitude and phase comparison could be used to create a hybrid direction finding algorithm that would be able to determine angle of arrival with extreme accuracy. By using the amplitude comparison system to determine the angle of a detected signal to within a few degrees of accuracy, the phase comparison system would be able to perform its calculations, and then select the ambiguous solution that is closest to the amplitude comparison's result. When restricting analysis of the ambiguous solutions returned by the phase comparison algorithm to only include the solution closest to the actual angle of arrival, this solution consistently exceeded our requirement of ±2.5° of accuracy, and the calculated angle was usually less than 1° in error from the actual angle of arrival. Therefore, we believe that the combination of amplitude and phase comparison systems would result in a highly accurate system.

Since the amplitude comparison system was intended to be implemented in our hardware, most of the experiments we did revolved around making the algorithm more efficient to achieve either the highest level of accuracy or the fastest computation while still achieving the required accuracy of ±2.5°. We determined that if the system was required to process very quickly or if there was limited space in the FPGA, our algorithm could compute angles of arrival across the entire 90° azimuth extent using a lookup table of only 18 elements and still meet the ±2.5° of accuracy over the entire extent for signals at +10 dBm. Additionally, if there was unlimited space in hardware and no requirement for processing time, the accuracy of the system could be greatly improved by increasing the size of the lookup table, and accordingly increasing the number of bits used to represent the ratio values in the table. Through simulation, we determined that using a lookup table of 2500 values, with 0.018° LUT resolution and 16-bits used to represent ratio values, enables our algorithm to determine angle of arrival across the 90° extent to within 0.2° of accuracy. However, these systems could not meet dynamic range specifications for resolving angles over the full azimuth extent for signals covering 40 dB dynamic range. The amplitude comparison system could be modified to utilize higher resolution ADC's to resolve angles of arrival over 40dB dynamic range to within the required accuracy of ±2.5° over the full azimuth extent.

6.3 Hardware Analysis

We designed and developed a prototype hardware direction finding system that functioned properly but was unable to meet our proposed system specifications. Testing each component that we designed separately allowed us to determine that the operation of each was functionally correct. Further, our overall system was able to receive full-scale power input signals and determine angles of arrival within the proposed ±2.5° accuracy for most of our 90° azimuth extent. However, errors stemming from ADC voltage biasing and lookup table clipping skewed our calculated angles of arrival. As such, we were not able to meet the accuracy

requirements for the system over the required azimuth extent, and we were also unable to perform an accurate measurement of dynamic range due to these issues. Fortunately, some additional hardware components could solve these two issues. The ADC bias could be eliminated using an internal bias with an opposite magnitude or, alternatively, a digital high-pass filter. Averaging calculated values within the hardware would mitigate the lookup table clipping and reduce the skew on the calculated angle of arrival. With these additional components, we believe our system would be capable of meeting the specifications as well as we had predicted.

Several additions and enhancements to our design could be made to make the system more robust. One such enhancement would allow the system to detect pulses on the input signal and only operate on these pulses. It would then be able to handle a much broader range of input signals. In addition, as the beacons this device would be used to detect would likely emit pulsed signals, this feature would make our device much more practical for real-world applications. Another functionality enhancement would be the ability to track multiple emitters simultaneously. Currently, our device only operates on one beacon signal. However, in practical applications, multiple signals may be encountered simultaneously at the input. Our device could be expanded to separate these input signals and perform direction finding for each of them in separate parallel channels. We had originally intended to implement both of these features in our hardware device but were forced to exclude them from our design due to time constraints. The addition of each of these performance improvements and functionality enhancements would make our system relatively accurate and robust for use in practical applications on airborne platforms.

Bibliography

Bowick, C., Blyler, J., & Ajluni, C. (2007). *RF circuit design* (2nd ed.) Newnes.

Broadbent, D. (2010, Q1). Do you know where your radios are? *Instrumentation Newsletter,* Retrieved from http://zone.ni.com/devzone/cda/pub/p/id/1010

Bucher, R., & Misra, D. (2002). A synthesizable VHDL model of the exact solution for three-dimensional hyperbolic positioning system. *VLSI Design, 15*, 507-520.

Carr, J. L., & Maxwell, M. S. (1989). *Direction finding method and apparatus* (342/430 ed.). United States: G01S 5/02.

Carter, G. C., Salt, J. E., & Yuan, Y. X. (1997). In The United States of America as represented by the Secretary of the Navy (Ed.), [Passive Direction Finding Device] (367/124 ed.). United States: G01S 3/80.

Chatterjee, R. (2006). *Antenna theory and practice* New Age International.

Eyre, J., & Bier, J. (2000). The evolution of DSP processors. *IEEE Signal Processing Magazine, 17*(2), 43-51.

Hennessy, J. L., Patterson, D. A., & Arpaci-Dusseau, A. C. (2007). *Computer architecture: A quantitative approach* (4th ed.) Morgan Kaufmann.

Innovative Integration. X5-400M XMC IO module [technical specifications sheet], 2007.

Kuon, I., Tessier, R., & Rose, J. (2008). FPGA architecture: Survey and challenges. *Foundations and Trends in Electronic Design Automation, 2*(2), 135-253.

Lioio, R. J., Clayton, G. E., & Deaton, R. A. (1998). In Hughes Electronics (Ed.), *Phase and time-difference precision direction finding system* (342/442 ed.) G01S 5/04.

Lipsky, S. E. (2004). *Microwave passive direction finding*. Raleigh: SciTech Publishing, Inc.

Lipták, B. G. (2006). *Instrument engineers' handbook: Process control and optimization* (4th ed.) CRC Press.

Mahafza, B. R. (1998). 9.2.3. amplitude comparison monopulse. In *Introduction to radar analysis* (pp. 244-244-251). CRC Press LLC, Boca Raton, Florida: CRC Press LLC.

Radhakrishnan, A. (2007). *Signal processing on a graphics card: An analysis of performance and accuracy.* (Unpublished Bachelor of Science in Engineering). University of Cape Town,

Skolnik, M. (2001). Monopulse tracking. In *Introduction to radar systems* (3rd Edition ed., pp. 213-214-224). The McGraw-Hill Companies, Inc. 1221 Avenue of the Americas, New York, NY 10020: McGraw-Hill.